JMMME

JOURNAL OF MATHEMATICAL MODELS AND METHODS IN ENGINEERING

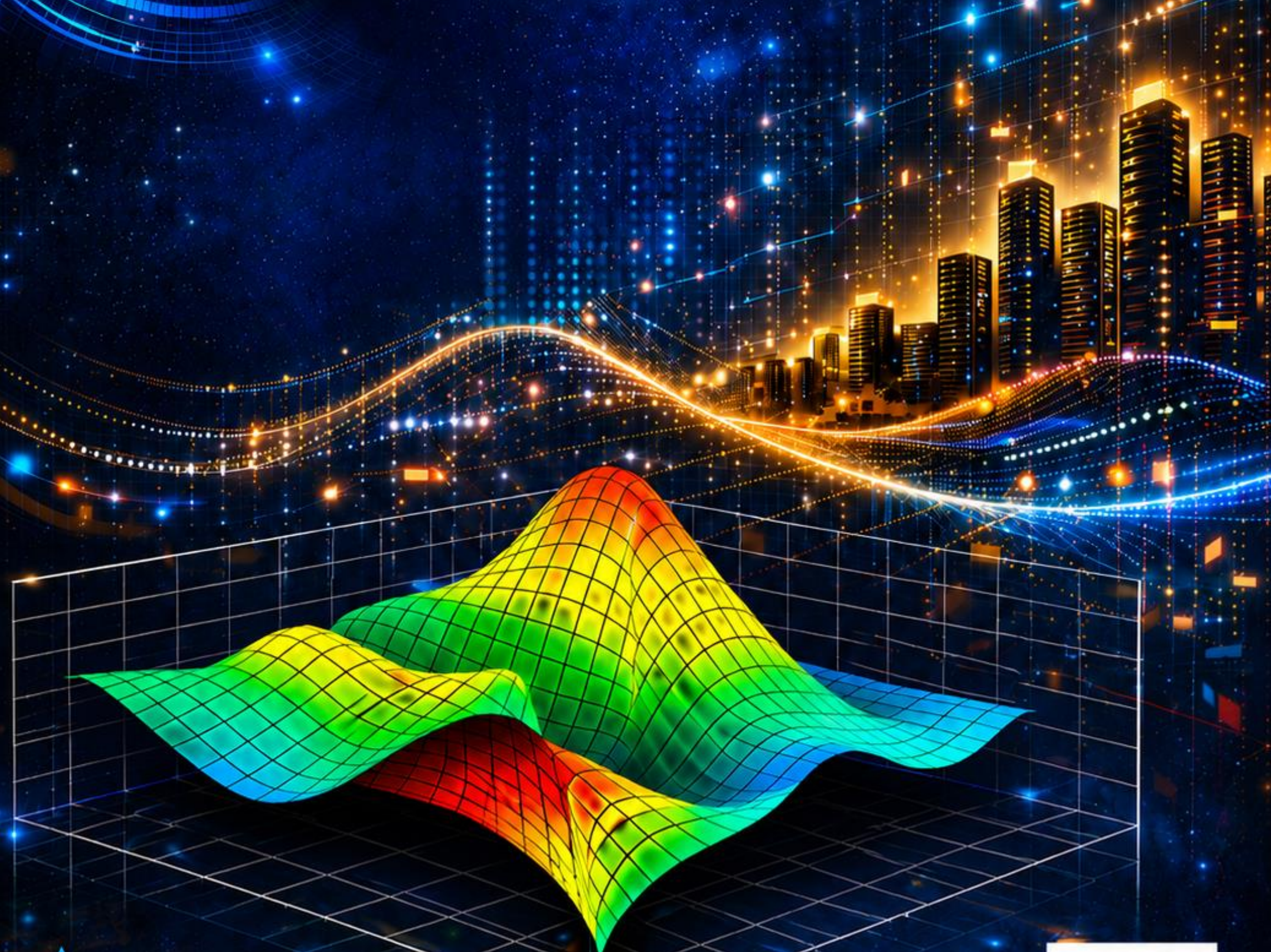

TIIAME
National Research University

JMMME

JOURNAL OF MATHEMATICAL MODELS AND METHODS IN ENGINEERING

JOURNAL INFORMATION

"Journal of Mathematical Models and Methods in Engineering" is an international, peer-reviewed, and open-access scientific journal established in the Republic of Uzbekistan by the National Research University "Tashkent Institute of Irrigation and Agricultural Mechanization Engineers" under Certificate No. 1648073 dated June 15, 2026.

The journal specializes in publishing scientific research on mathematical modeling, numerical methods, computational algorithms, optimization, and analytical approaches across various fields of engineering — including civil engineering, mechanical engineering, energy, hydraulic engineering, materials science, robotics, and environmental protection. It serves as a scientific platform for scholars, engineers, educators, and doctoral researchers to exchange theoretical and applied knowledge.

All submitted manuscripts undergo a double-blind peer review process and are published in strict compliance with high academic quality standards and publication ethics.

The journal has been published since June 15, 2026, once per quarter, that is, 4 times per year. Manuscripts are accepted in English and must be prepared in accordance with international IMRAD standards.

TIIAME
National Research University

FOUNDER	TIIAME National Research University
ADDRESS	39 Qori-Niyoziy Street, Mirzo Ulugbek District, Tashkent, Republic of Uzbekistan
PHONE	+998 (93) 397-12-39
WEBSITE	jmmme.uz
CERTIFICATE	No. 1648073, June 15, 2026
PUBLISHED	2026-06-15
LANGUAGE	English
FREQUENCY	Quarterly / 4 times per year
REVIEW	Double-blind peer review
STANDARD	International IMRAD standards

INDEXED AND DISCOVERABLE THROUGH

ISSN INTERNATIONAL STANDARD SERIAL NUMBER · Google Scholar · zenodo · doi · OpenAIRE · OPEN ACCESS

JMMME

JOURNAL OF MATHEMATICAL MODELS AND METHODS IN ENGINEERING

TIIAME National Research University

Journal of Mathematical Models and Methods in Engineering

journal homepage: https://jmmme.uz/index.php/journal

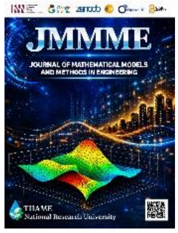

Mathematical description and analysis of oscillatory processes of thin-walled structures when they are flown by a gas stream

B.A.Khudayarov[1*], A.A. Verlan[2]

[1] *"Tashkent institute of irrigation and agricultural mechanization engineers" National Research University, Tashkent, 100000, Uzbekistan*
[2]*Norwegian University of Science and Technology, Norway*

ARTICLE INFO

Keywords:
modeling,
three-layer plates,
flutter,
supersonic flow,
critical velocities

ABSTRACT

The flutter of viscoelastic three-layer Elements of an Aircraft, flown around by a supersonic gas flow is studied in the article. Mathematical models of problems on the flutter of viscoelastic three-layer plates with a structure asymmetrical in thickness, flown around by a supersonic gas flow are developed. The flutter of viscoelastic three-layer plates is studied in linear formulations. The critical flutter velocities of elongated plates are compared with the results obtained in previously published studies, where the solutions were obtained in an elastic formulation. The flutter of viscoelastic three-layer plates with a rigid filler that resists transverse shear, flown from the outside by a supersonic flow, was studied. It is shown that an increase in the geometric parameter characterizing the flexural rigidity of the bearing layers of three-layer structures leads to an increase in the flutter velocity by 25–40%.

1. Introduction

Layered structures, in particular, three-layer plates and shells, are used in the aircraft industry and in other branches of mechanical engineering, and in the future, the scope of their application will undoubtedly expand. Three-layer structures have many qualities that conventional structures made of metal do not have. They have high specific rigidity and can withstand high specific loads. Layered plates and shells have good heat and sound insulation properties, damping and vibration-absorbing properties, certain radio technical characteristics, etc. Due to the fact that there are no fasteners of any kind on the outer surface of three-layer structures and the surface is perfectly smooth, they have high aerodynamic qualities.

Theoretical and experimental studies on three-layer structures made it possible to reveal their main advantages in relation to other types of structures. These advantages are due to the fact that core layers reinforced with filler can withstand high compressive stresses. As a result, these designs are optimal in bending and can significantly increase their critical loads at a minimal weight. Their implementation in various branches of technology entailed intensive research in the field of theory and calculation methods. As a result, over the past fifty years, a separate direction has developed in the mechanics of a deformable rigid body related to the development of the theory of multilayer (in particular, three-layer) plates and shells [1–5].

* Corresponding author. **B.A.Khudayarov**
E-mail addresses: bakht-flpo@yandex.ru

A great contribution to the development of the theory of multilayer plates and shells was made by E.I. Grigolyuk [3] and others. In [6], the main relations of the quadratic nonlinear theory of non-sloping multilayer anisotropic shells of an arbitrary form were presented.

In recent years, the needs of engineering have led to the fact that the bearing layers began to be made in different thicknesses. This greatly expands the scope of the use of three-layer structures.

Three-layer structures are effectively used in the aircraft industry and other branches of engineering. Therefore, three-layer structures have entailed intensive research in the field of flutter theory.

A number of publications [7, 8] are devoted to the issue of calculating vibrations of elastic three-layer plates and shells with a structure that is asymmetric in thickness. In the studies by A.I. Smirnov [7, 8], the supersonic flutter of three-layer plates and cylindrical shells was considered in an elastic formulation.

A mathematical model to investigate the effect of external average flow on sound transmission loss through composite sandwich panels filled with porous materials was built [9]. The equations of motion for multilayer composite plates were constructed using first-order shear deformation theory. A study of the influence of the external average flow, the angle of incidence, and the lamination scheme on the coincidence frequency and sound absorption of multilayer composite structures was conducted.

In [10], the study of the influence of free vibration on the behavior of a multifunctional sandwich plate using an advanced and reliable method was performed. The basic equation for the analysis of free vibrations was obtained, in which Reddy's third-order shear deformation theory was used.

In this article, the authors study the nonlinear flutter of viscoelastic three-layer plates and shallow shells with an asymmetric in thickness structure, which are flown around by a supersonic gas flow.

2.Equations of motion

Let us consider a rectangular three-layer plate with sides *a* and *b*, streamlined from the outside by a supersonic gas flow at an unperturbed velocity *V*, directed along the *Ox*-axis. The aerodynamic pressure is taken into account according to the linear piston theory [11]. Let us assume that the plates are hinged on all four edges.

The equation of motion of a viscoelastic three-layer plate in a gas flow in the absence of shear forces takes the following form:

$$\begin{gathered} D(1-R^*)(1-\Theta h^2\beta_3^{-1}\nabla^2)\nabla^4\chi - N_x\frac{\partial^2}{\partial x^2}(1-h^2\beta_3^{-1}\nabla^2)\chi - \\ - N_y\frac{\partial^2}{\partial y^2}(1-h^2\beta_3^{-1}\nabla^2)\chi - \Omega\frac{\partial^2}{\partial t^2}(1-h^2\beta_3^{-1}\nabla^2)\chi - q = 0. \end{gathered} \tag{1}$$

Here $\chi(x,y,t)$ is the displacement function related to the deflection $w(x, y, t)$ by the following relation:

$$w = (1-h^2\beta_3^{-1}\nabla^2)\chi\,, \tag{2}$$

where $\nabla^2=\partial^2/\partial x^2+\partial^2/\partial y^2$.

Values of D, Θ, β_3, Ω characterize the cylindrical stiffness of the three-layer package, the bending stiffness of the bearing layers, the shear stiffness of the filler, and the specific mass of the three-layer package, respectively; h is the package thickness; N_x, N_y are the external compressive (tensile) forces in the longitudinal and transverse directions; $q(x,y,t)$ is an aerodynamic load.

3.Numerical results

An approximate solution to equation (41) is sought in the following form:

$$\chi(x,y,t)=\sum_{n=1}^{N}\sum_{m=1}^{M}\chi_{nm}(t)\,\varphi_{nm}(x,y), \tag{3}$$

where functions $\varphi_{nm}(x,y)$ are chosen so that each term of the sum (3) satisfies the boundary conditions at the edges of the plate, and $\chi_{nm}(t)$ are some functions to be determined. Substituting (3) into equation (1) and applying the Bubnov-Galerkin method to this equation, we obtain a system of integrodifferential equations with respect to the coefficients (3). By introducing the following dimensionless parameters

$$\frac{x}{a},\quad \frac{y}{b},\quad \frac{\chi}{h},$$

and keeping the previous notation, we obtain

$$A_{kl}\,\ddot{\chi}_{kl}+B_{kl}\,\dot{\chi}_{kl}+\left[\left(1-R^{*}\right)C_{kl}+E_{kl}\right]\chi_{kl}-V_{*}\sum_{n=1}^{N}F_{k\ln m}\chi_{nl}=0\,. \tag{4}$$

Here A_{kl}, B_{kl}, C_{kl}, E_{kl}, F_{klnm}, , $V_*= \aleph p_\infty a^3 M^*/D$ are dimensionless parameters.

The calculation results are presented in Tables 1, 2.

4. Discussion of results

From Table 1 it can be seen that an increase in the viscosity coefficient A leads to a decrease in the critical flutter velocity $V_{*кр}$ by 59% [12-16]. For A=0 and A=0.1, the flutter velocity is 36 and 14.65, respectively. As seen from the table, the result obtained for the elastic plate (A=0) exactly coincides with the results given in [17].

The effect of external compressive (tensile) forces in the longitudinal and transverse directions was studied. Table 1 shows that an increase in compressive forces n_x ($n_x = N_x a^2/D$) in the direction of the flow velocity leads to a decrease in the critical flutter velocity. On the contrary, tensile forces n_x lead to the same proportional increase in the critical flutter velocity.

When the forces n_y ($n_y = N_y a^2/D$) change in the direction normal to the velocity of the flow V oncoming on the plates, the flutter velocity changes little.

An increase in parameter k_1 ($k_1 = h^2\beta_3^{-1}/a^2$) leads to a significant change in V_{*cr}. The studies were conducted for k_1=0.1; 0.2; 0.5 and 1.5. It can be seen that with a decrease in the shear stiffness of the filler (an increase in coefficient κ_1) the critical flutter velocity of the three-layer plate decreases.

With an increase in the plate elongation λ ($\lambda=a/b$), the plate length in the flow direction increases and the elongated edges of the plate approach each other. The latter contributes to an increase in the relative rigidity of the system and an increase in the critical flutter velocity, which is observed from the table 2.

The influence of parameter ε (aerodynamic damping) was also studied. With an increase in coefficient ε, an increase in the dimensionless critical flutter velocity was observed.

Table 1

Critical values of flutter velocity depending on on the viscoelastic properties of the material

A	α	β	$-n_x$	$-n_y$	k_1	λ	Θ	ε	V_{*cr}
0									**36**
0.001	0.25	0.05	0.75	0.45	1	1	0.05	0.1	**34.2**
0.01									**19.45**
0.1									**14.65**
	0.1								**18.17**
0.01	0.5	0.05	0.75	0.45	1	1	0.05	0.1	**20**
	0.7								**21**
		0.01							**19.5**
0.01	0.25	0.08	0.75	0.45	1	1	0.05	0.1	**19.43**
		0.1							**19.42**

Table 2

Critical values of flutter velocity depending on the physical-mechanical and geometric nature of the plate

A	α	β	$-n_x$	$-n_y$	k_1	λ	Θ	ε	V_{*cr}
			3						**6.38**
			1.5						**15.1**
0.01	0.25	0.05	1	0,45	1	1	0.05	0.1	**17.93**
			0						**23.77**
			-0.5						**26.5**
			-1						**29.6**
			0.75	2.75					**17.15**
				0.5					**19.4**
0.01	0.25	0.05		0	1	1	0.05	0.1	**19.9**
				-0.5					**20.35**
				-1.5					**21.3**

				-4					**23.7**
					0.1				**70.5**
0.01	0.25	0.05	0.75	0.45	0.2	1	0.05	0.1	**45.5**
					0.5				**26.4**
					1.5				**16.99**
						1.2			**17.67**
0.1	0.25	0.05	0.75	0.45	1	1.5	0.05	0.1	**23.5**
						2			**36.82**
							0.03		**12.83**
0.01	0.25	0.05	0.75	0.45	1	1	0.07	0.1	**25.7**
								0	**19.4**
0.01	0.25	0.05	0.75	0.45	1	1	0.05	0.5	**19.6**
								5	**21.82**

5. Conclusions

1. Mathematical models of flutter problems for viscoelastic three-layer plates with a structure asymmetric in thickness, flown around by a supersonic gas flow, were constructed and developed.

2. A computational algorithm was developed based on the elimination of singularities of integrodifferential equations with singular kernels, followed by the use of quadrature formulas, for solving practically important linear and nonlinear problems of the hereditary theory of viscoelasticity.

3. When modeling flutter problems for viscoelastic three-layer plates, a number of new effects were obtained:

- it was determined that an account for the viscoelastic properties of the material of the three-layer elements of the aircraft leads to a decrease in the critical flutter velocity by 30 - 60%;
- it was found that an increase in compressive forces in the direction of the flow velocity leads to a decrease in the critical flutter velocity of three-layer plates. On the contrary, tensile forces lead to the same proportional increase in the critical flutter velocity;
- it was shown that an increase in the geometric parameter characterizing the flexural rigidity of the bearing layers of three-layer structures leads to an increase in the flutter velocity by 25–40%;
- it was determined that a decrease in the shear stiffness of the filler leads to a decrease in the flutter velocity.

References

[1] E.I. Grigolyuk, Finite deflections of three-layer shells with rigid filler, News of the AS USSR, OTN 1 (1958) 26–34.

[2] E.I. Grigolyuk, P.P. Chulkov, On the general theory of three-layer shells with a large deflection, Reports of the AS USSR, 150(5) (1963) 1012–1014.

[3] E.I. Grigolyuk, P.P. Chulkov, Stability and vibrations of three-layer shells. Moscow, "Engineering", 1973.
[4] V.A. Ivanov, V.N. Paimushin, Refined statement of dynamic problems of three-layer shells with transversally rigid filler and numerical-analytical method for their solution, Applied Mechanics and Technical Physics 36(4) (1995) 137-151.
[5] V.P. Paimushin, Theory of Stability of Three-Layer Plates and Shells (Stages of Development, State of the Art and Directions for Further Research), Proceedings of the Russian Academy of Sciences. Mechanics of a rigid body, 2 (1998) 148–162.
[6] E.I. Grigolyuk, V.I. Mamai, Nonlinear deformation of thin-walled structures, Moscow, Nauka. Fizmatlit, 1997.
[7] A.I. Smirnov, Dynamic stability and vibrations of three-layer panels in a supersonic gas flow, Reports of AS USSR, 180 (5) (1968) 1060–1063.
[8] A.I. Smirnov, Natural oscillations and flutter of three-layer cylindrical shells in a supersonic gas flow, Reports of AS USSR, 186(3) (1969) 533–536.
[9] Rasool Moradi-Dastjerdi, Kamran Behdinan, Free vibration response of smart sandwich plates with porous CNT-reinforced and piezoelectric layers, Applied Mathematical Modelling 96 (2021) 66-79. https://doi.org/10.1016/j.apm.2021.03.013.
[10] E.I. Grigolyuk, P.P. Chulkov, Critical loads of three-layer cylindrical and conical shells. Novosibirsk, Western-Siberian publishing house, 1966.
[11] A.A. Ilyushin, The law of plane sections in aerodynamics of high supersonic speeds, Applied Mathematics and Mechanics, XX (6) (1956) 733–755.
[12] B.A. Khudayarov, F.Z. Turaev, Nonlinear supersonic flutter for the viscoelastic orthotropic cylindrical shells in supersonic flow. Aerospace Science and Technology 84 (2019) 120-130.
[13] B.A. Khudayarov, F.Z. Turaev, Nonlinear vibrations of fluid transporting pipelines on a viscoelastic foundation. Magazine of Civil Engineering 86(2) (2019) 30-45.
[14] B.A. Khudayarov, Modeling of supersonic nonlinear flutter of plates on a viscoelastic foundation. Advances in Aircraft and Spacecraft Science 6(3) (2019) 257-272.
[15] B.A. Khudayarov, F.Z. Turaev, Mathematical Simulation of Nonlinear Oscillations of Viscoelastic Pipelines Conveying Fluid. Applied Mathematical Modelling 66 (2019) 662-679.
[16] B.A. Khudayarov, Kh.M. Komilova, Vibration and dynamic stability of composite pipelines conveying a two-phase fluid flows. Engineering Failure Analysis 104 (2019) 500-512.
[17] A.I. Smirnov, Supersonic flutter of three-layer plates, Reports of the Academy of Sciences of the USSR, 183(3) (1968) 540–543.

Journal of Mathematical Models and Methods in Engineering 1 (2026)

Journal of Mathematical Models and Methods in Engineering

journal homepage: https://jmmme.uz/index.php/journal

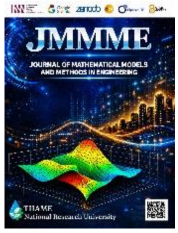

Reduction formulas for hypergeometric functions and their application to the comparison of problems solutions for the Laplace equation and singular elliptic equations

M.O.Abbasova[1], T.G.Ergashev[2*], A.R. Ryskan[3]

[1] Namangan State University, Namangan, 160107, Uzbekistan
[2] "Tashkent institute of irrigation and agricultural mechanization engineers" National Research University, Tashkent, 100000, Uzbekistan
[3]University of California, 1 Shields Ave, Davis, CA 95616, USA

ARTICLE INFO

Keywords:
hypergeometric functions Gauss,
Appell and Lauricella,
reduction formulas,
Dirichlet problem,
Neumann problem,
Laplace equation,
elliptic equation with singular coefficients.

ABSTRACT

The main goal of this work is to prove a number of reduction formulas for the first Lauricella function, i.e. to determine the set of those numerical parameters for which the hypergeometric function is expressed in elementary functions. Currently, tables of partial values for Appell functions of two variables are known; however, these formulas are insufficient for applications, and therefore, it is necessary to establish more general relations for hypergeometric functions whose number of variables exceeds 2. In the first part of the work, we will prove new reduction formulas for the Lauricella function of three or more variables, generalizing previously known results. The second part of the paper is devoted to applying the obtained reduction formulas to the study of the properties of solutions to the Dirichlet and Neumann problems for the Laplace equation and a singular elliptic equation. The main result of this study is that, using reduction formulas for hypergeometric functions, it is proven that the solutions to the Dirichlet and Neumann problems for elliptic equations with vanishing singular coefficients coincide with the solutions to similar problems for the Laplace equation.

1. Introduction

It is well known [1,2] that the solution of a wide variety of problems related to heat conduction and dynamics, electromagnetic oscillations and aerodynamics, quantum mechanics, and potential theory leads to special functions. They most often arise when solving partial differential equations using separation of variables or the Green's function method. The diversity of problems leading to special functions has led to a rapid increase in the number of functions used in applications.

The great success of the theory of hypergeometric series in one variable has stimulated the development of a corresponding theory in two and more variables. Appell [3] has defined, in 1880, four double series F_1 to F_4, which are all analogous to Gauss' $F(a,b;c;z)$. Following the Appell's work, Lauricella [4] has defined, in 1893, four hypergeometric series $F_A^{(n)}$, $F_B^{(n)}$, $F_C^{(n)}$

* Corresponding author. **T.G.Ergashev**
E-mail addresses: ergashev.tukhtasin@gmail.com

and $F_D^{(n)}$, which are natural generalizations of the classical Gauss hypergeometric function F and the Appell functions $F_1 - F_4$ to the case in n complex variables and the corresponding complex parameters.

The Appell and Lauricella hypergeometric functions play an important role in mathematical physics. In particular, solutions to a number of boundary value problems for singular elliptic equations are given in terms of the Appell hypergeometric function F_2 [5,6] and the Lauricella hypergeometric function $F_A^{(n)}$ [7,8,9,10]. Under exceptional circumstances, multiple hypergeometric functions can be expressed in terms of simpler functions, notably in terms of hypergeometric functions of one variable or, in general, with fewer variables or in terms of elementary functions. In such cases we speak of *reducible* hypergeometric functions and of *reduction formulas*. Certain trivial reduction formulas are obvious: for example, if one of the two variables is zero in any of the double series, the hypergeometric series in two variables can be expressed in terms of series in one variable: such trivial reductions are disregarded in the sequel.

The monographs [11, 12, 13] contain a systematic exposition of summation, reduction, and transformation formulas, as well as various other developments, covering not only each of the four Appell functions, but also several families of functions in two variables. Furthermore, the works [14] and [15] compiled an extensive tables of reduction formulas for the double Appell F_2 and triple Lauricella $F_A^{(3)}$ functions, respectively.

In this paper, for the first time, reduction formulas are established for the Lauricella hypergeometric function $F_A^{(n)}$ in n variables and the results obtained are applied to the study of the properties of solutions of the Dirichlet and Neumann problems for the Laplace equation and the elliptic equation with singular coefficients in the infinite parts (half-space, quarter-space, half-quarter-space, in general, 1/2 -part of space) of m-dimensional Euclidean space.

2.Reduction formulas for Gauss and Appell functions at zero parameter values

The Gauss hypergeometric function is defined inside the circle $|z|<1$ as the sum of the hypergeometric series [12, p. 109, eq. 2.8(1)]

$$F(a,b;c;z) \equiv F\left(\begin{matrix} a,b; \\ c; \end{matrix} z\right) = \sum_{n=0}^{\infty} \frac{(a)_n (b)_n}{(c)_n} \frac{z^n}{n!}, \tag{1}$$

and for $|z|>1$, as its analytic continuation. Here $a,b\in\mathbb{C}$ и $c\in\mathbb{C}\setminus\mathbb{Z}_0^-$; $\mathbb{Z}_0^{-1}:=\{0,-1,-2,...\}$, and the expression $(\nu)_n$ denotes the Pochhammer symbol: $(\nu)_0:=1,\ (\nu)_n:=\nu(\nu+1)...(\nu+n-1)$, $\nu\in\mathbb{C}$, $n\in\mathbb{N}$, written through the gamma function $\Gamma(\nu)$ in the form $(\nu)_n=\Gamma(\nu+n)/\Gamma(\nu),\ n\in\{0\}\cup\mathbb{N};$ $\mathbb{N}$ is the set of natural numbers.

In general, an extensive table is known [16, Chapter 7, Section 7.3], in which the hypergeometric function for certain particular values of numerical parameters is written in terms of elementary functions, for example,

$$F\left(a+1,1;2;z\right) = \frac{1}{az}\left[(1-z)^{-a}-1\right], a\neq 0, \tag{2}$$

$$F\left(1,1;2;z\right) = -\frac{1}{z}\ln(1-z). \tag{3}$$

The Appell hypergeometric function F_2 has a form [12, p. 224, eq. 5.7(7)]

$$F_2\left(a,b,b';c,c';x,y\right)\equiv F_2\left(\begin{matrix}a,b,b';\\ c,c';\end{matrix}x,y\right)$$
$$=\sum_{m,n=0}^{\infty}\frac{(a)_{m+n}\left(b\right)_m\left(b'\right)_n}{\left(c\right)_m\left(c'\right)_n}\frac{x^m}{m!}\frac{y^n}{n!},|x|+|y|<1, \tag{4}$$

where $a,b,b'\in\mathbb{C}$ and $c,c'\in\mathbb{C}\setminus\mathbb{Z}_0^-$.

J.Murley and N.Saad [14] compiled an extensive tables of the Appell functions F_2. Let us list some of them that we need to continue our research:

$$F_2\left(\begin{matrix}a+2,1,1;\\ 2,2;\end{matrix}x,y\right)=\frac{1}{a(a+1)xy}\left[1-\frac{1}{(1-x)^a}-\frac{1}{(1-y)^a}+\frac{1}{(1-x-y)^a}\right],a\neq 0,-1, \tag{5}$$

$$F_2\left(2,1,1;2,2;x,y\right)=\frac{1}{xy}\ln\frac{(1-x)(1-y)}{1-x-y}\equiv\frac{1}{xy}\ln\left(1+\frac{xy}{1-x-y}\right). \tag{6}$$

However, the table [14] of Appell functions $F_2\left(a,b,1;c,2;x,y\right)$ cannot claim to be complete in this direction, because in applications of the Appell function F_2 it is necessary to calculate the values of this function, i.e. to express it in elementary functions, when some of its parameters, which are in the numerator and denominator, simultaneously tend to zero.

Hypergeometric functions can be expressed through elementary functions when the same number of parameters of the numerator and denominator are simultaneously equal to zero.

The following reduction formulas are valid:

$$\lim_{b\to 0}F\left(a,b;kb;x\right)=\frac{1}{k}\left[(1-x)^{-a}+k-1\right],\ k\neq 0. \tag{7}$$

$$\lim_{b\to 0}F\left(a+\lambda,b+\lambda;kb+\lambda;x\right)=(1-x)^{-a-\lambda},\ k\neq 0,\ \ \lambda\neq 0. \tag{8}$$

Reduction formulas (5) – (8) can be proved by comparing coefficients of equal powers of variables on both sides.

Theorem 1. *For* $|x|+|y|<1$, *the Appell function* F_2 *is given by*

$$F_2\left(a,b,b';kb,k'b';x,y\right)\Big|_{b=b'=0}$$
$$=\frac{1}{kk'}\left[(k-1)(k'-1)+\frac{k'-1}{(1-x)^a}+\frac{k-1}{(1-y)^a}+\frac{1}{(1-x-y)^a}\right],\ k\neq 0,k'\neq 0; \tag{9}$$

$$F_2\left(a+1,1,b;2,kb;x,y\right)\Big|_{b=0}$$
$$=-\frac{1}{akx}\left[k-1-\frac{k-1}{(1-x)^a}+\frac{1}{(1-y)^a}-\frac{1}{(1-x-y)^a}\right],\ a\neq 0,\ k\neq 0; \tag{10}$$

$$F_2\left(1,1,b;2,kb;x,y\right)\Big|_{b=0}=-\frac{1}{x}\ln(1-x)+\frac{1}{kx}\ln\left(1+\frac{xy}{1-x-y}\right). \tag{11}$$

Proof. The well-known Burchnall-Chaundy expansion [17]

$$F_2\left(\begin{matrix}a,b,b';\\ c,c';\end{matrix}x,y\right)=\sum_{n=0}^{\infty}\frac{(a)_n(b)_n(b')_n}{n!(c)(c')_n}x^ny^nF\left(\begin{matrix}a+n,b+n;\\ c+n;\end{matrix}x\right)F\left(\begin{matrix}a+n,b'+n;\\ c'+n;\end{matrix}y\right)$$

allows one to easily derive the reduction formula (9). Indeed,

$$
\begin{aligned}
&F_2\left(a,b,b';kb,k'b';x,y\right)=F(a,b;kb;x)F(a,b';k'b';y)\\
&+\frac{a}{k\cdot k'}xyF(a+1,b+1;kb+1;x)F(a+1,b'+1;k'b'+1;y)\\
&+\frac{a(a+1)(b+1)(b'+1)}{2k\cdot k'(kb+1)(k'b'+1)}x^2y^2F(a+2,b+2;kb+2;x)\times\\
&\times F(a+2,b'+2;k'b'+2;y)+.... \qquad (12)
\end{aligned}
$$

Next, passing to the limit in both parts of equality (12) as $b\to 0$ and $b'\to 0,$ by virtue of the formulas (7) and (8), after reducing similar ones, we obtain the reduction formula (9).

Applying the formula (7) to the expansion [16, p. 413, eq. 6.7.1(4)]

$$F_2\left(a,b,b';c,c';x,y\right)=\sum_{n=0}^{\infty}\frac{(a)_n(b')_n}{n!(c')_n}y^nF(a+n,b;c;x),\ \ |x|+|y|<1$$

for $b'=1,\ c'=2$, and passing to the limit as $b\to 0,$ we obtain the required formula (10).

Formula (11) follows directly from the reduction formula (3). Theorem 1 is completely proven.

3.Reduction formulas for the multiple Lauricella function $F_A^{(n)}$

We introduce a following notation:

$$\mathbf{b}:=\left(b_1,...,b_n\right),\ \mathbf{c}:=\left(c_1,...,c_n\right),\ \mathbf{x}:=\left(x_1,...,x_n\right);\ |\mathbf{k}|:=k_1+...+k_n,\ k_1\ge 0,...,k_n\ge 0.$$

The Lauricella hypergeometric function $F_A^{(n)}$ in $n\in N$ (real or complex) variables is defined as [4] (see also [11, p.114])

$$
\begin{aligned}
F_A^{(n)}\left(a,\mathbf{b};\mathbf{c};\mathbf{x}\right)&\equiv F_A^{(n)}\left(\begin{matrix}a,b_1,...,b_n;\\ c_1,...,c_n;\end{matrix}x_1,...,x_n\right)\\
&=\sum_{|\mathbf{k}|=0}^{\infty}(a)_{|\mathbf{k}|}\prod_{j=1}^{n}\left[\frac{(b_j)_{k_j}}{(c_j)_{k_j}}\frac{x_j^{k_j}}{k_j!}\right],\ \ \sum_{j=1}^{n}|x_j|<1, \qquad (13)
\end{aligned}
$$

where $a,b_1,...,b_n\in\mathbb{C},\ c_1,...,c_n\in\mathbb{C}\setminus\mathbb{Z}_0^-$.

Clearly, in definition (13) we have $F_A^{(1)}\equiv F$ and $F_A^{(2)}\equiv F_2,$ where F and F_2 are Gauss and Appell series defined in (1) and (4), respectively.

Using the properties of the Pochhammer symbol, the Lauricella function $F_A^{(n)}$ can be expanded into hypergeometric functions with fewer variables:

$$F_A^{(n)}\left(a,\mathbf{b};\mathbf{c};\mathbf{x}\right)=\sum_{m_n=0}^{\infty}\frac{(a)_{m_n}\left(b_n\right)_{m_n}}{\left(c_n\right)_{m_n}}\frac{x_n^{m_n}}{m_n!}F_A^{(n-1)}\left(a+m_n,\mathbf{b}';\mathbf{c}';\mathbf{x}'\right) \qquad (14)$$

$$=\sum_{|\mathbf{m}'|=0}^{\infty}(a)_{|\mathbf{m}'|}\prod_{j=1}^{n-1}\left[\frac{(b_j)_{m_j}}{(c_j)_{m_j}}\frac{x_j^{m_j}}{m_j!}\right]F\left(a+|\mathbf{m}'|,b_n;c_n;x_n\right), \qquad (15)$$

where $\mathbf{b}':=\left(b_1,...,b_{n-1}\right),\ \ \mathbf{c}':=\left(c_1,...,c_{n-1}\right),\ \ \mathbf{x}':=\left(x_1,...,x_{n-1}\right),\ |\mathbf{m}'|:=m_1+...+m_{n-1}$

.

Theorem 2. *For* $\sum_{j=1}^{n}|x_j|+|y|<1,$ *the function* $F_A^{(n+1)}$ *in* $n+1$ *variables is given by*

$$F_A^{(n+1)}\left(\begin{matrix} a+1,\mathbf{b},1; \\ \mathbf{c},2; \end{matrix} \mathbf{x},y\right) = -\frac{1}{ay} F_A^{(n)}\left(\begin{matrix} a,\mathbf{b}; \\ \mathbf{c}; \end{matrix} \mathbf{x}\right) + \frac{1}{ay(1-y)^a} F_A^{(n)}\left(\begin{matrix} a,\mathbf{b}; \\ \mathbf{c}; \end{matrix} \frac{\mathbf{x}}{1-y}\right), \tag{16}$$

where $a \neq 0$; $b_1,...,b_n \in \mathbb{C}$, $c_1,...,c_n \in \mathbb{C}\setminus\mathbb{Z}_0^-$.

Proof. Using expansions (14) and (15), the Lauricella function $F_A^{(n+1)}$ in $n+1$ variables can be easily represented in the form

$$F_A^{(n+1)}\left(\begin{matrix} a+1,\mathbf{b},1; \\ \mathbf{c},2; \end{matrix} \mathbf{x},y\right) = \sum_{|\mathbf{k}|=0}^{\infty} (a+1)_{|\mathbf{k}|} \prod_{j=1}^{n} \left[\frac{(b_j)_{k_j}}{(c_j)_{k_j}} \frac{x_j^{k_j}}{k_j!}\right] F\left(a+1+|\mathbf{k}|,1;2;y\right). \tag{17}$$

Applying the well-known reduction formula

$$F\left(a+1,1;2;z\right) = \frac{1}{az}\left[(1-z)^{-a}-1\right], a \neq 0,$$

to the right-hand side of (17), we obtain

$$F_A^{(n+1)}\left(\begin{matrix} a+1,\mathbf{b},1; \\ \mathbf{c},2; \end{matrix} \mathbf{x},y\right) = \frac{1}{y} \sum_{|\mathbf{k}|=0}^{\infty} \frac{(a+1)_{|k|}}{a+|\mathbf{k}|} \prod_{j=1}^{n} \left[\frac{(b_j)_{k_j}}{(c_j)_{k_j}} \frac{x_j^{k_j}}{k_j!}\right] \left[(1-y)^{-a-|k|}-1\right].$$

The last equality directly implies equality (16). Theorem 2 is proved.

Corollary 1. *If* $a \neq 0,-1,...,-(n-1)$; $b \in \mathbb{C}$, $c \in \mathbb{C}\setminus\mathbb{Z}_0^-$, *then the following reduction formulas*

$$F_A^{(n+1)}\left(\begin{matrix} a+n,\underbrace{1,...,1}_{n},b; \\ \underbrace{2,...,2}_{n},c; \end{matrix} \mathbf{x},y\right) = \frac{(-1)^n}{(a)_n \Pi\left(x_n\right)} \sum_{I_s \subseteq \{1,...,n\}} \frac{(-1)^{|I_n|}}{\left(1-X_{I_n}\right)^a} F\left(a,b;c;\frac{y}{1-X_{I_s}}\right), \tag{18}$$

$$F_A^{(n)}\left(a+s,\underbrace{1,...,1}_{s}, b_{s+1},...,b_n;\underbrace{2,...,2}_{s}, c_{s+1},...,c_n;x_1,...,x_n\right) = \frac{(-1)^s}{(a)_s \Pi\left(x_s\right)} \times$$

$$\times \sum_{I_s \subseteq \{1,...,s\}} \frac{(-1)^{|I_s|}}{\left(1-X_{I_s}\right)^a} F_A^{(n-s)}\left(a,b_{s+1},...,b_n;c_{s+1},...,c_n;\frac{x_{s+1}}{1-X_{I_s}},...,\frac{x_n}{1-X_{I_s}}\right) \tag{19}$$

are valid.

Here and below, I_n denotes any subset of the set of first n natural numbers $\{1,2,...,n\}$, i.e., the right-hand sides of the reduction formulas (18) and (19) consist of 2^n and 2^s pieces of terms, respectively; $X_{I_n} = \sum_{i \in I_n} x_i$, $X_{\varnothing} = 0$; $|I_n|$ is an element's number of set I_n, $|\varnothing| = 0$; $\Pi\left(x_k\right)$ is a product of the first k variables of the Lauricella function $\left(1 \leq k \leq n\right)$.

Examples.

$$F_A^{(n)}\left(a+n,\underbrace{1,...,1}_{n};\underbrace{2,...,2}_{n};\mathbf{x}\right) = \frac{(-1)^n}{(a)_n \Pi\left(x_n\right)} \sum_{I_n \subseteq \{1,...,n\}} \frac{(-1)^{|I_n|}}{\left(1-X_{I_n}\right)^a}, \tag{20}$$

$$F_A^{(n)}\left(n,\underbrace{1,...,1}_{n};\underbrace{2,...,2}_{n};\mathbf{x}\right) = \frac{(-1)^n}{(n-1)!\Pi\left(x_n\right)} \sum_{I_n \subseteq \{1,...,n\}} (-1)^{|I_n|} \ln \frac{1}{1-X_{I_n}}. \tag{21}$$

It should be noted that formulas (20) and (21) are natural generalizations of the reduction formulas (2), (5) and (3), (6), respectively.

Theorem 3. *For* $\sum_{j=1}^{n} |x_j| < 1,$ *and* $k_1 \neq 0$ *,...,* $k_n \neq 0,$ *the function* $F_A^{(n)}$ *is given by*

$$F_A^{(n)}\left(\begin{matrix} a,b_1,...,b_n; \\ k_1b_1,...,k_nb_n; \end{matrix} x_1,...,x_n\right)\Bigg|_{\mathbf{b}=0} = \frac{1}{k_1k_2...k_n}\sum_{I_n}\frac{1}{\left(1-X_{I_n}\right)^a}. \tag{22}$$

Proof. We prove the reduction formula (22) by mathematical induction. Formula (22) is true for $n=1$ and $n=2$ (see eq. (7) and (9), respectively).

Let us assume that formula (22) is valid for any natural number n. We will prove that it is also true for $n \sim n+1$. We write the expansion (14) in the form

$$F_A^{(n+1)}\left(\begin{matrix} a,b_1,...,b_n,b_{n+1}; \\ k_1b_1,...,k_nb_n,k_{n+1}b_{n+1}; \end{matrix} x, x_{n+1}\right)$$
$$= \sum_{s=0}^{\infty}\frac{(a)_s\left(b_{n+1}\right)_s}{\left(k_{n+1}b_{n+1}\right)_s}\frac{x_{n+1}^s}{s!}F_A^{(n)}\left(\begin{matrix} a+s,b_1,...,b_n; \\ k_1b_1,...,k_nb_n; \end{matrix} x\right)$$
$$= F_A^{(n)}\left(\begin{matrix} a,b_1,...,b_n; \\ k_1b_1,...,k_nb_n; \end{matrix} x\right) + \frac{1}{k_{n+1}}\sum_{s=1}^{\infty}\frac{(a)_s\left(1+b_{n+1}\right)_{s-1}}{\left(1+k_{n+1}b_{n+1}\right)_{s-1}}\frac{x_{n+1}^s}{s!}F_A^{(n)}\left(\begin{matrix} a+s,b_1,...,b_n; \\ k_1b_1,...,k_nb_n; \end{matrix} x\right).$$

Passing to the limit in the last expression as $\mathbf{b} \to 0$ and $b_{n+1} \to 0$, by virtue of (22), we obtain

$$F_A^{(n+1)}\left(\begin{matrix} a,b_1,...,b_n,b_{n+1}; \\ k_1b_1,...,k_nb_n,k_{n+1}b_{n+1}; \end{matrix} x, x_{n+1}\right)\Bigg|_{\mathbf{b}=0,b_{n+1}=0}$$
$$= \frac{1}{k_1k_2...k_n}\sum_{I_n\subseteq\{1,...,n\}}\frac{1}{\left(1-X_{I_n}\right)^a}\left[k_{n+1}+\sum_{s=1}^{\infty}\frac{(a)_s}{s!}\left(\frac{x_{n+1}}{1-X_{I_n}}\right)^s\right].$$

Now, taking into account the easily verified equality

$$\sum_{s=1}^{\infty}\frac{(a)_s}{s!}\left(\frac{x_{n+1}}{1-X_I}\right)^s = \frac{\left(1-X_{I_n}\right)^a}{\left(1-X_{I_n}-x_{n+1}\right)^a}-1,$$

after several transformations, we have

$$F_A^{(n+1)}\left(\begin{matrix} a,b_1,...,b_n,b_{n+1}; \\ k_1b_1,...,k_nb_n,k_{n+1}b_{n+1}; \end{matrix} x, x_{n+1}\right)\Bigg|_{b=0,b_{n+1}=0} = \frac{1}{k_1k_2...k_nk_{n+1}}\sum_{I_{n+1}\subseteq\{1,...,n+1\}}\frac{1}{\left(1-X_{I_{n+1}}\right)^a},$$

which is what was required to be proved. Theorem 3 is proven.

Theorem 4. *Let* s *be a natural number* $(1 \le s \le n)$ *and* n *be the number of variables of the Lauricella function* $F_A^{(n)}$. *For* $\sum_{j=1}^{n} |x_j| < 1,$ *and* $k_{s+1} \neq 0$ *,...,* $k_n \neq 0,$ *the function* $F_A^{(n)}$ *is given by*

$$F_A^{(n)}\left(a+s,\underbrace{1,...,1}_{s},b_{s+1},...,b_n;\underbrace{2,...,2}_{s},k_{s+1}b_{s+1},...,k_nb_n;x_1,...,x_n\right)\Bigg|_{\substack{b_{s+1}=0\\ ...\\ b_n=0}}$$

$$=\frac{(-1)^s}{(a)_s\Pi\left(x_s\right)k_{s+1}...k_n}\sum_{I_s\subseteq\{1,...,s\}}(-1)^{|I|}\sum_{J_n\subseteq\{s+1,...,n\}}\frac{1}{\left(1-X_{I_s}-X_{J_n}\right)^a}. \qquad (23)$$

Proof. Reduction formula (23) is proved by mathematical induction, similar to the proof of the reduction formula (22).

4.Applications of the obtained results

Let $\Re_m$ be m-multidimensional Euclidean space ($m\geq 2$), $x:=\left(x_1,...,x_m\right)$ be an arbitrary point in it, n be a natural number, where $n\leq m.$ We define the 2^n th part of the Euclidean space $\Re_m$ as follows:

$$\Omega\equiv\Omega_m^{n+}=\left\{x\in\Re_m:x_i>0,\ i=1,...,n;-\infty<x_j<+\infty,\ j=n+1,...,m\right\}.$$

We consider the Laplace equation

$$\Delta u\equiv\sum_{i=1}^m\frac{\partial^2u}{\partial x_i^2}=0 \qquad (24)$$

and generalized singular elliptic equation

$$L_\alpha^{(m,n)}(u)\equiv\sum_{i=1}^m\frac{\partial^2u}{\partial x_i^2}+\sum_{j=1}^n\frac{2\alpha_j}{x_j}\frac{\partial u}{\partial x_j}=0 \qquad (25)$$

in $\Omega,$ where $\alpha:=\left(\alpha_1,...,\alpha_n\right)$ is a vector and α_j are real numbers: $0<2\alpha_j<1,\ j=1,...,n.$

In the case $m=2$ the detailed bibliography and exposition of studies of basic boundary value problems for equations (14) and (25) can be found un the monographs [18] – [20].

In this paper we set $m>2.$

We denote:

$$S_k=\left\{\begin{matrix}x:x_i>0,\ ...,x_{k-1}>0,\ x_k=0,x_{k+1}>0,...,x_n>0;\\ -\infty<x_j<+\infty,\ j=n+1,...,m\end{matrix}\right\};$$

$$\tilde{x}_k:=\left(x_1,...,x_{k-1},x_{k+1},...,x_n,...,x_m\right)\in S_k\subset\Re_{m-1};\quad \rho_k:=\sqrt{\textstyle\sum_{i=1,i\neq k}^m x_k^2};$$

$$\xi:=\left(\xi_1,...,\xi_m\right)\in\Re_m;\ \ \tilde{\xi}_k:=\left(\xi_1,...,\xi_{k-1},\xi_{k+1},...,\xi_n,...,\xi_m\right)\in S_k\subset\Re_{m-1};$$

$$r=\sqrt{\sum_{j=1}^m\left(x_j-\xi_j\right)^2};\ \ r_{I_n}=\sqrt{\sum_{j\in I_n}\left(x_j+\xi_j\right)^2+\sum_{j\in\{1,...,m\}\setminus I_n}\left(x_j-\xi_j\right)^2};\ r_\varnothing\equiv r.$$

Dirichlet problem $D_{m,n}^{\infty}$. Find a solution $u\left(x\right)\in C\left(\overline{\Omega}\right)\cap C^2(\Omega)$ to the Laplace equation (to the singular equation (25)), satisfying the conditions

$$u(x)\Big|_{x_k=0}=\tau_k(\tilde{x}_k),\quad \tilde{x}_k\in\overline{S}_k,\quad k=\overline{1,n},\quad \lim_{R\to\infty}u(x)=0,$$

where $\tau_k\left(\tilde{x}_k\right)$ are given functions such that $\tau_k\left(\tilde{x}_k\right)=O\left(\theta_k^{-\varepsilon}\right),\ \theta_k\to\infty,\ \varepsilon>0,k=\overline{1,n}.$

In addition, the functions $\tau_k\left(\tilde{x}_k\right)$ satisfy the concordance conditions

$$\tau_k(\mathbf{0}) = \tau_j(\mathbf{0}),\ \tau_k(\tilde{x}_k)\Big|_{x_j=0} = \tau_j(\tilde{x}_j)\Big|_{x_k=0},\ \ k \neq j,\ k,j=\overline{1,n},\ \mathbf{0} := (0,...,0) \in \Re_{m-1}.$$

The solution $u_0^{(n)}(x)$ of the Dirichlet problem $D_{m,n}^{\infty}$ for the Laplace equation (24) in Ω has a form [21]

$$u_0^{(n)}(x) = \frac{\Gamma(m/2)}{\pi^{m/2}} \sum_{k=1}^{n} x_k \underbrace{\int_0^\infty ... \int_0^\infty}_{n-1} \underbrace{\int_{-\infty}^\infty ... \int_\infty^\infty}_{m-n} \tau_k(\tilde{\xi}_k) \sum_{I_{n\setminus k}} \frac{(-1)^{|I_{n\setminus k}|}}{r_{I_{n\setminus k}}^m} d\tilde{\xi}_k, \tag{26}$$

and the solution $u_\alpha^{(n)}(x)$ of the Dirichlet problem $D_{m,n}^{\infty}$ for the singular elliptic equation (25) in Ω is also known [8]:

$$u_\alpha^{(n)}(x) = \sum_{k=1}^{n} \underbrace{\int_0^\infty ... \int_0^\infty}_{n-1} \underbrace{\int_{-\infty}^\infty ... \int_\infty^\infty}_{m-n} \tau_k(\tilde{\xi}_k) T_{\alpha,k}^{(n)}(x;\tilde{\xi}_k) d\tilde{\xi}_p, \tag{27}$$

where

$$T_{\alpha,k}^{(n)}(x,\tilde{\xi}_k) = (1-2\alpha_k)\gamma_n x^{(1-2\alpha)} \tilde{\xi}_k^{(1)} \times$$

$$\times R_k^{-2\beta_n} F_A^{(n-1)}\left(\begin{matrix} \beta_n, 1-\alpha_1,...,1-\alpha_{k-1},1-\alpha_{k+1},...,1-\alpha_n; \\ 2-2\alpha_1,...,2-2\alpha_{k-1},2-2\alpha_{k+1},...,2-2\alpha_n; \end{matrix} \tilde{\rho}_k\right),$$

$$\tilde{\rho}_k := (\rho_1,...,\rho_{k-1},\rho_{k+1},...,\rho_n),\quad \rho_j = -\frac{4x_j\xi_j}{R_k^2}, j \neq k, j = \overline{1,n},$$

$$\beta_n = \frac{m-2}{2} + n - \sum_{j=1}^{n} \alpha_j,\quad \gamma_n = 2^{2\beta_n - m} \frac{\Gamma(\beta_n)}{\pi^{m/2}} \prod_{j=1}^{n} \left[\frac{\Gamma(1-\alpha_j)}{\Gamma(2-2\alpha_j)}\right];$$

$$x^{(1-2\alpha)} = \prod_{j=1}^{n} \left[x_j^{1-2\alpha_j}\right],\quad \tilde{\xi}_k^{(1)} = \prod_{j=1, j\neq k}^{n} [\xi_k],\ 1 \le k \le n.$$

Theorem 5. *Let the functions* $u_0^{(n)}(x)$ *and* $u_\alpha^{(n)}(x)$*, defined by equalities (26) and (27), be solutions of the Dirichlet problems* $D_{m,n}^{\infty}$ *for the Laplace equation (24) and the singular elliptic equation (25), respectively. Then the limit relation*

$$\lim_{\alpha \to 0} u_\alpha^{(n)}(x) = u_0^{(n)}(x) \tag{28}$$

is valid.

Proof. To prove the validity of the limit relation (28), we use the reduction formula (20) for $a \sim m/2$ and $n \sim n-1$:

$$F_A^{(n-1)}\left(\begin{matrix} \frac{m}{2}+n-1, \underbrace{1,...,1}_{n-1}; \\ \underbrace{2,...,2}_{n-1}; \end{matrix} \tilde{\rho}_k\right) = \frac{(-1)^{n-1}}{(m/2)_{n-1}\Pi_{n-1}(\tilde{\rho}_k)} \sum_{I_n \subseteq \{1,...,n\}\setminus\{k\}} \frac{(-1)^{|I_n|}}{(1-X_{I_n})^{m/2}}. \tag{29}$$

Now, passing to the limit in $J_{\alpha,k}^{(n)}\left(x,\tilde{\xi}_k\right)$ as $\alpha\to 0$ and substituting (29) into $\lim\limits_{\alpha\to 0} u_\alpha^{(n)}(x)$, we obtain the solution (26) to the Dirichlet problem $D_{m,n}^{\infty}$ for the Laplace equation (24). Theorem 5 is proven.

Let $D_n=\bigcup\limits_{k=1}^{n} S_k$ be the union of all n lateral faces of Ω.

Neumann problem $N_{m,n}^{0,\infty}$. Find a solution $u(x)\in C\left(\overline{\Omega}\right)\cap C^1\left(\Omega\cup D_n\right)\cap C^2(\Omega)$ to the Laplace equation (24), satisfying the conditions

$$\left.\frac{\partial u}{\partial x_k}\right|_{x_k=0}=\nu_k(\tilde{x}_k),\ \ \tilde{x}_k\in S_k,\ \ k=\overline{1,n},\quad \lim_{R\to\infty}u(x)=0,$$

where $\nu_k\left(\tilde{x}_k\right)$ are given functions such that at the origin they can become infinite of integrable order, i.e. less than $m-1$, and $\nu_k\left(\tilde{x}_k\right)=O\left(\theta_k^{-\varepsilon-1}\right),\ \theta_k\to\infty,\ \varepsilon>0,\ k=\overline{1,n}.$

Neumann problem $N_{m,n}^{\alpha,\infty}$. Find a solution $u(x)\in C\left(\overline{\Omega}\right)\cap C^1\left(\Omega\cup D_n\right)\cap C^2(\Omega)$ to the singular elliptic equation (25), satisfying the conditions

$$\left.\left(x_k^{2\alpha_k}\frac{\partial u}{\partial x_k}\right)\right|_{x_k=0}=\nu_k(\tilde{x}_k),\ \ \tilde{x}_k\in S_k,\ \ k=\overline{1,n},\quad \lim_{R\to\infty}u(x)=0,$$

where $\nu_k\left(\tilde{x}_k\right)$ are given functions such that at the origin they can become infinite of integrable order, i.e. less than $m-1-2\alpha_k$, and $\nu_k\left(\tilde{x}_k\right)=O\left(\theta_k^{2\alpha_k-\varepsilon-1}\right),\ \theta_k\to\infty,\ \varepsilon>0,\ k=\overline{1,n}.$

The solution $\tilde{u}_0^{(n)}(x)$ of the Neumann problem $N_{m,n}^{0,\infty}$ for the Laplace equation (24) in Ω has a form [22]

$$\tilde{u}_0^{(n)}(x)=-\frac{1}{2\pi^{m/2}}\Gamma\left(\frac{m-2}{2}\right)\sum_{k=1}^{n}\underbrace{\int_0^\infty\!\!\cdots\!\int_0^\infty}_{n-1}\underbrace{\int_{-\infty}^\infty\!\!\cdots\!\int_{\infty}^\infty}_{m-n}\nu_k\left(\tilde{\xi}_k\right)\sum_{I_{n\backslash k}}\frac{1}{r_{I_{n\backslash k}}^{m-2}}d\tilde{\xi}_k, \tag{30}$$

and the solution $\tilde{u}_\alpha^{(n)}(x)$ of the Neumann problem $N_{m,n}^{\alpha,\infty}$ for the singular elliptic equation (25) in Ω is also known [9]:

$$\tilde{u}_\alpha^{(n)}(x)=-\sum_{k=1}^{n}\underbrace{\int_0^\infty\!\!\cdots\!\int_0^\infty}_{n-1}\underbrace{\int_{-\infty}^\infty\!\!\cdots\!\int_{-\infty}^\infty}_{m-n}\nu_k\left(\tilde{\xi}_k\right)N_{\alpha,k}^{(n)}\left(x;\tilde{\xi}_k\right)d\tilde{\xi}_k, \tag{31}$$

where $$N_{\alpha,k}^{(n)}\left(x,\tilde{\xi}_k\right)=\gamma_0 R_k^{-2\beta_0}F_A^{(n-1)}\left(\begin{matrix}\beta_0,\alpha_1,\ldots,\alpha_{k-1},\alpha_{k+1},\ldots,\alpha_n;\\ 2\alpha_1,\ldots,2\alpha_{k-1},2\alpha_{k+1},\ldots,2\alpha_n;\end{matrix}\tilde{\rho}_k\right),$$

$$\beta_0=\frac{m-2}{2}+\sum_{j=1}^{n}\alpha_j,\quad \gamma_0=2^{2\beta_0-m}\frac{\Gamma(\beta_0)}{\pi^{m/2}}\prod_{j=1}^{n}\left[\frac{\Gamma(\alpha_j)}{\Gamma(2\alpha_j)}\right].$$

Theorem 6. *Let the functions* $\tilde{u}_0^{(n)}\left(x\right)$ *and* $\tilde{u}_\alpha^{(n)}\left(x\right)$, *defined by equalities (30) and (31), be solutions of the Neumann problems* $N_{m,n}^{0,\infty}$ *and* $N_{m,n}^{\alpha,\infty}$ *for the Laplace equation (24) and the singular elliptic equation (25), respectively. Then the limit relation*

$$\lim_{\alpha\to 0}\tilde{u}_\alpha^{(n)}(x)=\tilde{u}_0^{(n)}(x) \tag{32}$$

is valid.

Proof. To prove the validity of the limit relation (32), we use the reduction formula (20) for $a\sim(m-2)/2$, $n\sim n-1$ and $k_1=...=k_n=2$:

$$F_A^{(n-1)}\left(\begin{matrix}\dfrac{m-2}{2},\alpha_1,...,\alpha_{k-1},\alpha_{k+1},...,\alpha_n; \\ 2\alpha_1,...,2\alpha_{k-1},2\alpha_{k+1},...,2\alpha_n;\end{matrix} x_1,...,x_{k-1},x_{k+1},...,x_n\right)\Bigg|_{\tilde{\alpha}_k=0}=\frac{1}{2^{n-1}}\sum_{I_{n\backslash k}}\frac{1}{\left(1-X_{I_{n\backslash k}}\right)^{(m-2)/2}},$$

where $\tilde{\alpha}_k:=\left(\alpha_1,...,\alpha_{k-1},\alpha_{k+1},...,\alpha_n\right).$

5. Conclusions

1. The well-known tables for the Appell hypergeometric function are supplemented with new reduction formulas at zero values of Appell function.
2. For the first time, reduction formulas for the Lauricella hypergeometric function in three or more variables were established
3. The proved reduction formulas for hypergeometric functions were applied to the comparison of solutions of the Dirichlet and Neumann problems for the Laplace equations and singular elliptic equations in infinite parts of Euclidean space.

References

[1] L.Bers, Mathematical aspects of subsonic and transonic gas dynamics. New York, Wiley, 1961.
[2] A.W.Niukkanen, Generalised hypergeometric series arising in physical and quantum chemical applications, Journal of Physics. A: Math. Gen., 16 (1983) 1813 – 1825. DOI:10.1088/0305-4470/16/9/007
[3] Appell P. Sur les séries hypergéométriques de deux variables, et sur des équations différentielles linéaires aux dérivées partielles. C.R. Acad. Sci., Paris, 90 (1880) 296 – 298.
[4] G.Lauricella, Sulle funzione ipergeometriche a più variabili, Rend.Circ. Mat. Palermo, 7 (1893) 111 – 158. DOI:10.1007/BF03012437
[5] E.T.Karimov, On a boundary problem with Neumann's condition for 3D singular elliptic equations, Applied Mathematics Letters, 23 (2010) 517 – 522. DOI: 10.1016/j.aml.2010.01.002
[6] E.T.Karimov, J.J.Nieto, The Dirichlet problem for a 3D elliptic equation with two singular coefficients, Computers and Mathematics with Applications, 62 (2011) 214 – 224. DOI: 10.1016/j.camwa.2011.04.068
[7] T.G.Ergashev, Generalized Holmgren problem for an elliptic equation with several singular coefficients, Differential Equations, 56(7) (2020) 842–856. DOI: 10.1134/S0012266120070046.
[8] T.G.Ergashev, Z.R.Tulakova, The Dirichlet problem for an elliptic equation with several singular coefficients in an infinite domain, Russian Mathematics, 65(7) (2021) 71–80. DOI: 10.3103/S1066369X21070082
[9] T.G.Ergashev, Z.R.Tulakova, The Neumann problem for a multidimensional elliptic equation with several singular coefficients in an infinite domain. Lobachevskii Journal of Mathematics, 43(1) (2022) 199 – 206. DOI: 10.1134/S19950802220401026

[10] A.S. Berdyshev, A.R.Ryskan. The Neumann and Dirichlet problems for one four-dimensional degenerate elliptic equation. Lobachevskii Journal of Mathematics, 41(6) (2020) 1051–1066. DOI: 10.1134/S1995080220060062
[11] P.Appell, J.Kampe de Feriet, Fonctions Hypergeometriques et Hyperspheriques; Polynomes d'Hermite. Paris: Gauthier – Villars, 1926.
[12] A.Erdelyi, W.Magnus, F.Oberhettinger, F.G.Tricomi, Higher transcendental functions. New York, Toronto, London, McGraw-Hill, 1953.
[13] H.M.Srivastava, P.W.Karlsson, Multiple Gaussian hypergeometric series. New York,Chichester,Brisbane and Toronto: Halsted Press, 1985.
[14] J.Murley, N.Saad, Tables of the Appell hypergeometric functions F_2, ArXiv:0809.5203v2 (2008)
[15] M.O.Abbasova, T.G.Ergashev, Tables of the Lauricella hypergeometric functions $F_A^{(3)}$, Vestnik KRAUNC. Fiz.-Mat. Nauki, 54(1) (2026) 9 – 32. DOI:10.26117/2079-6641-2026-54-1-9-32
[16] A.P.Prudnikov, Yu.A.Brychkov, O.I.Marichev. Integrals and Series. Vol. 3. More Special Functions. Amsterdam, Gordon and Breach Science Publishers, 1990.
[17] J.L.Burchnall, T.W.Chaundy, Expansions of Appell's double hypergeometric functions,The Quarterly J. of Mathematics, Oxford, 11 (1940) 249 – 270.
[18] R.Gilbert, Function Theoretic methods in partial differential equations. New York, London, Academic Press, 1969.
[19] A.V.Bitsadze, Some classes of partial differential equations. Moscow, Nauka, 1981.
[20] M.M.Smirnov, Degenerating elliptic and hyperbolic equations. Moscow, Nauka, 1966.
[21] M.O.Abbasova, T.G.Ergashev, Dirichlet problems for the Laplace equation in infinite domains of Euclidean space, Scientific Bulletin of Namangan State University, 1 (2026) 15 – 20.
[22] M.O.Abbasova, T.G.Ergashev, Neumann problems for Laplace in infinite parts of Euclidean space, Scientific Bulletin of the Bukhara State University, 1 (2026) 44 – 50.

Journal of Mathematical Models and Methods in Engineering

journal homepage: https://jmmme.uz/index.php/journal

A three-variable analogue of the Humbert function with applications to solving Dirichlet problem for a singular Helmholtz equation

Z.O.Arzikulov[1*], R.I.Parovik[2], R.T. Zunnunov[3]

[1] *Fergana State Technical University, Fergana, 150107, Uzbekistan*
[2] *Laboratory of Modeling Physical Processes, Institute of Cosmophysical Research and Radio Wave Propagation FEB RAS, Mirnaya Str., 7, Paratunka 684034, Russia*
[3] *Laboratory of Mathematical Modeling of Nonlinear System, V. I. Romanovskiy Institute of Mathematics, Uzbekistan Academy of Sciences, University Street 9, Tashkent 100174, Uzbekistan*

ARTICLE INFO

Keywords:
confluent hypergeometric function of three variables; system of partial differential equations; asymptotic formula; three-dimensional Helmholtz equation with three singular coefficients; Dirichlet problem in the first infinite octant

ABSTRACT

In this paper we introduce a new confluent hypergeometric function of three variables, list its elementary properties, and construct a system of partial differential equations that the new function satisfies. We study the behavior of the function and establish an asymptotic formula for a large values of arguments. The results obtained are applied to solving the Dirichlet problem for the three-dimensional Helmholtz equation with three singular coefficients in the first infinite octant. The uniqueness of the solution of the Dirichlet problem in an infinite domain is proved using the extremum principle for elliptic equations. Thanks to the established properties of the confluent hypergeometric function of three variables, the unique solution to the posed boundary value problem is written out in explicit form.

1. Introduction

In study of many applied problems involving thermal conductivity and dynamics, electromagnetic oscillation and aerodynamics, and quantum mechanics and potential theory arise a hypergeometric (higher and special or transcendent) functions [1, 2, 3] which are often referred to as special functions of mathematical physics.

The success of the theory of Gaussian hypergeometric function stimulated the development of the corresponding theory in two or more variables. Much credit for the further development of the theory of hypergeometric functions in two variables goes to Horn [4], who gave a more general definition and introduced the concept of the order of double hypergeometric series. He investigated the convergence of the double hypergeometric functions and established systems of partial differential equations that they satisfy. He divided hypergeometric functions into complete and confluent functions and compiled a list (Horn List) of the second order hypergeometric functions in two variables. There are essentially 34 (14 complete and 20 confluent) convergent functions of the second order.

* Corresponding author. **Z.O.Arzikulov**
E-mail addresses: zafarbekarzikulov1984@gmail.com

Lauricella [5, p. 114] first introduced 14 complete triple hypergeometric series (functions) of the second order and Saran [6] systematically studied of these ten hypergeometric functions in three variables which belong to the Lauricella's set. Other hypergeometric functions in three variables studied in the literature include, in addition to the three-variable analogues of the hypergeometric functions in many variables, the functions introduced by Dhawan [7], Samar [8], and Exton [9]. An expansion of the results on the triple hypergeometric series together with references to the original literature are to be found in the book by Srivastava and Karlsson [10], which is a normal work on the subject. This monograph also contains a full list of all relevant articles up to 1985. For instance, Srivastava and Karlsson [10] presented a table of 205 distinct complete Gaussian functions in three variables together with their sources, if known.

Despite many applications of confluent forms of hypergeometric functions of more than two variables, they have been relatively little studied. In the works of Jain [11] and Exton [12], some functions were studied that are confluent forms of the complete hypergeometric functions in three variables.

When the number of the variables exceeds two or three, some confluent forms of the multiple Lauricella functions are defined in [10, pp. 34 - 36] as an applications of which, the self-similar and fundamental solutions of the second order multidimensional systems of partial differential equations with singular coefficients are constructed in explicit forms (see [13]).

The plan of this paper is as follows. In Section 2 we briefly give some preliminary information, which will be used later. In Section 3 we define new confluent hypergeometric function in three variables, write the system of partial differential equations, which satisfies new confluent function, find behavior and asymptotic expansion formulas. Sections 4 and 5 are devoted to the applications of the confluent hypergeometric functions. In Section 4 we formalize the Dirichlet problem for the Helmholtz equation with the three singular coefficients in the first infinite octant and prove the uniqueness of the solution to the problem. In Section 5 we find the solution of the Dirichlet in explicit form.

2. Preliminaries

The Gaussian hypergeometric function of the complex varible z is defined inside the circle $|z|<1$ as the sum of the hypergeometric series [14] :

$$F(a,b;c;z)=\sum_{n=0}^{\infty}\frac{(a)_n(b)_n}{(c)_n}\frac{z^n}{n!}, c\neq 0,-1,-2,... \tag{1}$$

where a, b, c are arbitrary complex numbers which are called the parameters of the hypergeometric function; $(\lambda)_n=\Gamma(\lambda+n)/\Gamma(\lambda), n=0,1,2,...$; $\Gamma(z)$ is a famous Euler's gamma-function.

The following function

$${}_pF_q\left[\begin{matrix}\alpha_1,...,\alpha_p;\\ \beta_1,...,\beta_q;\end{matrix} z\right]=\sum_{n=0}^{\infty}\frac{(\alpha_1)_n\cdots(\alpha_p)_n}{(\beta_1)_n\cdots(\beta_q)_n}\frac{z^n}{n!}, \tag{2}$$

is known as the generalized Gaussian function [14], or simply, the generalized hypergeometric function. Here p and q are positive integers or zero (interpreting an empty product as 1), and we assume that the variable z, the numerator parameters $\alpha_1,...,\ \alpha_p$, and the denominator parameters $\beta_1,\ ...,\ \beta_q$ take on complex values, provided that $\beta_j\neq 0,-1,-2,...$; $j=1,...,q$.

The Bessel function is defined as a special case of the generalized hypergeometric function:

$$J_\alpha(z)=\frac{1}{\Gamma(\alpha+1)}\left(\frac{z}{2}\right)^{\alpha}{}_0F_1\left(\alpha+1;-\frac{z^2}{4}\right)=\sum_{m=0}^{\infty}\frac{(-1)^m}{m!\Gamma(m+\alpha+1)}\left(\frac{z}{2}\right)^{2m+\alpha}.$$

Appel has defined, in 1880, four hypergeometric functions, F_1 to F_4 which are all analogous to Gauss' $F(a,b;c;z)$. For instance [15],

$$F_3\left(a,a',b,b';c;x,y\right)=\sum_{m,n=0}^{\infty}\frac{(a)_m\left(a'\right)_n(b)_m\left(b'\right)_n}{(c)_{m+n}}\frac{x^m}{m!}\frac{y^n}{n!},\max\{|x|,|y|\}<1. \qquad (3)$$

One of the confluent forms of the Appell function (3) is a following Humbert function

$$\Xi_2\left(a,b;c;x,y\right)=\sum_{m,n=0}^{\infty}\frac{(a)_m(b)_m}{(c)_{m+n}}\frac{x^m}{m!}\frac{y^n}{n!},|x|<1. \qquad (4)$$

which satisfies system of partial differential equations

$$\begin{cases} x(1-x)u_{xx}+yu_{xy}+\left[c-\left(a+b+1\right)x\right]u_x-abu=0, \\ yu_{yy}+xu_{xy}+cu_y-u=0, \end{cases} \qquad (5)$$

where $u\equiv\Xi_2(a,b;c;x,y)$.

At first we clarify the behavior of $\Xi_2(a,b;c;x,y)$ as $x\to\infty$. It follows from (4) that the representation

$$\Xi_2\left(a,b;c;x,y\right)=\sum_{n=0}^{\infty}\frac{y^n}{(c)_n n!}F(a,b;c+n;x) \qquad (6)$$

is true. Substituting an expansion of the Gaussian hypergeometric function of the form [16, p. 183, Eq. (10.13)]

$$F(a,b;c;z)=O\left(z^{-b}\right)+O\left(z^{-b}\right),a-b\neq 0,\pm 1,\pm 2,...,z\to\infty$$

into (6) we obtain the following leading term of (6) as $x\to\infty$, $|\arg(-x)|<\pi$ [16, p. 809, Eq. (40.42)]:

$$\Xi_2\left(a,b;c;x,y\right)\sim\frac{\Gamma(c)\Gamma(b-a)}{\Gamma(b)\Gamma(c-a)}\,{}_0F_1(c-a;y)(-x)^{-a}$$

$$+\frac{\Gamma(c)\Gamma(a-b)}{\Gamma(a)\Gamma(c-b)}\,{}_0F_1(c-b;y)(-x)^{-b},a\neq b, \qquad (7)$$

where ${}_0F_1(a;y)$ is the generalized Gaussian function defined in (2).

Now we use the asymptotic expansion (see [17, p. 76])

$${}_0F_1(\nu;-y)=O\left[y^{(1-2\nu)/4}\cos\left(2\sqrt{y}+\frac{(1-2\nu)\pi}{4}\right)\right]\text{as } y\to\infty. \qquad (8)$$

Then from (7) we find that

$$\Xi_2\left(a,b;c;x,y\right)=O\left(x^{-a}y^{(1+2a-2c)/4}\right)+O\left(x^{-b}y^{(1+2b-2c)/4}\right),a\neq b,\ x,y\to\infty. \qquad (9)$$

The Humbert function $\Xi_2(a,b;c;x,y)$, a PDE-system (1.5), the behavior formula (7) and the asymptotic expansion (9) have important applications: in the work [18] an explicit solution of the Dirichlet problem for the equation

$$u_{xx}+u_{yy}+\frac{2\alpha}{x}u_x+\frac{2\beta}{y}u_y-\lambda^2u=0,0<2\alpha,2\beta<1,-\infty<\lambda<+\infty \qquad (10)$$

in the infinite first quadrant $(x,y): x\ge 0, y\ge 0$ is written out through a function (4), the satisfaction of which for the equation (10) is established thanks to the system (5), and the formulas (7) and (9) help to show the fulfillment of the conditions of the Dirichlet problem.

3. Confluent hypergeometric function $\Xi_{22}^{(3)}$ in three variables

This section is devoted to the study of the one confluent form of the triple Lauricella function $F_B^{(3)}$. The new function under consideration is analogous to Humbert's confluent hypergeometric function of two variables $\Xi_2(a,b;c;x,y)$ defined in (1.4), and this work is in some degree complementary to the investigation by Exton [12] on the triple confluent hypergeometric functions.

The Lauricella hypergeometric function $F_B^{(3)}$ is defined by the formula [5]

$$F_B^{(3)}\left(a,a',a'',b,b',b'';c;x,y,z\right)=\sum_{m,n,p=0}^{\infty}\frac{(a)_m\left(a'\right)_n\left(a''\right)_p(b)_m\left(b'\right)_n\left(b''\right)_p}{(c)_{m+n+p}}\frac{x^m}{m!}\frac{y^n}{n!}\frac{z^p}{p!},\quad(11)$$

$$\max\{|x|,|y|,|z|\}<1.$$

The function (11) has 6 confluent forms [12], one of which can be written as follows

$$\Xi_{22}^{(3)}\left(a,b,a',b';c;x,y,z\right)=\sum_{m,n,p=0}^{\infty}\frac{(a)_m(b)_m\left(a'\right)_n\left(b'\right)_n}{(c)_{m+n+p}}\frac{x^m}{m!}\frac{y^n}{n!}\frac{z^p}{p!},\max\{|x|,|y|\}<1.\quad(12)$$

Note, the multidimensional analogous of the confluent hypergeometric function $\Xi_{22}^{(3)}$ is found in [13].

If one sets

$$\theta=x\frac{\partial}{\partial x},\phi=y\frac{\partial}{\partial y},\psi=z\frac{\partial}{\partial z},\quad(13)$$

it is clear that the new function $\Xi_{22}^{(3)}$ defined in (12) satisfies the following system of PDE [12]:

$$\begin{cases}\left[\theta(\theta+\phi+\psi+c-1)-x(a+\theta)(b+\theta)\right]\Xi_{22}^{(3)}=0,\\ \left[\phi(\theta+\phi+\psi+c-1)-y(a'+\phi)(b'+\phi)\right]\Xi_{22}^{(3)}=0,\\ \left[\psi(\theta+\phi+\psi+c-1)\right]\Xi_{22}^{(3)}=0.\end{cases}$$

Using the operators (13), it is easy to get

$$\begin{cases}x(1-x)u_{xx}+yu_{xy}+zu_{xz}+\left[c-\left(a+b+1\right)x\right]u_x-abu=0,\\ y(1-y)u_{yy}+xu_{xy}+zu_{yz}+\left[c-\left(a'+b'+1\right)y\right]u_y-a'b'u=0,\\ zu_{zz}+xu_{xz}+yu_{yz}+cu_z-u=0,\end{cases}\quad(14)$$

where $u\equiv\Xi_{22}^{(3)}\left(a,b,a',b';c;x,y,z\right)$.

At first we clarify the behavior of $\Xi_{22}^{(3)}\left(a,b,a',b';c;x,y,z\right)$ as $x,y\to\infty$. It follows from (12) that the representation

$$\Xi_{22}^{(3)}\left(a,b,a',b';c;x,y,z\right)=\sum_{n=0}^{\infty}\frac{(a')_n(b')_n y^n}{n!(c)_n}\Xi_2\left(a,b;c+n;x,z\right) \tag{15}$$

is true, where Ξ_2 is the Humbert function defined in (4). Substituting an expansion (9) of the Humbert function Ξ_2 into (15) we obtain the following leading term of (15) as $x,y\to\infty$, $|\arg(-x)|<\pi$, $|\arg(-y)|<\pi$:

$$\Xi_{22}^{(3)}\left(a,b,a',b';c;x,y,z\right)\sim\frac{\Gamma(c)\Gamma(b-a)\Gamma(b'-a')}{\Gamma(b)\Gamma(b')\Gamma(c-a-a')}\,{}_0F_1(c-a-a';z)(-x)^{-a}(-y)^{-a'}+$$

$$+\frac{\Gamma(c)\Gamma(b-a)\Gamma(a'-b')}{\Gamma(b)\Gamma(a')\Gamma(c-a-b')}\,{}_0F_1(c-a-b';z)(-x)^{-a}(-y)^{-b'}+$$

$$+\frac{\Gamma(c)\Gamma(a-b)\Gamma(b'-a')}{\Gamma(a)\Gamma(b')\Gamma(c-b-a')}\,{}_0F_1(c-b-a';z)(-x)^{-b}(-y)^{-a'}+$$

$$+\frac{\Gamma(c)\Gamma(a-b)\Gamma(a'-b')}{\Gamma(a)\Gamma(a')\Gamma(c-b-b')}\,{}_0F_1(c-b-b';z)(-x)^{-b}(-y)^{-b'},\ a\neq b,\ a'\neq b'. \tag{16}$$

Now we use the asymptotic expansion (8). Then from (16) we find that

$$\Xi_{22}^{(3)}\left(a,b,a',b';c;x,y,z\right)=O\left(x^{-a}y^{-a'}z^{(1-2c+2a+2a')/4}\right)$$
$$+O\left(x^{-a}y^{-b'}z^{(1-2c+2a+2b')/4}\right)+O\left(x^{-b}y^{-a'}z^{(1-2c+2b+2a')/4}\right)$$
$$+O\left(x^{-b}y^{-b'}z^{(1-2c+2b+2b')/4}\right),\ a\neq b,\ a'\neq b';\ x,y,z\to\infty. \tag{17}$$

4. The Dirichlet problem in the first octant for the Helmholtz equation with three singular coefficients

Let us consider the following singular Helmholtz equation

$$u_{xx}+u_{yy}+u_{zz}+\frac{2\alpha}{x}u_x+\frac{2\beta}{y}u_y+\frac{2\gamma}{z}u_z-\lambda^2u=0,\ 0<2\alpha,2\beta,2\gamma<1 \tag{18}$$

in the infinite domain $\Omega\equiv\{(x,y,z):x>0,y>0,z>0\}$.

The Dirichlet problem. Find a regular solution $u(x,y,z)$ to the singular Helmholtz equation (18) which belongs to the class of functions $C\left(\overline{\Omega}\right)\cup C^2(\Omega)$, satisfying the conditions

$$u(x,y,0)=\tau_1(x,y),\ 0\le x,y<\infty, \tag{19}$$

$$u(x,0,z)=\tau_2(x,z),\ 0\le x,z<\infty, \tag{20}$$

$$u(0,y,z)=\tau_3(y,z),\ 0\le y,z<\infty, \tag{21}$$

$$\lim_{R\to\infty}u(x,y,z)=0,\ R=\sqrt{x^2+y^2+z^2}, \tag{22}$$

where $\tau_k(t,s)$ are given functions such that

$$\tau_1(x,y)=\frac{\tilde{\tau}_1(x,y)}{\left(1+x^2+y^2\right)^{(1+\alpha+\beta-\gamma+\varepsilon_1)/2}},\tilde{\tau}_1(x,y)\in C(0\le x,y<\infty),\varepsilon_1>2-2\alpha-2\beta, \quad (23)$$

$$\tau_2(x,z)=\frac{\tilde{\tau}_2(x,z)}{\left(1+x^2+z^2\right)^{(1+\alpha-\beta+\gamma+\varepsilon_2)/2}},\tilde{\tau}_2(x,z)\in C(0\le x,z<\infty),\varepsilon_2>2-2\alpha-2\gamma, \quad (24)$$

$$\tau_3(y,z)=\frac{\tilde{\tau}_3(y,z)}{\left(1+y^2+z^2\right)^{(1-\alpha+\beta+\gamma+\varepsilon_3)/2}},\tilde{\tau}_3(y,z)\in C(0\le y,z<\infty),\varepsilon_3>2-2\beta-2\gamma. \quad (25)$$

In addition, the functions $\tau_1(x,y)$, $\tau_2(x,z)$ and $\tau_3(y,z)$ satisfy the concordance conditions in origin $\tau_1(0,0)=\tau_2(0,0)=\tau_3(0,0)$, and in the lateral ribs of the domain Ω:

$$\tau_1(x,0)=\tau_2(x,0),\tau_1(0,y)=\tau_3(y,0),\tau_2(0,z)=\tau_3(0,z)\,0\le x,y,z<\infty. \quad (26)$$

In the two-dimensional case the Dirichlet problem for the Helmholtz equation (10) in the infinite first quadrant is studied in [18].

In the paper [19] the Dirichlet problem for an elliptic equation with two singular coefficients

$$u_{xx}+u_{yy}+\frac{2\alpha}{x}u_x+\frac{2\beta}{y}u_y=0,0<2\alpha,2\beta<1$$

in the arbitrary domain bounded in the first quarter $\{(x,y):x>0,y>0\}$ of the xOy-plane is solved by a potential theory method and in the paper [20] a solution of the Dirichlet problem for multidimensional elliptic equation with two singular coefficients

$$\sum_{j=1}^{m}u_{x_jx_j}+\frac{2\alpha}{x_1}u_{x_j}+\frac{2\beta}{x_2}u_{x_2}=0,0<2\alpha,2\beta<1$$

in the quarter of the multidimensional ball is found in the explicit form. In the work [21] a spatial mixed problems and Neumann problem for a three- dimensional elliptic equation with two singular coefficients

$$u_{xx}+u_{yy}+u_{zz}+\frac{2\alpha}{x}u_x+\frac{2\beta}{y}u_y=0,0<2\alpha,2\beta<1$$

are investigated.

Conditions (23) – (25) are essential for the unique solvability of the Dirichlet problem. A similar problem for the equation (18) under more severe constraints on the data is solved in [22].

Theorem 1. *The Dirichlet problem for equation (18) in an unbounded domain Ω can have at most one solution.*

Proof. For the proof of the theorem, it is sufficient to show that the corresponding homogeneous problem has a trivial solution. For that we denote by Ω_R the finite part of domain Ω, which is bounded by planes $x=0$, $y=0$, $z=0$ and a part of the sphere

$$\sigma_R:=\{(x,y,z):x^2+y^2+z^2,x>0,y>0,z>0\}.$$

Let

$$\tau_1(x,y)=0,\tau_2(x,z)=0,\tau_3(y,z)=0. \quad (27)$$

The validity of theorem follows from the extremum principle for the elliptic equations [23]. Indeed, in the domain $\overline{\Omega}_R$ due to (10), the function $u(x,y,z)$ can attain its positive maximum and negative minimum on σ_R only.

Let (x,y,z) be an arbitrary point of domain Ω_R. Let us take an arbitrary small number $\varepsilon>0$ and, taking into account (10), we choose R so large that $|u(x,y,z)|<\varepsilon$ on σ_R. With suffuciently large R, this point belongs to the domain Ω_R and therefore $|u(x,y,z)|<\varepsilon$. In view of arbitrariness of ε we have $u(x,y,z)=0$. Then $u(x,y,z)=0$ in the domain Ω.

5. Existence of the solution to the Dirichlet problem

We will seek a solution to the Dirichlet problem (18) – (26) in the form

$$u(x,y,z)=\sum_{i=1}^{3}u_i(x,y,z),$$

where $u_1(x,y,z)$, $u_2(x,y,z)$, $u_3(x,y,z)$ are a solutions to the equation (18), satisfying the boundary conditions

$$u_1(x,y,0)=\tau_1(x,y), u_1(x,0,z)=0, u_1(0,y,z)=0, \tag{28}$$

$$u_2(x,y,0)=0, u_2(x,0,z)=\tau_2(x,z), u_2(0,y,z)=0, \tag{29}$$

$$u_3(x,y,0)=0, u_3(x,0,z)=0, u_3(0,y,z)=\tau_3(y,z), \tag{30}$$

respectively.

Lemma 1. *If a function $\tau_1(x,y)$ can be represented by the formula (23), then the function*

$$u_1(x,y,z)=\sum_{j=1}^{4}(-1)^{j+1}u_{1j}(x,y,z) \tag{31}$$

is a regular solution of the equation (18) in the domain Ω, satisfying the boundary conditions(28) and vanishing at infinity, where

$$u_{1j}(x,y,z)=\frac{2(1-2\gamma)x^{-\alpha}y^{-\beta}z^{1-2\gamma}}{\pi}\int_0^\infty\int_0^\infty\frac{\tau_1(t,s)t^{\alpha}s^{\beta}}{\rho_{1j}^{3-2\gamma}}\times$$

$$\times\Xi_{22}^{(3)}\left(\alpha,1-\alpha,\beta,1-\beta;\gamma-\frac{1}{2};\frac{\rho_{1j}^2}{-4xt};\frac{\rho_{1j}^2}{-4ys};\frac{\lambda^2}{4}\rho_{1j}^2\right)dtds,\ j=1,2,3,4; \tag{32}$$

$$\rho_{11}=\sqrt{(t-x)^2+(s-y)^2+z^2},\rho_{12}=\sqrt{(t+x)^2+(s-y)^2+z^2},$$

$$\rho_{13}=\sqrt{(t+x)^2+(s+y)^2+z^2},\rho_{14}=\sqrt{(t-x)^2+(s+y)^2+z^2},$$

and $\Xi_{22}^{(3)}$ is confluent hypergeometric function in three variables defined in (12).

Proof. First, we need to make sure that function (32) satisfies the equation

$$W_{xx}+W_{yy}+W_{zz}+\frac{2\alpha}{x}W_x+\frac{2\beta}{y}W_y+\frac{2\gamma}{z}W_z-\lambda^2W=0 \tag{33}$$

in the arguments x, y and z. For this purpose, consider the function

$$W(x,y,z)=x^{-\alpha}y^{-\beta}z^{1-2\gamma}\rho^{\gamma-\frac{3}{2}}\omega(\xi,\eta,\zeta),$$

where

$$\omega(\xi,\eta,\zeta)=\Xi_{22}^{(3)}\left(\alpha,1-\alpha,\beta,1-\beta;\gamma-\frac{1}{2};\frac{\rho}{-4xt};\frac{\rho}{-4ys};\frac{\lambda^2}{4}\rho\right), \tag{34}$$

$$\rho=(x-t)^2+(y-s)^2+z^2,\xi=-\frac{\rho}{4xt},\eta=-\frac{\rho}{4ys},\zeta=\frac{\lambda^2}{4}\rho.$$

Calculating the necessary derivatives of function W with respect to variables x, y, z and substituting them into equation (33), we obtain a following system of partial differential equations

$$\begin{cases} \xi(1-\xi)\omega_{\xi\xi} + \eta\omega_{\xi\eta} + \zeta\omega_{\xi\zeta} + \left(\gamma - \frac{1}{2} - 2\xi\right)\omega_{\xi} - \alpha(1-\alpha)\omega = 0, \\ \eta(1-\eta)\omega_{\eta\eta} + \xi u_{\xi\eta} + \zeta\omega_{\eta\zeta} + \left(\gamma - \frac{1}{2} - 2\eta\right)\omega_{\eta} - \beta(1-\beta)\omega = 0, \\ \zeta\omega_{\zeta\zeta} + \xi\omega_{\xi\zeta} + \eta\omega_{\eta\zeta} + \left(\gamma - \frac{1}{2}\right)\omega_{\zeta} - \omega = 0. \end{cases} \tag{35}$$

Comparing the system of equations (35) with the system of hypergeometric type equations (14), we can conclude that the function $\omega(\xi,\eta,\zeta)$ defined by formula (34), is a solution to system of equations (35). Thus, function (32) satisfies equation (18).

Now we will show that function $u_{11}(x,y,z)$ satisfies condition (19) of the Dirichlet problem.

By setting $t = x + z\mu, s = y + z\nu,$ we transform formula (32) for $j=1$ to the form

$$u_{11}(x,y,z) = \frac{2(1-2\gamma)}{\pi}\int_0^\infty\int_0^\infty \frac{\tau_1(x+z\mu, y+z\nu)}{w^{(3-2\gamma)/2}}\left(\frac{x+z\mu}{x}\right)^{\alpha}\left(\frac{y+z\nu}{y}\right)^{\beta} \times$$

$$\times\Xi_{22}^{(3)}\left(\alpha,1-\alpha,\beta,1-\beta;\gamma-\frac{1}{2};\frac{wz^2}{-4x(x+z\mu)};\frac{wz^2}{-4y(y+\nu)};\frac{\lambda^2}{4}wz^2\right)d\mu d\nu, \tag{36}$$

where $w := 1+\mu^2+\nu^2$ for brevity.

On the right-hand side of (36) we pass to the limit as $z \to 0$ and get

$$\lim_{z\to 0} u_{11}(x,y,z) = \tau_1(x,y)\frac{2(1-2\gamma)}{\pi}\int_0^\infty\int_0^\infty \frac{d\mu d\nu}{\left(1+\mu^2+\nu^2\right)^{(3-2\gamma)/2}}.$$

Using consistently the well-known identity [24, p. 612, Eq. 4.623]

$$\int_0^\infty\int_0^\infty \varphi\left(a^2x^2+b^2y^2\right)dxdy = \frac{\pi}{2ab}\int_0^\infty \varphi\left(x^2\right)xdx, \tag{37}$$

we obtain

$$\lim_{z\to 0} u_{11}(x,y,z) = \tau_1(x,y).$$

Likewise, everyone can easily get

$$\lim_{z\to 0} u_{1j}(x,y,z) = 0,\ j = 2,3,4.$$

So, the following equality is true for the function $u_1(x,y,z)$ defined in (31):

$$\lim_{z\to 0} u_1(x,y,z) = \tau_1(x,y).$$

Applying the behavior formula (16) to (32) and taking into account the obvious equalities

$$\rho_{11}\big|_{x=0} = \rho_{12}\big|_{x=0}, \rho_{11}\big|_{y=0} = \rho_{14}\big|_{y=0}, \rho_{12}\big|_{y=0} = \rho_{13}\big|_{y=0}, \rho_{13}\big|_{x=0} = \rho_{14}\big|_{x=0},$$

we establish that for $\alpha < \frac{1}{2}$ and $\beta < \frac{1}{2}$ there exist a following limits

$$\lim_{x\to 0} u_1(x,y,z) = 0, \lim_{y\to 0} u_1(x,y,z) = 0.$$

It is easy to see that as the point (x,y,z) tends to infinity, i.e. $R\to\infty$, function (32) tends to zero. To do this, we will use the formula (17) that describes the behavior of the function $\Xi_{22}^{(3)}$ at infinity. Then, by virtue of (23), we get

$$\left|u_{11}(x,y,z)\right|\le C_{11}z^{1-2\gamma}\int_0^\infty\int_0^\infty\frac{t^{2\alpha}s^{2\beta}dtds}{\left(1+t^2+s^2\right)^{(1+\alpha+\beta-\gamma+\varepsilon_1)/2}\rho_{11}^{2+\alpha+\beta-\gamma}}$$

$$+C_{12}y^{1-2\beta}z^{1-2\gamma}\int_0^\infty\int_0^\infty\frac{t^{2\alpha}sdtds}{\left(1+t^2+s^2\right)^{(1+\alpha+\beta-\gamma+\varepsilon_1)/2}\rho_{11}^{3+\alpha-\beta-\gamma}}$$

$$+C_{13}x^{1-2\alpha}z^{1-2\gamma}\int_0^\infty\int_0^\infty\frac{ts^{2\beta}dtds}{\left(1+t^2+s^2\right)^{(1+\alpha+\beta-\gamma+\varepsilon_1)/2}\rho_{11}^{3+\beta-\gamma-\alpha}}$$

$$+C_{14}x^{1-2\alpha}y^{1-2\beta}z^{1-2\gamma}\int_0^\infty\int_0^\infty\frac{tsdtds}{\left(1+t^2+s^2\right)^{(1+\alpha+\beta-\gamma+\varepsilon_1)/2}\rho_{11}^{4-\alpha-\beta-\gamma}}. \qquad (38)$$

At the right-hand sides of inequalities (38), change the variables as follows: $t=R\mu$, $s=R\nu$. We obtain the inequalities

$$|u_{11}|\le\frac{1}{R^{2\alpha+2\beta-2+\varepsilon_1}}\left(\frac{z}{R}\right)^{1-2\gamma}\left[\frac{C_{11}}{R^{2-2\alpha-2\beta}}K_1(x,y,z;R)+\frac{C_{12}}{R^{1-2\alpha}}\left(\frac{y}{R}\right)^{1-2\beta}K_2(x,y,z;R)\right.$$

$$\left.+\frac{C_{13}}{R^{1-2\beta}}\left(\frac{x}{R}\right)^{1-2\alpha}K_3(x,y,z;R)+C_{14}\left(\frac{x}{R}\right)^{1-2\alpha}\left(\frac{y}{R}\right)^{1-2\beta}K_4(x,y,z;R)\right],$$

where

$$K_1(x,y,z;R)=\int_0^\infty\int_0^\infty\frac{\mu^{2\alpha}\nu^{2\beta}d\mu d\nu}{\Lambda^{(1+\alpha+\beta-\gamma+\varepsilon_1)/2}\Upsilon^{(2+\alpha+\beta-\gamma)/2}},$$

$$K_2(x,y,z;R)=\int_0^\infty\int_0^\infty\frac{\mu^{2\alpha}\nu d\mu d\nu}{\Lambda^{(1+\alpha+\beta-\gamma+\varepsilon_1)/2}\Upsilon^{(3+\alpha-\beta-\gamma)/2}},$$

$$K_3(x,y,z;R)=\int_0^\infty\int_0^\infty\frac{\mu\nu^{2\beta}d\mu d\nu}{\Lambda^{(1+\alpha+\beta-\gamma+\varepsilon_1)/2}\Upsilon^{(3+\beta-\gamma-\alpha)/2}},$$

$$K_4(x,y,z;R)=\int_0^\infty\int_0^\infty\frac{\mu\nu d\mu d\nu}{\Lambda^{(1+\alpha+\beta-\gamma+\varepsilon_1)/2}\Upsilon^{(4-\beta-\gamma-\alpha)/2}},$$

$$\Lambda=\frac{1}{R^2}+\mu^2+\nu^2,\Upsilon=1+\mu^2+\nu^2-\frac{2}{R}(\mu x+\nu y).$$

Let us show that these proper double integrals are bounded. Indeed, using the formula (37) and passing to the limit as $R\to\infty$, we find the relations

$$\lim_{R\to\infty}R_j(x,y,z;R)=M_j,\ j=1,2,3,4, \qquad (39)$$

where

$$M_1=\frac{\Gamma\left(\alpha+\frac{1}{2}\right)\Gamma\left(\beta+\frac{1}{2}\right)\Gamma\left(\frac{1+\alpha+\beta+2\gamma+\varepsilon_1}{2}\right)\Gamma\left(\frac{2-2\gamma+\varepsilon_1}{2}\right)}{4\Gamma(1+\alpha+\beta)\Gamma\left(\frac{2+\alpha+\beta-\gamma}{2}\right)},$$

$$M_2=\frac{\Gamma\left(\frac{2+\alpha-\beta+\gamma-\varepsilon_1}{2}\right)\Gamma\left(\frac{1-2\gamma+\varepsilon_1}{2}\right)}{2(1+2\alpha)\Gamma\left(\frac{3+\alpha-\beta-\gamma}{2}\right)},$$

$$M_3=\frac{\Gamma\left(\frac{2-\alpha+\beta+\gamma-\varepsilon_1}{2}\right)\Gamma\left(\frac{1-2\gamma+\varepsilon_1}{2}\right)}{2(1+2\beta)\Gamma\left(\frac{3-\alpha+\beta-\gamma}{2}\right)},$$

$$M_4=\frac{\Gamma\left(\frac{3-\alpha-\beta+\gamma-\varepsilon_1}{2}\right)\Gamma\left(\frac{1-2\gamma+\varepsilon_1}{2}\right)}{4\Gamma\left(\frac{4-\alpha-\beta-\gamma}{2}\right)}.$$

From (39), it intermediately follows that

$$\left|u_{11}(x,y,z)\right|\le\frac{C}{R^{2\alpha+2\beta-2+\varepsilon_1}},\varepsilon_1>2-2\alpha-2\beta, \tag{40}$$

where C is a constant.

Now, it intermediately follows from estimate (40) that the function (32) vanishes at infinity. The **Lemma 1** is proved.

Similar statements are also true for functions $u_2(x,y,z)$ and $u_3(x,y,z)$ that satisfy the conditions (29) and (30), respectively, and vanish at infinity, where

$$u_i(x,y,z)=\sum_{j=1}^{4}(-1)^{j+1}u_{ij}(x,y,z), i=2,3,$$

$$u_{2j}(x,y,z)=\frac{2(1-2\beta)}{\pi}x^{-\alpha}y^{1-2\beta}z^{-\gamma}\int_0^\infty\int_0^\infty\frac{\tau_2(t,s)t^\alpha s^\gamma}{\rho_{2j}^{3-2\beta}}\times$$

$$\times\Xi_{22}^{(3)}\left(\alpha,1-\alpha,\gamma,1-\gamma;\beta-\frac{1}{2};\frac{\rho_{2j}^2}{-4xt};\frac{\rho_{2j}^2}{-4zs};\frac{\lambda^2}{4}\rho_{2j}^2\right)dtds, \tag{41}$$

$$\rho_{21}=\sqrt{(t-x)^2+y^2+(s-z)^2},\ \rho_{22}=\sqrt{(t+x)^2+y^2+(s-z)^2},$$

$$\rho_{24}=\sqrt{(t-x)^2+y^2+(s+z)^2},\ \rho_{23}=\sqrt{(t+x)^2+y^2+(s+z)^2},$$

$$u_{3j}(x,y,z)=\frac{2(1-2\alpha)}{\pi}x^{1-2\alpha}y^{-\beta}z^{-\gamma}\int_0^\infty\int_0^\infty\frac{\tau_3(t,s)t^\beta s^\gamma}{\rho_{3j}^{3-2\alpha}}\times$$

$$\times \Xi_{22}^{(3)}\left(\beta,1-\beta,\gamma,1-\gamma;\alpha-\frac{1}{2};\frac{\rho_{3j}^2}{-4yt};\frac{\rho_{3j}^2}{-4zs};\frac{\lambda^2}{4}\rho_{3j}^2\right)dtds, \tag{42}$$

$$\rho_{31}=\sqrt{x^2+(t-y)^2+(s-z)^2},\ \rho_{32}=\sqrt{x^2+(t+y)^2+(s-z)^2},$$
$$\rho_{34}=\sqrt{x^2+(t-y)^2+(s+z)^2},\ \rho_{33}=\sqrt{x^2+(t+y)^2+(s+z)^2}.$$

Thus, we have proved the following theorem

Theorem 2. *Function* $u(x,y,z)=\sum_{i=1}^{3}\sum_{j=1}^{4}(-1)^{j+1}u_{ij}(x,y,z)$, *where the functions* u_{ij} *are defined in (32), (41) and (42), is a regular solution of equation (18) in the domain* Ω, *satisfying the boundary conditions (19) to (22).*

6. Conclusion

In this paper we dealt with the three-dimensional singular Helmholtz equation of the second order. In the future, the study can be developed in two directions: firstly, towards increasing the dimensionality of the equation, secondly, towards increasing the order of the equation, it would be necessary to consider the above-studied problem at least for the third order singular partial differential equation.

Because, at the present all fundamental solutions of the multidimensional Helmholtz equation with the singular coefficents

$$\sum_{i=1}^{m}\frac{\partial^2 u}{\partial x_i^2}+\sum_{k=1}^{n}\frac{2\alpha_i}{x_k}\frac{\partial u}{\partial x_k}-\lambda^2 u=0, 0<2\alpha_k<1, m\geq 2, 1\leq n\leq m \tag{43}$$

are expressed by a multiple confluent hypergeometric function defined in [25]. In addition, particular solutions of the more general equation

$$\sum_{j=1}^{k}\frac{\partial^2 u}{\partial x_j^2}+\sum_{j=1}^{k}\frac{2\alpha_j}{x_j}\frac{\partial u}{\partial x_j}=\sum_{j=k+1}^{n}\frac{\partial^2 u}{\partial x_j^2}+\sum_{j=k+1}^{n}\frac{2\alpha_j}{x_j}\frac{\partial u}{\partial x_j}, k=\overline{1,n-1}$$

are currently known [26].

In the multidimensional case, only Kapilevič [27], in 1952, has solved the Dirichlet problem for the Helmholtz equation with the single singular coefficient (i.e. $n=1$ in Eq. (43)) in the half-space.

To study third-order partial differential equations, all results on the high-order hypergeometric functions are required. For instance, the following degenerating model parabolic equation of the third order

$$x^n y^m u_t - t^k y^m u_{xxx} - t^k x^n u_{yyy} = 0, m,n,k = const > 0$$

has 9 linearly independent particular solutions [28] which are expressed by, so called, a Kampé de Fériet's hypergeometric functions in two variables [10, p. 27] the order of which exceeds two. For the study of high-order hypergeometric functions, expansion formulas are very important, which allow us to express a given multiple hypergeometric function by the infinite sum of hypergeometric functions of lower order. In a recent work [29], expansions of the Kampé de Fériet's functions are established.

The study can be started with solving the Dirichlet problem for a four-dimensional equation

$$u_{xx}+u_{yy}+u_{zz}+u_{tt}+\frac{2\alpha}{x}u_x+\frac{2\beta}{y}u_y+\frac{2\gamma}{z}u_z+\frac{2\delta}{t}u_t-\lambda^2 u=0,\ 0<\alpha,\beta,\gamma,\delta<1/2 \tag{44}$$

using the results of the work [30] devoted to the Dirichlet problem for equation (44) at $\lambda=0$.

References

[1] L.Bers, Mathematical aspects of subsonic and transonic gas dynamics.(AM-206). New York, Dover Publications Inc, 1958.

[2] G. Lohofer, "Theory of an electromagnetically deviated metal sphere. 1: Abcorbed power" , SIAM Journal Applied Mathematics, 49(1989) 567–581.

[3] A.W. Niukkanen, "Generalized hypergeometric series ${}^{N}F\left(x_1,...,x_N\right)$ arising in physical and quantum chemical applications" , J.Phys.A:Math.Gen., 16(9) (1983) 1813–1825.

[4] J. Horn, "Über die Convergenz der hypergeometrischen Reihen zweier und dreier Veränderlichen" , Math. Ann., 34(4) (1889) 544–600.

[5] G. Lauricella, "Sulle funzioni ipergeometriche a piu variabili" , Rend. Circ. Mat. Palermo., 7 (1893) 111–158.

[6] S. Saran, "Hypergeometric functions of three variables" , Ganita., 5 (1954) 77–91, Corrigendum. *ibid.*, 7(1956) 65.

[7] G.K. Dhawan, "Hypergeometric functions in three variables" , Proc. Nat. Acad. Sci. India Sect. A., 40 (1970) 43-48.

[8] M.S. Samar, "Some definite integrals" , Vijnana Parishad Anusandhan Patrika., 16 (1973) 7–11.

[9] H. Exton, "Hypergeometric functions of three variables" , J. Indian Acad. Math., 4 (1982) 113–119.

[10] H.M. Srivastava, P.W. Karlsson, Multiple Gaussian Hypergeometric Series. (AM-428). New York, Chichester, Brisbane and Toronto: Halsted Press, 1985.

[11] R.N. Jain, "The confluent hypergeometric functions of three variables" , Proc. Nat.Acad.Sci.India. Sect. A., 36 (1966) 395-408.

[12] H. Exton, "On certain confluent hypergeometric of three variables", Ganita., 21(2) (1970) 79–92.

[13] Z.O. Arzikulov, T.G. Ergashev, "Some systems of PDE associated with the multiple confluent hypergeometric functions and their applications", Lobachevskii Journal of Mathematics., 45(2) (2024) 591 – 603.

[14] A. Erdélyi, W. Magnus, F. Oberhettinger, F.G. Tricomi, Higher Transcendental Functions, (AM-302). New York; Toronto; London: McGraw-Hill Book Company, 1953.

[15] P. Appell. "Sur les séries hypergéométriques de deux variables, et sur des équations différentielles linéaires aux dérivées partielles", C.R. Acad. Sci. Paris., 90 (1880) 296–298.

[16] S.G. Samko, A.A. Kilbas, O.I. Marichev, Fractional integrals and derivatives. Theory and applications., (AM-976). Amsterdam: Gordon and Breach Science Publishers, 1993.

[17] O.I. Marichev, Handbook of integral transforms of higher transcendental functions, theory and algorithmic tables., (AM-336). Chichester, New York: Ellis Horwood Ltd, 1982.

[18] O.A. Repin, M.E. Lerner, "On the Dirichlet problem for the generalized bioxially symmetric Helmholtz equation in the first quadrant" , Vestnik Samarsk. Gos. Tekh. Universiteta, Ser. fiz.-matem. nauki., 6 (1998) 5–8.

[19] A. Hasanov, T.G. Ergashev, "On potential theory for the generalized bi-axially symmetric elliptic equation in the plane", KazNU Bulletin Mathematics Mechanics Computer Science Series., 1 (2021) 3–24.

[20] N.J. Komilova, "Dirichlet problem for multidimensional elliptic equation with two singular coefficients", Uzbek Mathematical Journal., 65(1) (2021) 98 – 109.

[21] Z.R. Tulakova, "Spatial mixed problems and Neumann problem for the three-dimensional elliptic equation with the two singular coefficients" Uzbek Mathematical Journal., 68(3) (2024) 150 –157.

[22] Z.O. Arzikulov, A. Hasanov, T.G. Ergashev, "Confluent hypergeometric functions and their application to the solution of Dirichlet problem for the Helmholtz equation with three singular coefficients" , Vestn. Samar. Gos. Tekhn. Univ., Ser. Fiz.-Mat. Nauki [J. Samara State Tech. Univ., Ser. Phys. Math. Sci.], 29(3) (2025) 407–429.

[23] C. Miranda, Partial Differential Equations of Elliptic Type, Second Revised Edition., (AM-256). Translated from the Italian edition by Z. C. Motteler, Ergebnisse der Mathematik und ihrer Grenzgebiete, Band **2**, Berlin, Heidelberg and New York: Springer-Verlag, 1970.
[24] I.S. Gradshteyn, I.M. Ryzhik, Table of integrals, series and products, 7 th ed., (AM-1172). Amsterdam, Boston, Heidelberg, London, New York, Oxford, Paris, San Diego, San Fransisco, Singapore, Sydney, Tokyo: Academic Press, 2007.
[25] T.G. Ergashev. "Fundamental solutions of the generalized Helmholtz equation with several singular coefficients and confluent hypergeometric functions of many variables" , Lobachevskii Journal of Mathematics., 41(1) (2020) 15–26.
[26] A.R. Ryskan, Z.O. Arzikulov, T.G. Ergashev, "Particular solutions of multidimensional generalized Euler-Poisson-Darboux equations of various (elliptic or hyperbolic) types" , KazNU Bulletin Mathematics Mechanics Computer Science Series., 1(121) (2024) 76–88.
[27] M.B. Kapilevich, "On an equation of mixed elliptic-hyperbolic type" , Matematicheskiy sbornik., 30(72)(1) (1952) 11–38.
[28] A. Hasanov, M. Ruzhansky, "Hypergeometric expansions of solutions of the degenerating model parabolic equations of the third order" , Lobachevskii Journal of Mathematics., 41(1) (2020) 27–31.
[29] N.J. Komilova, A. Hasanov, T.G. Ergashev, "Expansions of Kampé de Fériet hypergeometric functions", KazNU Bulletin Mathematics Mechanics Computer Science Series., 2(122) (2024) 48–63.
[30] A.S. Berdyshev, A.R.Ryskan. The Neumann and Dirichlet problems for one four-dimensional degenerate elliptic equation. Lobachevskii Journal of Mathematics, 41(6) (2020) 1051–1066. DOI: 10.1134/S1995080220060062

Journal of Mathematical Models and Methods in Engineering

journal homepage: https://jmmme.uz/index.php/journal

Neural networks with configurable affinity functions for binary object classification

S.Yu. Leonov[1*], **O.V. Lipchanska**[2]

[1,2]*Department of Computer Engineering and Programming, "Kharkiv Polytechnic Institute" National Technical University, Kharkiv, 61000, Ukraine*

ARTICLE INFO

Keywords:
computer systems for recognition;
computing systems;
data transmission;
Hamming neural network;
affinity functions;
diagnostics of systems for determining operability;
classification of discrete objects;
binary vectors

ABSTRACT

The paper addresses computer systems for the recognition of discrete objects encoded by binary and bipolar feature vectors. It is shown that the well-known Hamming neural network, which uses the scalar product of bipolar vectors and the Hamming distance for recognition, does not allow the application of more refined similarity functions when object features are binary-encoded. Modifications of the network architecture are proposed, implementing computing systems for evaluating object similarity using the Jaccard, Russell-Rao, Sokal-Michener, Kulczynski, and Yule functions. Neuron and neural block structures are developed that ensure data transmission between the network's layers and perform diagnostics of systems for determining the operability of recognition algorithms through the parallel computation of match/mismatch variables for the features of compared binary vectors. A numerical example is given, confirming the correctness of the proposed computer tools for classification. It is shown that the developed approach extends the scope of application of neural-network-based computer systems for recognition and makes it possible to synthesize networks that determine several equally valid solutions simultaneously.

1. Introduction

The scalar product of vectors is often used in solving a variety of problems involving the determination of affinity (similarity or relationship) between different binary objects. In particular, the Hamming neural network [1 – 3], which uses the *DB* scalar product of two bipolar *n*-bit vectors $D=(d_1,\ldots,d_n)$, $B=(b_1,\ldots,b_n)$

$$DB=\sum_{k=1}^{n} d_k b_k = a_{eq} - r = 2a_{eq} - n \qquad (1)$$

where a_{eq} is the number of identical bipolar components in vectors *D* and *B*; *r* is the Hamming distance between vectors *D* and *B* (the number of distinct components in the vectors under consideration) $a_{eq}+r=n$, used in black-and-white image recognition based on the number of matching bipolar components, taking the Hamming distance into account

* Corresponding author. **S.Yu. Leonov**
E-mail addresses: serleomail@gmail.com

$$a_{eq} = n/2 + \frac{1}{2}\sum_{k=1}^{n} d_k b_k \tag{2}$$

The number of identical bipolar components in the vectors can be regarded as a measure of similarity between these vectors. For identical vectors, this measure of similarity reaches a maximum value equal to the number of binary bits in the vectors being compared. The similarity measure takes its minimum value, equal to zero, when the vectors being compared do not share a single binary bit with identical components.

The concept of the Hamming distance and measures of similarity (2) is based on the number of mismatched or matching bits in the binary vectors being compared. However, in [4 – 10], it is noted that a more refined classification can be introduced for the compared binary vectors using the special Table 1 when binary encoding the vectors $D = (d_1, \ldots, d_n)$, and $B = (b_1, \ldots, b_n)$, which contain the encoded features of certain compared objects.

Table 1

Relationship between the features of a pair of objects (binary vectors)

D \ B	1	0
1	a	e
0	f	b

The variable *a* in Table 1 is introduced to calculate the number of features (the number of components of binary vectors that are 1) that are present in both objects *D* and *B* simultaneously. It is calculated using the following formula:

$$a = \sum_{v=1}^{n} d_v b_v \tag{3}$$

The scalar product (3) of the binary vectors *D* and *B* is used to compute the similarity parameter (a measure of similarity between binary vectors) in the ART-1 discrete neural network [1, 2]. However, using only the nonzero components to assess the similarity of two binary vectors significantly limits the ability to make a more nuanced comparison of these vectors. To do this, knowledge of the variables *b*, *f*, and *e* (Table 1) is required.

The variable *b* in Table 1 is used to count the number of features (the number of zero components in the vectors) that the objects under consideration do not simultaneously possess

$$b = \sum_{v=1}^{n} (1 - d_v)(1 - b_v) \tag{4}$$

The variable *f* is used to count the number of attributes that object (vector) *B* has but object *D* does not. The variable *e*, on the other hand, is used to count the attributes that object *B* does not have but object *D* does:

$$f = \sum_{v=1}^{n} (1 - d_v) b_v \tag{5}$$

$$e = \sum_{v=1}^{n} d_v (1 - b_v) \tag{6}$$

An analysis of relations (3) – (6) shows that the measure of similarity between objects *D* and *B* increases as the affinity function *a* increases. The same cannot be said unequivocally about function (4), since the mere absence of identical features among objects can indicate either similarity between the objects or their belonging to different classes (when this is the only property they share). With regard to functions (5) and (6), it can be said that the measure of similarity between objects *D* and *B* is symmetric with respect to these functions.

Various combinations of functions (3) through (6) yield a wide range of affinity functions for binary vectors (objects whose presence or absence of features is encoded by binary components) [4 – 10]. Here are some of them:

Russell–Rao affinity function:

$$S_1 = \frac{a}{a+b+f+e} = \frac{a}{n} \tag{7}$$

Jaccard affinity function:

$$S_2 = \frac{a}{a+f+e} = \frac{a}{n-b} \tag{8}$$

Sokal–Michener affinity function:

$$S_3 = \frac{a+b}{n} \tag{9}$$

Kulczynski 1 and 2 affinity functions:

$$S_4 = \frac{a}{f+e} \tag{10}$$

$$S_5 = \frac{a}{2(a+e)} + \frac{a}{2(a+f)} \tag{11}$$

Dice affinity function:

$$S_6 = \frac{a}{2a+e+f} \tag{12}$$

Yule affinity function:

$$S_7 = \frac{ab-ef}{ab+ef} \tag{13}$$

Here is the research gap. Despite the effectiveness of the Hamming neural network for bipolar-encoded objects, it cannot be applied directly when the components of the compared objects are encoded with a binary (0/1) alphabet, nor can it evaluate affinity using functions such as Jaccard, Sokal–Michener, Kulczynski, and others. The large number of such affinity functions indicates the absence of a single universal function, and there are no generally accepted recommendations for choosing among them. This motivates the need for a systematic method of synthesizing neural networks that can compute arbitrary affinity functions for binary-encoded objects and, optionally, return several solutions.

The aim of this work is to develop modifications of the Hamming neural network that make it possible to solve recognition problems for discrete objects whose components are described using binary components, and where affinity functions of the form (7) – (13) serve as the proximity measure.

2. Methods

2.1 Illustrative comparison of the affinity functions

To characterize the behaviour of the affinity functions, we first perform a numerical experiment.

Example 1. Using the affinity functions (3) – (13) and the Hamming distance r, we compare three pairs of vectors D and B:

D = (1 1 0 1 1 1 0 0 0 1);

B = (1 0 1 0 1 1 1 0 0 1);

D = B = (1 1 0 1 1 1 0 0 0 1) and vectors D and B_1 = (0 0 1 0 0 0 1 1 1 0). The results of the calculations are presented in Table 2.

An analysis of Table 2 shows that the affinity functions $S_1 - S_7$ behave similarly:

– they take on minimum values for vectors with opposite binary components;

– they take on maximum values for pairs of identical binary vectors;

– if the vectors being compared are neither identical nor have opposite components, then the affinity functions $S_1 - S_7$ take on values between their maximum and minimum values.

The Hamming distance behaves, in a sense, in the opposite way—it takes on its minimum value for identical binary vectors and its maximum value for vectors that do not share a single identical binary bit.

Affinity functions are not limited to the relations (3) – (13) [4 – 10]. The large number of these functions indicates that there is no single universal function suitable for comparing any binary vectors with binary-coded components. Nor are there any universally accepted recommendations for the application of known functions.

Table 2

Values of the affinity functions for various pairs of vectors

Case	a	b	e	f	S_1	S_2	S_3	S_4	S_5	S_6	S_7	r
Values of similarity functions for vectors D and B.	4	2	2	2	0,4	0,5	0,6	1	2/3	1/3	0,5	4
Similarity function values for identical vectors D = B = (1101110001).	6	4	0	0	0,6	0,75	1	∞	1	0,5	1	0
Similarity function values for vectors D and B_1 with opposite components.	0	0	6	4	0	0	0	0	0	0	–1	10

The choice of an affinity function is typically made by analyzing the results of computer simulations in feature space, encoded by binary components.

2.2 Reference architecture: the Hamming neural network

Hemming's neural network [1 – 3]. It has n input neurons $S_1, \ldots, S_n$ (Fig. 1), which receive information about the bipolar components of the input images $D^q = (d_1^q, \ldots, d_n^q)$, $q = \overline{1, L}$. The output signals of the S-elements replicate their input signals: $U_{outS_i} = U_{inputS_i} = d_i^q$, $i = \overline{1, n}$. Each element of the S-layer is connected to each neuron of the Z-layer (Fig. 1). The weights (

$w_{1p}^1, w_{2p}^1, \ldots, w_{np}^1$) of the connections of neuron Z_p ($p = \overline{1, m}$) contain information about the p-th reference image: $B^p = (b_1^p, \ldots, b_n^p)$: $w_{1p}^1 = b_1^p/2, \ldots, w_{np}^1 = b_n^p/2$, where the superscript in the connection weights indicates the layer of Z-neurons.

The activation functions of the elements of the Z-layer are given by:

$$g_z(U_{input}) = \begin{cases} 0, \text{ if } U_{input} \leq 0, \\ k_1 U_{input}, \text{ if } 0 \leq U_{input} \leq U_n, \\ U_n, \text{ if } U_{input} > U_n, \end{cases} \tag{14}$$

where U_{input} is an input signal of a neuron of Z- layer; k_1, U_n are constants.

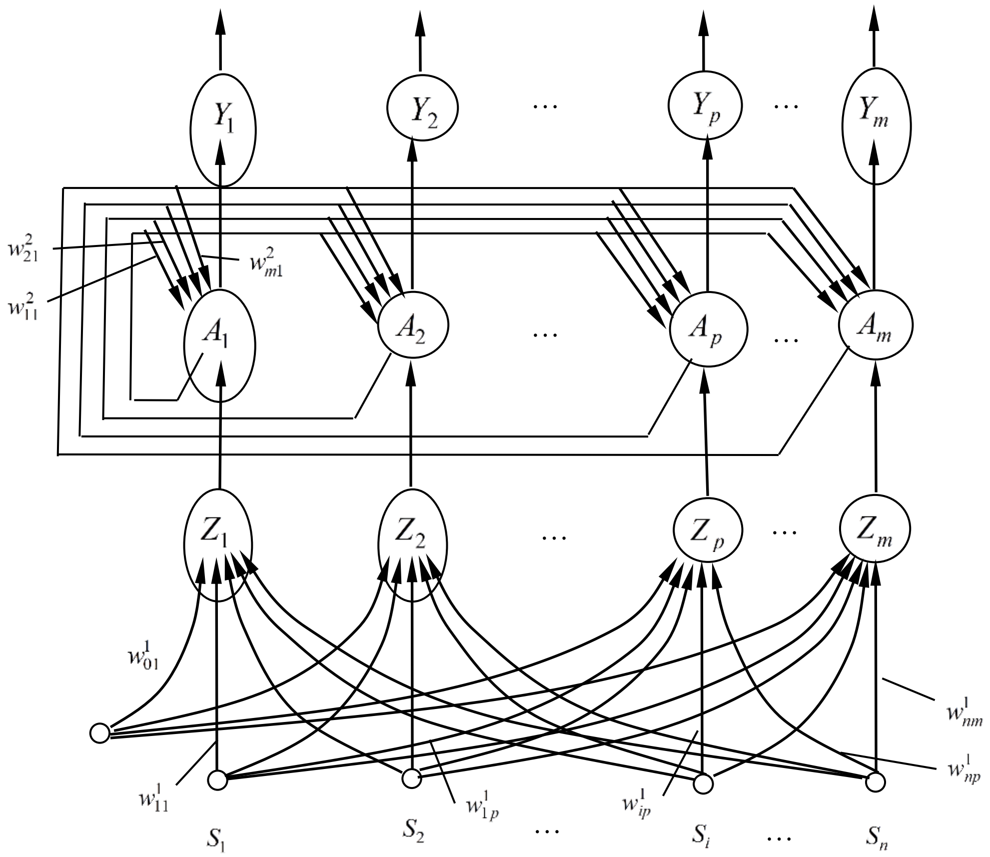

Fig. 1. The Hamming Neural Network

When an image $D^* = (d_1^*, \ldots, d_n^*)$ is fed into the neural network, each Z-element determines its input and output signals according to expressions of the form (2) and (14):

$$U_{inputZp} = n/2 + \frac{n}{2}\sum_{i=1}^{n} w_{ip} d_i^*,$$

$$U_{outZp} = g_z(U_{inputZp}) = a_p, \ p = \overline{1, m}.$$

The output signals from the neurons in the Z-layer are fed to the corresponding inputs of the elements in the A-layer (Fig. 1), which have activation functions described by the equation

$$U_{outAp} = g(U_{inputp}) = \begin{cases} U_{inputp}, \text{ if } U_{inputp} > 0, \\ 0, \text{ if } U_{inputp} \leq 0, \quad p = \overline{1, m}. \end{cases}$$

The weights of the connections between neurons in layer A are determined by the ratio

$$w_{ij}^2 = \begin{cases} 1, \quad \text{if } \ i = j, \\ -\varepsilon, \quad \text{if } \ i \neq j, \quad i, j = \overline{1, m}, \end{cases}$$

where ε is a a constant that satisfies the expression $0 < \varepsilon \leq 1/m$.

The layer of *A*-neurons operates cyclically, and the output signals of its elements are described by the relationship

$$U_{outAj}(t+1) = g(U_{outAj}(t) - \varepsilon \sum_{p=1,\ p\neq j}^{m} U_{outAp}(t)),\ \ j = \overline{1, m}$$

under initial conditions $U_{inputAj}(0) = a_j,\ \ j = \overline{1, m}$.

If there is a single largest input signal among the input signals a_p ($p = \overline{1, m}$), then as a result of the iterative process, only one neuron A_j will have an output signal greater than zero. Since the output signals of the elements in layer *A* are fed to the inputs of the neurons in layer *Y*, which have activation functions of the form

$$g_Y(U_{input}) = \begin{cases} 1, \text{ if } U_{input} > 0, \\ 0, \text{ if } U_{input} \leq 0, \end{cases}$$

then the output of the Hemming network will consist of only one neuron Y_j with a unit output signal. This signal indicates that, in terms of image similarity (2), the input image $D^* = (d_1^*, \ldots, d_n^*)$ is closest to the reference image $B^j = (b_1^j, \ldots, b_n^j)$.

2.3 Modular representation and the proposed synthesis method

Hemming's neural network can also be represented in a more general form (Fig. 2).

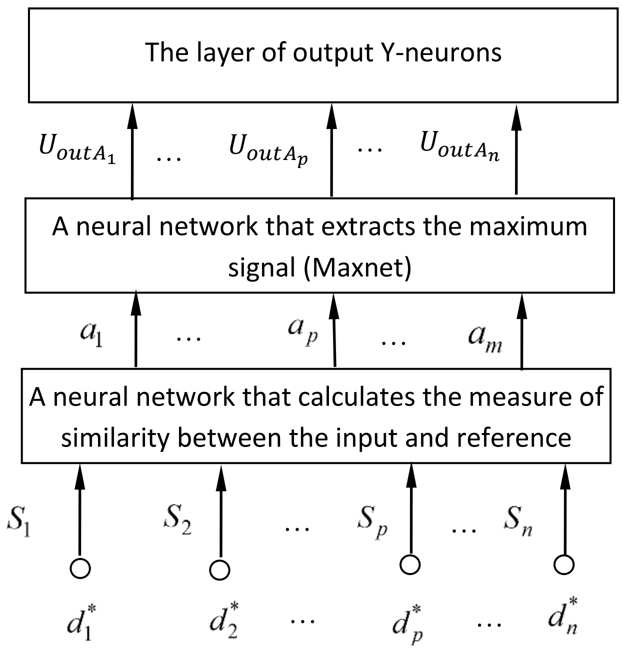

(input image $D^* = (d_1^*, d_2^*, \ldots, d_{p,}^*\ \ldots, d_n^*)$

Fig. 2. Block diagram of the Hamming neural network

This representation of the Hamming neural network shows that the two main blocks of the network can be modified independently of one another. In particular, instead of a Maxnet, a neural network that identifies several identical maximum signals can be used. This makes it possible to find reference images that are all at the same minimum distance from the input [3, 11]. It also follows from the network architecture (Fig. 2) that the block calculating the measure of proximity between the input and reference images can compute various measures of proximity. The relative independence of the main blocks in the Hamming neural network makes it possible to propose neural networks both for working with binary images (vectors) and for using various affinity functions of the form (7) – (13) between the input and reference binary images.

In the Hamming neural network (Fig. 1), the scalar product of two binary vectors $D = (d_1, \ldots, d_n)$, $B = (b_1, \ldots, b_n)$ is computed as follows:

$$DB = \sum_{i=1}^{n} d_i b_i = (a+b) - (f+e) \tag{15}$$

where *a*, *b*, *f*, and *e* are variables defined by equations (3) – (6), with vector *D* being the input vector and vector *B* being the vector of neuron connection weights used to compute the scalar product. Since $(a+b)+(f+e)=n$, we can derive from (15) that

$$\sum_{i=1}^{n} d_i b_i = 2(a+b) - n$$

or

$$(a+b) = \frac{n}{2} + \frac{1}{2}\sum_{i=1}^{n} d_i b_i \ .$$

In a Hamming neural network, the value of the expression (*a* + *b*) is computed using a single neuron (Fig. 3). In the case of binary encoding of object features or binary vectors, it is not possible to use a Hamming network to compute the scalar product of two vectors. Most of the affinity functions (7) – (13) cannot be computed using a single neuron either. To compute these functions, one must first determine functions (3) – (6) using separate neurons and then use them to compute the affinity functions (7) – (13).

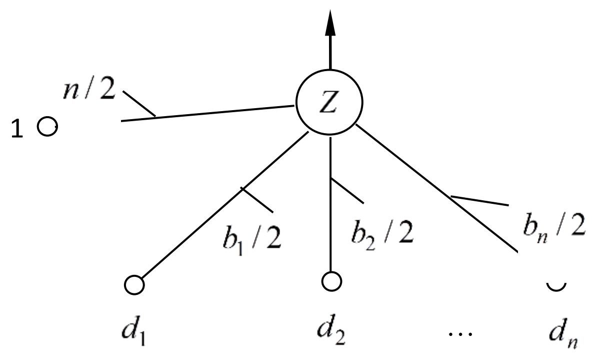

Fig. 3. A neuron for computing the scalar product of two bipolar vectors in a Hamming neural network;

$n/2$, $b_1/2$, $b_2/2$, …, $b_n/2$ are the neuron's connection weights; d_1, d_2, …, d_n are the components of the input vector.

Figure 4 shows a neuron for computing the variable *a*. The neuron's G_1 input signals are determined by the components of the binary vector *D*, and the connection weights are determined by the components of the binary vector $B = (b_1, \ldots, b_n)$. Figure 5 shows a block for computing the variable *b* (Equation (4)). In this block, using the summing elements Σ_1, … , Σ_n the input signals $(1-d_1)$, $(1-d_2)$, …, $(1-d_n)$ of neuron G_2 are first computed; these are then multiplied by the corresponding weight coefficients $(1-b_1)$, $(1-b_2)$, …, $(1-b_n)$ and subsequently summed by the element G_2. This leads to the computation of Equation (4). If, in Fig. 5, the input signals d_1, d_2, …, d_n are applied to the inputs of neuron G_2 instead of the signals $(1-d_1)$, $(1-d_2)$, …, $(1-d_n)$ computed by the summation elements, then neuron G_2 will compute the variable *e* (Equation (6)).

To compute the variable f (Equation (5)) in Fig. 5, it suffices to replace the weight coefficients $(1-b_1)$, $(1-b_2)$, …, $(1-b_n)$ with the corresponding weight coefficients $(b_1, \ldots, b_n)$.

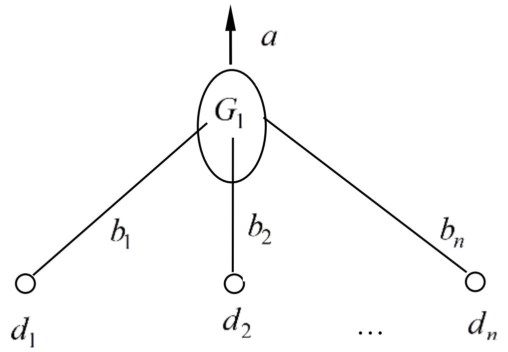

Fig. 4. A neuron for computing the variable a; b_1, b_2, …, b_n are the neuron's connection weights; d_1, d_2, …, d_n are the components of the input vector.

Given neurons or neural components for computing the variables *a, b, f,* and *e,* it is straightforward to derive neural networks for computing any of the affinity functions (7) – (13). Let us consider the most complex of these — the Kulchinsky 2 affine function. The neural network for calculating the proximity measure between the input and reference images is shown in Fig. 6.

Similarly, a neural network can be synthesized to compute any other affine function from the given list. In particular, Fig. 7 shows a neural network for computing the Yule affine function (equation (13)).

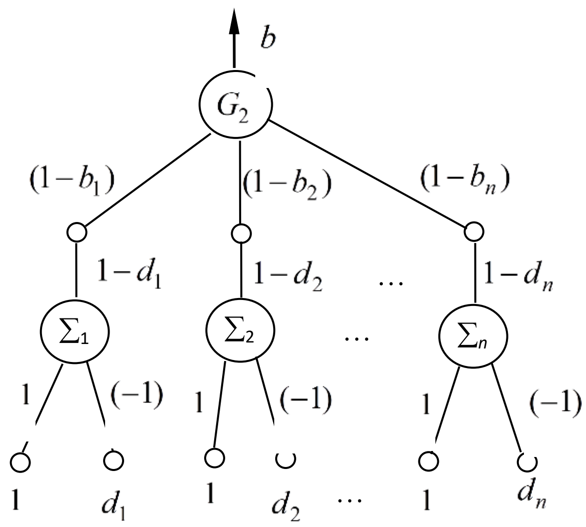

Fig. 5. A neuron for computing the variable b. The following notation is used in the figure: $(1-b_1)$, $(1-b_2)$, …, $(1-b_n)$ are the connection weights of the neuron ; G_2; Σ_1, …, Σ_n are summing elements for computing the G_2 neuron's input signals.

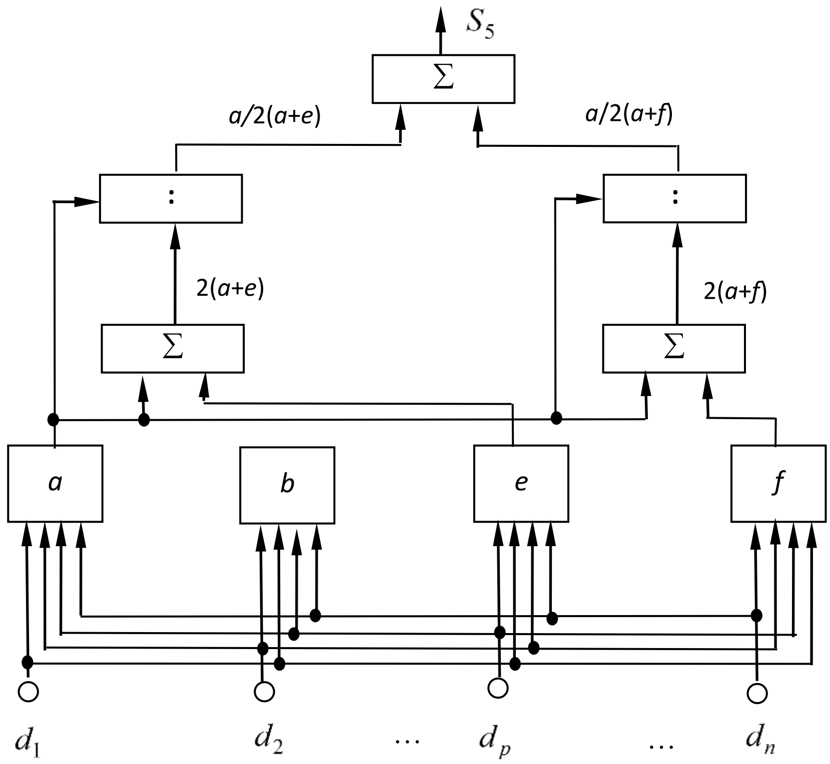

Fig. 6. Neural network computing the Kulchinsky function 2.

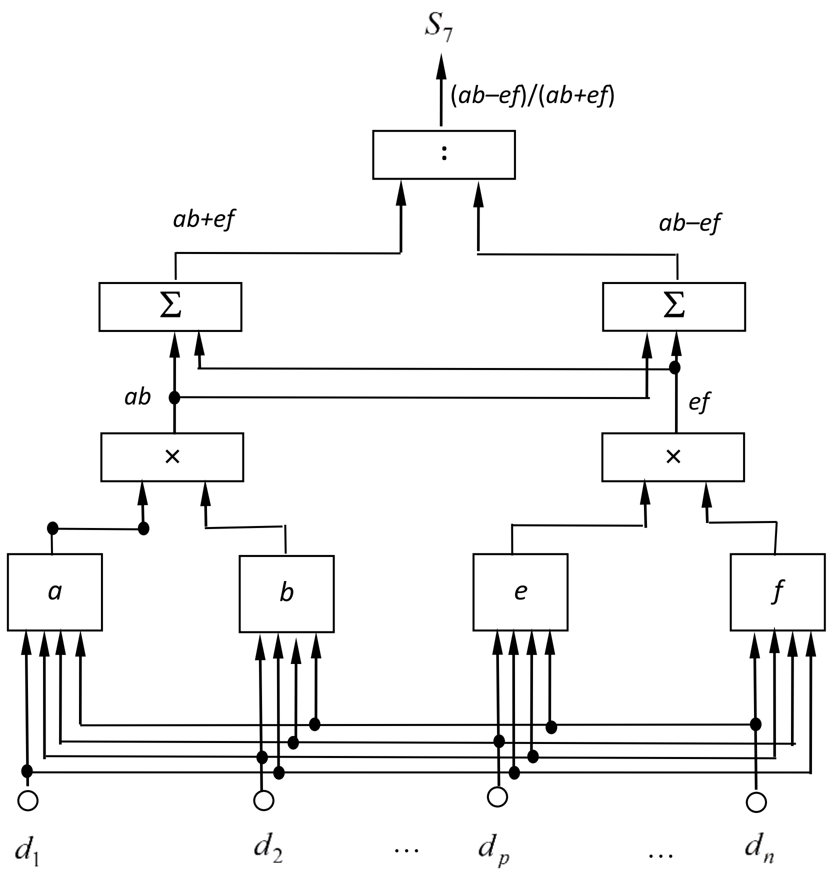

Fig. 7. Neural network that computes the Eul's affinity function.

3. Results

The numerical experiment (Example 1, Table 2) yields the following primary findings on the behavior of the affinity functions S1 – S7:

- they attain their minimum values for vectors with opposite binary components.
- they attain their maximum values for a pair of identical binary vectors.
- for vectors that are neither identical nor opposite, S1 – S7 take intermediate values between their maxima and minima.

In contrast, the Hamming distance behaves oppositely: minimal for identical vectors and maximal for vectors sharing no identical digit.

The affinity functions are not exhausted by (3) – (13) [4 – 10]; their large number indicates the absence of a single universal function, and there are no generally accepted recommendations for their application. In practice, the affinity function is chosen through computer simulation in the binary-encoded feature space.

The methodological results form a complete constructive synthesis procedure:

- elementary blocks compute a (Fig. 4), b, e, f (Fig. 5) directly from binary inputs;
- composite networks realize complex functions: Kulczynski 2 (Fig. 6, S5) and Yule (Fig. 7, S7);
- the modular architecture (Fig. 2) permits independent substitution of both the similarity-measure block (any of S1 – S7) and the Maxnet block (several solutions).

Thus, networks were obtained that operate directly on binary vectors and evaluate a broad family of affinity measures, whereas the original Hamming network is restricted to bipolar encoding and the similarity of Eq. (2).

4. Discussion

The results confirm and extend prior work [4 – 7] on the diversity of affinity measures for binary objects. Whereas the standard Hamming network [1 – 3] relies solely on the bipolar scalar product and effectively on a single criterion (Eq. 2), our modular reinterpretation (Fig. 2) reveals that the proximity-measure block and the decision block are functionally decoupled — the key insight enabling direct realization of the whole family S1 – S7.

Comparison with the Hamming distance (Table 2) clarifies why the bipolar network cannot be reused for binary encoding: the Hamming distance and the affinity functions respond in opposite directions, and functions such as Jaccard (8), Sokal–Michener (9), Kulczynski (10) – (11), Dice (12) and Yule (13) require the joint quantities a, b, e, f, which the single scalar-product neuron (Fig. 3) cannot produce. Our method resolves this by materializing a, b, e, f as separate blocks (Figs. 4 – 5) and composing them with adders, multipliers and dividers (Figs. 6 – 7), generalizing the ART-1 use of the binary scalar product [1, 2] far beyond the single feature a.

Replacing Maxnet by a network isolating several equal maximal signals [3, 11] allows reporting multiple equidistant reference images — particularly relevant since different measures can produce ties.

A recognized limitation, consistent with [4 – 10], is that no single affinity function is universally optimal; the choice remains task-dependent and is settled through simulation. The proposed method does not remove this need but provides a uniform, replicable way to instantiate whichever function is selected, lowering the cost of experimentation.

5. Conclusions

The Hamming neural network is an effective tool for recognizing and classifying discrete objects encoded with a bipolar alphabet, where the proximity measure is the difference between the number of identical bipolar components and the Hamming distance. However, it cannot be applied under binary encoding, nor can it evaluate affinity using the Jaccard, Sokal–Michener, Kulczynski and similar functions.

To overcome this, a method for synthesizing neural networks that assess binary-vector proximity using these affinity measures has been developed. Building on elementary blocks that compute a, b, e, f, the method constructs networks for arbitrarily complex functions, as demonstrated for

Kulczynski 2 (Fig. 6) and Yule (Fig. 7). This extends the applicability of neural networks to tasks relying on finer proximity features of binary-encoded objects.

Moreover, because the modular architecture allows Maxnet to be replaced by a network that can determine several solutions (when they exist), it is possible to synthesize networks returning a predefined number of solutions. The main significance of the study is twofold: it broadens the class of similarity criteria realizable by Hamming-type networks, and it provides a uniform, replicable synthesis procedure for both the proximity-measure and the decision stages.

References

[1] Ke-Lin Du , M.N.S. Swamy. Neural Networks and Statistical Learning, 2nd edition. Springer (2019).

[2] M.T. Hagan, H.B. Demuth, M.H. Beale, O. De Jesús. Neural Network Design, 2nd edition (2014).

[3] Dmitrienko, V.D., Zakovorotny, A.Yu., and Leonov, S.Yu. Hamming neural network for solving problems with several solutions, Bulletin of NTU "KPI, , Kharkiv, NTU "KPI", No. 50 (1271) (2017). 119-129.

[4] Babichev, S.A. Theoretical and practical principles of information technology for processing gene expression profiles for gene network reconstruction. Dissertation for the degree of Doctor of Technical Sciences (2018).

[5] Dmitrienko, V.D., Khavina, I.P., Zakovorotny, A.Yu., Lipchansky, M.V., and Mezentsev, N.V. Methods and algorithms of artificial intelligence systems, Kiev, Kafedra, (2014).

[6] Richard O. Duda, Peter E. Hart, David G. Stork — Pattern Classification, 2nd edition. Wiley (2001).

[7] Christopher M. Bishop. Pattern Recognition and Machine Learning. Springer (2006).

[8] Andrew R. Webb, Keith D. Copsey. Statistical Pattern Recognition, 3rd edition. Wiley (2011).

[9] Lynne Billard, Edwin Diday. Symbolic Data Analysis: Conceptual Statistics and Data Mining. Wiley (2006).

[10] Charu C. Aggarwal, Chandan K. Reddy (eds.) Data Clustering: Algorithms and Applications. CRC Press (2013).

[11] N. Ikeda, P. Watta, M. Artiklar, M. Hassoun. A two-level Hamming network for high performance associative memory. Neural Networks (2001).

Journal of Mathematical Models and Methods in Engineering

journal homepage: https://jmmme.uz/index.php/journal

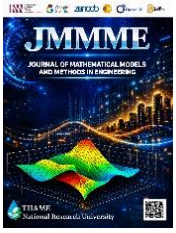

Some identities involving hypergeometric functions

A.B.Okboev[1*], A.A.Verlan [2]

[1] *"Tashkent institute of irrigation and agricultural mechanization engineers" National Research University, Tashkent, 100000, Uzbekistan*
[2]*National Technical University of Ukraine "Igor Sikorsky Kyiv Polytechnic Institute", Kyiv, Ukraine*

ARTICLE INFO

Keywords:
Hypergeometric functions,
Mathematical identities,
Laplace transform,
Kampé de Fériet function,
Differential equations

ABSTRACT

This paper focuses on formulating and proving some identities involving hypergeometric functions. The main result generalizes an identity previously proven for specific cases, specifically for $m=1$ and $m=2$ with $b=a-1$. To prove the primary identity, the Laplace transform method is employed. The mathematical proof also utilizes the notations introduced by Srivastava and Daoust, as well as the properties of the Kampé de Fériet function. Additionally, a second identity is formulated and presented. These generalized identities can be actively applied to analyze and solve various boundary-value problems in the theory of differential equations.

1. Introduction

Hypergeometric functions have a wide range of practical applications in physics, engineering, mathematical statistics, and various other scientific fields. Notably, they are extensively used as a powerful mathematical tool for analyzing and solving complex problems within the theory of differential equations.

In the existing literature, numerous boundary-value problems and fundamental solutions have been successfully constructed by utilizing the unique properties of hypergeometric functions [1-6]. For instance, Salakhitdinov and Urinov explored eigenvalue problems for mixed-type equations featuring two singular coefficients [1]. Similarly, hypergeometric functions have been instrumental in finding fundamental solutions for the generalized bi-axially symmetric Helmholtz equation [3, 4] and certain classes of three-dimensional elliptic equations with singular coefficients [5].

Furthermore, obtaining explicit solutions to specific boundary-value problems often requires the use of mathematical identities containing hypergeometric functions [7-11]. Such identities have played a crucial role in solving the Cauchy problem for degenerating hyperbolic equations of the second kind [7, 9]. They have also been actively applied to the Tricomi problem for elliptic-hyperbolic and parabolic-hyperbolic type equations [8, 10] , as well as for solving non-local boundary-value problems [11].

The present work builds directly upon these foundational studies. Specifically, the core identity (1) discussed in this paper was initially proven by N. K. Mamadaliev for the specific case where

* Corresponding author. A.B.Okboev
E-mail addresses: a_oqboev@tiiame.uz

$m=1$ and $b=a-1$ [8]. In a subsequent study, this result was extended and proven for the case where $m=2$ and $b=a-1$ [10]. Motivated by these previous achievements, this article aims to formulate and rigorously prove a generalized identity involving hypergeometric functions, which can further broaden their application in the theory of differential equations.

2. Preliminaries and Notation

To establish our main identities, we first need to recall some foundational definitions and notations. Multiple hypergeometric series can often become cumbersome to write and manipulate. However, they can be elegantly and compactly represented using the generalized Kampé de Fériet function. According to the notation formally introduced by Srivastava and Daoust (1969), this function in multiple variables is defined as follows:

$$F^{A:B^{(1)};...;B^{(n)}}_{C:D^{(1)};...;D^{(n)}}\left(\begin{matrix}\left[a:\theta^{(1)},...,\theta^{(n)}\right]:\left[b^{(1)}:\varphi^{(1)}\right];...;\left[b^{(n)}:\varphi^{(n)}\right];\\ x_1,...,x_n\\ \left[c:\psi^{(1)},...,\psi^{(n)}\right]:\left[d^{(1)}:\delta^{(1)}\right];...;\left[d^{(n)}:\delta^{(n)}\right];\end{matrix}\right)=\sum_{m_1,...,m_n=0}^{\infty}\Omega\left(m_1,...,m_n\right)\frac{x_1^{m_1}}{m_1!}...\frac{x_n^{m_n}}{m_n!}$$

where the multiple sequence $\Omega\left(m_1,...,m_n\right)$ is given by the quotient of products of the Pochhammer symbols:

$$\Omega\left(m_1,...,m_n\right)=\frac{\prod_{j=1}^{A}\left(a_j\right)_{m_1\theta_j^{(1)}+...+m_n\theta_j^{(n)}}\prod_{j=1}^{B^{(1)}}\left(b_j^{(1)}\right)_{m_1\varphi_j^{(1)}}...\prod_{j=1}^{B^{(n)}}\left(b_j^{(n)}\right)_{m_n\varphi_j^{(n)}}}{\prod_{j=1}^{C}\left(c_j\right)_{m_1\psi_j^{(1)}+...+m_n\psi_j^{(n)}}\prod_{j=1}^{D^{(1)}}\left(d_j^{(1)}\right)_{m_1\delta_j^{(1)}}...\prod_{j=1}^{D^{(n)}}\left(d_j^{(n)}\right)_{m_n\delta_j^{(n)}}}$$

By utilizing this compact notation, we can transform complex multiple sums into a more manageable and recognizable form. Specifically, if we expand the left-hand side of our proposed identity (1) into a power series and systematically rearrange the terms, it can be sequentially rewritten in the following manner:

$$\sum_{k_1=0}^{n_1}...\sum_{k_m=0}^{n_m}\prod_{i=1}^{m}\binom{n_i}{k_i}\frac{(-1)^k(1/2-b)_k}{(n+a)_k}(4x)^kF(n-k+b,-n+k-b+1,n+k+a;x)=$$
$$=\sum_{k_1=0}^{n_1}...\sum_{k_m=0}^{n_m}\sum_{l=0}^{\infty}\prod_{i=1}^{m}\frac{(-n_i)_{k_i}(1/2-b)_k}{(n+a)_k}\frac{(n-k+b)_l(-n+k-b+1)_l}{(n+k+a)_l}\frac{(4x)^{k_i}}{k_i!}\frac{x^l}{l!}=$$
$$=\sum_{k_1=0}^{n_1}...\sum_{k_m=0}^{n_m}\sum_{l=0}^{\infty}\prod_{i=1}^{m}\frac{(-n_i)_{k_i}(1/2-b)_k}{(n+a)_{k+l}}\frac{(-1)^l(1-n-b)_{k+l}}{(1-n-b)_{k-l}}\frac{(4x)^{k_i}}{k_i!}\frac{x^l}{l!}=$$
$$=F^{2:m;...;0}_{2:0;...;0}\left(\begin{matrix}[1/2-b:1,...,1,0],[1-n-b:1,...,1,1]:[-n_1:1],...,[-n_m:1];-;...;-\\ 4x,...,4x,-x\\ [n+a:1,...,1,1],[1-n-b:1,...,1,-1]:---------;-;...;-;\end{matrix}\right).$$

This preliminary transformation is crucial, as it sets the stage for the rigorous proof of our main theorems using integral transforms.

3. Main Results

In this section, we present the primary findings of our research. The core result is a generalized mathematical identity that equates a complex multiple summation involving Gaussian hypergeometric functions to a single hypergeometric function.

Theorem 1. Let the real parameters satisfy $a\ge b>0$ and let $x\ge 0$. Then, the following identity holds true:

$$\sum_{k_1=0}^{n_1}...\sum_{k_m=0}^{n_m}\prod_{i=1}^{m}\binom{n_i}{k_i}\frac{(-1)^k(1/2-b)_k}{(n+a)_k}(4x)^kF(n-k+b,-n+k-b+1,n+k+a;x)=$$
$$=F(1+n-b,-n+b,n+a;x). \quad (1)$$

In the formulation above, the integer parameters are defined such that $m, n_j \in \mathbb{N}$ for $j = 1, 2, ..., m$. Furthermore, the sums of the respective indices are denoted concisely as $n = n_1 + ... + n_m$ and $k = k_1 + ... + k_m$. The binomial coefficients and the Pochhammer symbol (rising factorial) utilized in the identity are defined in the standard mathematical manner:

$$\binom{n}{k} = \frac{n!}{k!(n-k)!} = (-1)^k \frac{(-n)_k}{k!}$$

$$(a)_k = \begin{cases} 1, & k = 0; \\ a(a+1)\cdot ...\cdot (a+k-1), & k \in \mathbb{N}. \end{cases}$$

Following a similar logical framework and methodology, we can establish a second significant identity, which further broadens the scope of our results.

Theorem 2. Assuming that the variable $z \geq 0$ and the parameters satisfy the condition $\pm a, 2b \neq -1, -2, ...$, the following equality is satisfied:

$$\sum_{k_1=0}^{n_1} ... \sum_{k_m=0}^{n_m} \prod_{i=1}^{m} \binom{n_i}{k_i} \frac{(a-n)_k}{(1/2+b)_k} \left(\frac{z}{2}\right)^{2k} F\left(c+k, a+b+2k-2n; 2b+2k; z\right) =$$

$$= \frac{\Gamma(2b)\Gamma(a)}{\Gamma(a+b)\Gamma(b)} z^{1-2b} (1-z)^{-a+n} F(1-a-b, 1-b; 1-a; 1-z).$$

4. Proofs of the Main Results

In this section, we provide the detailed proof for our primary result.

Proof of Theorem 1. To prove Theorem 1, we employ the Laplace transform method. Let us rewrite the left-hand side of identity (1) in the following form:

$$= x^{-a-n+1} B(a, b, n; x) \tag{2}$$

where the function $B(a, b, n; x)$ is defined as:

$$B(a,b,n;x) = \sum_{k_1=0}^{n_1} ... \sum_{k_m=0}^{n_m} \prod_{i=1}^{m} \binom{n_i}{k_i} \frac{(-1)^k (1/2-b)_k}{(n+a)_k} 4^k \times$$

$$\times x^{a+n+k-1} F(n-k+b, -n+k-b+1, n+k+a; x) \tag{3}$$

By making the substitution $x = 1 - e^{-t}$ (where $t > 0$) in equation (3), we obtain:

$$B(a,b,n;1-e^{-t}) = \sum_{k_1=0}^{n_1} ... \sum_{k_m=0}^{n_m} \prod_{i=1}^{m} \binom{n_i}{k_i} \frac{(-1)^k (1/2-b)_k}{(n+a)_k} 4^k \times$$

$$\times (1-e^{-t})^{a+n+k-1} F(n-k+b, -n+k-b+1, n+k+a; 1-e^{-t}).$$

Next, let us introduce the Laplace transform of this function with respect to the variable t:

$$\Phi(a,b;n;p) = \int_0^{+\infty} e^{-pt} B(a,b,n;1-e^{-t}) dt \leftrightarrow B(a,b,n;1-e^{-t}).$$

Using the standard tables of integral transforms (e.g., Bateman and Erdélyi [13]), we use the following known operational relation:

$$(1-e^{-t})^{c-1} F(a,b,c;1-e^{-t}) \leftrightarrow \frac{\Gamma(p)\Gamma(c-a-b+p)\Gamma(c)}{\Gamma(c-a+p)\Gamma(c-b+p)} \tag{4}$$

Applying formula (4), we find the image $\Phi(a,b;n;p)$ as:

$$\Phi(a,b;n;p) = \sum_{k_1=0}^{n_1} ... \sum_{k_m=0}^{n_m} \prod_{i=1}^{m} \binom{n_i}{k_i} \frac{(-1)^k (1/2-b)_k}{(n+a)_k} 4^k \times$$

$$\times \frac{\Gamma(p)\Gamma(a+k+n+p-1)\Gamma(a+n+k)}{\Gamma(a+2k-b+p)\Gamma(a+2n+b+p-1)}.$$

To simplify the gamma terms, we utilize the generalized reduction formula:

$$\Gamma(n+\gamma) = (\gamma)_n \Gamma(\gamma), \quad \gamma > 0 \tag{5}$$

along with the identity:

$$(a)_{2k} = 4^k (a/2)_k (a/2+1/2)_k . \qquad (6)$$

Using these relations, we can rewrite $\Phi(a,b;n;p)$ in terms of the Kampé de Fériet function:

$$\Phi(a,b;n;p) = \frac{\Gamma(p)\Gamma(a+n+p-1)\Gamma(a+n)}{\Gamma(a-b+p)\Gamma(a+2n+b+p-1)} \times$$

$$\times F^{2:1;...;1}_{2:0;...;0}\left(\begin{matrix} [1/2-b, a+n+p-1]:[-n_1];...;[-n_m] \\ 1,...,1 \\ [a/2-b/2+p/2, a/2-b/2+p/2+1/2]:-;...;- \end{matrix}\right).$$

By applying the reduction formula for the Kampé de Fériet function (as provided in [12, p. 39, eq. 32]), this multiple series collapses into a generalized hypergeometric series ${}_3F_2$:

$$\Phi(a,b;n;p) = \frac{\Gamma(p)\Gamma(a+n+p-1)\Gamma(a+n)}{\Gamma(a-b+p)\Gamma(a+2n+b+p-1)} \times$$

$$\times {}_3F_2\left(\begin{matrix} -n, 1/2-b, a+n+p-1; \\ a/2-b/2+p/2, a/2-b/2+p/2+1/2 \end{matrix} 1\right)$$

Next, we evaluate the ${}_3F_2$ series at unit argument using Prudnikov's formula (see [14, p. 454, eq. 87]):

$$\Phi(a,b;n;p) = \frac{\Gamma(p)\Gamma(a+n+p-1)\Gamma(a+n)}{\Gamma(a-b+p)\Gamma(a+2n+b+p-1)} \times$$

$$\times \frac{(a/2+b/2+p/2-1/2)_n(-a/2-b/2-p/2-n+1)_n}{(a/2-b/2+p/2)_n(-a/2+b/2-p/2+1/2-n)_n}$$

Applying the property $(a-n)_n = (-1)^n(1-a)_n$, together with formulas (5) and (6), the expression drastically simplifies to:

$$\Phi(a,b;n;p) = \frac{\Gamma(p)\Gamma(a+n+p-1)\Gamma(a+n)}{\Gamma(a-b+p+2n)\Gamma(a+b+p-1)}.$$

Now, we find the original function (inverse Laplace transform) according to our previously stated relation (4):

$$\Phi(a,b;n;p) \leftrightarrow (1-e^{-t})^{a+n-1} F(b-n, 1-b+n; a+n; 1-e^{-t}) = B(a,b,n;1-e^{-t}) .$$

Making the reverse substitution $e^{-t} = 1-x$, we obtain the explicit form for B(a,b,n;x):

$$B(a,b,n;x) = x^{a+n-1} F(b-n, 1-b+n; a+n; x) .$$

Finally, substituting this resulting expression for $B(a,b,n;x)$ back into equation (2) directly yields the right-hand side of identity (1). This concludes the proof of Theorem 1.

The proof of Theorem 2 proceeds along the same logical lines and methodology as the proof of Theorem 1. By rewriting the multiple summation and applying the Laplace transform method, the expression can be similarly represented in terms of the Kampé de Fériet function. Utilizing the relevant operational relations for integral transforms and the generalized reduction formulas for hypergeometric series, the complex series simplifies directly to the explicit form presented on the right-hand side. Since the underlying analytical steps are strictly analogous to those demonstrated in detail for Theorem 1, they are omitted here for the sake of brevity.

5. Conclusion

In this paper, we have successfully formulated and rigorously proven generalized mathematical identities involving Gaussian hypergeometric functions. By systematically employing the Laplace transform method and utilizing the properties of the generalized Kampé de Fériet function, we demonstrated that complex multiple summations can be elegantly reduced to a single hypergeometric function.

These main results significantly extend previous foundational studies in this area, specifically generalizing the identities that were previously established only for restricted cases (such as $m=1$ and $m=2$). The newly proven identities not only contribute to the theoretical development of special functions but also hold substantial potential for broader mathematical applications. In particular, we anticipate that these generalized identities will be actively utilized as an effective analytical tool for constructing fundamental solutions and solving various complex boundary-value problems within the theory of differential equations.

References

[1] Salakhitdinov, M. S., & Urinov, A. K. (2007). Eigenvalue problems for a mixed-type equation with two singular coefficients. *Siberian Mathematical Journal*, 48(4), 707-717.

[2] Juraev, T. D., & Apakov, Yu. P. (2007). On self-similar solution of one third order equation with multiple characteristics (in Russian). Vestn. Sam. Gos. Tekn. Un-ta. Ser. Fiz.-mat. Nauki, 2(15), 18–26.

[3] Hasanov, A. (2007). Fundamental solutions of generalized bi-axially symmetric Helmholtz equation. *Complex Variables and Elliptic Equations*, 52(8), 673-683.

[4] Urinov, A. K., & Ergashev, T. G. (2018). Confluent hypergeometric functions of many variables and their application to the finding of fundamental solutions of the generalized Helmholtz equation with singular coefficients. Vestn. Tomsk. Gos. Univ. Mat. Mekh., 55, 45–56.

[5] Hasanov, A., & Karimov, E. T. (2009). Fundamental solutions for a class of three-dimensional elliptic equations with singular coefficients. *Applied Mathematics Letters*, 22(12), 1828-1832.

[6] Irgashev, B. Y. (2023). Application of hypergeometric functions to the construction of particular solutions. *Complex Variables and Elliptic Equations*. DOI: 10.1080/17476933.2023.2270910.

[7] Salakhitdinov, M. S., & Ergashev, T. G. (1995). Integral representation of the generalized solution of the Cauchy problem in the class Rl2k for a hyperbolic type equation of the second kind (in Russian). *Uzbek Mathematical Journal*, 1, 67-75.

[8] Mamadaliev, N. K. (2014). Tricomi problem for an elliptic-hyperbolic equation of the second kind. *Eurasian Mathematical Journal*, 5(3), 80-92.

[9] Ergashev, T. G., & Komilova, N. J. (2022). The Kampe de Feriet series and the regular solution of the Cauchy problem for degenerating hyperbolic equation of the second kind. Lobachevskii Journal of Mathematics, 43(11), 3112-3124.

[10] Okboev, A. B. (2020). Tricomi problem for second kind parabolic hyperbolic type equation. Lobachevskii Journal of Mathematics, 41(1), 58-70.

[11] Urinov, A. K., & Okboev, A. B. (2020). Nonlocal boundary-value problem for a parabolic-hyperbolic equation of the second kind. *Lobachevskii Journal of Mathematics*, 41(9), 1886-1897.

[12] Srivastava, H. M., & Daoust, M. C. (1969). On Eulerian integrals associated with Kampé de Fériet’s function. Publ. Inst. Math. (Beograd).

[13] Bateman, H., & Erdélyi, A. (1954). Tables of Integral Transforms (in Russian). Vol 1.

[14] Prudnikov, A. P., Brychkov, Yu. A., & Marichev, O. I. (2003). Integrals and Series. Vol. 3. Special Functions. Supplementary Chapters (2nd ed., in Russian). Moscow: FIZMATLIT.

[15] Srivastava, H. M., & Karlsson, P. W. (1985). Multiple Gaussian Hypergeometric Series. Halsted Press (Ellis Horwood Limited, Chichester); Wiley, New York, Chichester, Brisbane, and Toronto.

Journal of Mathematical Models and Methods in Engineering 1 (2026)

Journal of Mathematical Models and Methods in Engineering

journal homepage: https://jmmme.uz/index.php/journal

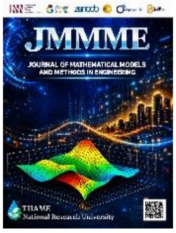

Effect of support conditions on nonlinear parametric vibrations of a viscoelastic anisotropic reinforced composite plate

Bakhtiyor Eshmatov[1*], Abdurakhmon Rayimov[2]

[1] *Department of Higher Mathematics, "Tashkent institute of irrigation and agricultural mechanization engineers" National Research University, Tashkent, 100000, Uzbekistan*
[2] *Department of Mechanics and Computer Simulation, "Tashkent institute of irrigation and agricultural mechanization engineers" National Research University, Tashkent, 100000, Uzbekistan*

ARTICLE INFO

Keywords:
anisotropic reinforced plate,
viscoelasticity,
Koltunov–Rzhanitsyn kernel,
Timoshenko theory,
geometric nonlinearity,
parametric vibrations,
nonlinear dynamics,
effect of boundary conditions,
fiber orientation

ABSTRACT

This study considers the nonlinear dynamics of a rectangular reinforced plate made of glass-reinforced plastic subjected to a periodic compressive load along one pair of edges. The model is based on a refined Timoshenko-type theory, which retains transverse shear and rotary inertia, and it includes geometric nonlinearity together with Boltzmann–Volterra hereditary viscoelasticity governed by the weakly singular Koltunov–Rzhanitsyn kernel. The anisotropy of the structure is described by transformed reduced stiffnesses at an arbitrary reinforcement angle. Applying the Bubnov–Galerkin method reduces the problem to a system of nonlinear integro-differential equations, which are integrated numerically once the singularity of the kernel has been removed. Two sets of boundary conditions are considered: simple support and clamping of all edges, with the material, geometry, rheological parameters, and loading law kept identical, which makes it possible to attribute the difference in the results to the type of support. The sensitivity of the response to the reinforcement angle is shown to be governed by the support conditions: for simple support, rotating the fibers from 0° to 45° reduces the deflection at the midpoint by roughly a factor of three, whereas for clamping the same rotation changes the amplitude by about 10% and in the opposite direction. Taking hereditary properties into account turns undamped vibrations into a decaying process without external damping, in the same way for both types of support. The clamped plate is found to require nine retained modes compared with four for simple support, and the reason for the difference is identified.

1. Introduction

Laminated polymer composites are used in aircraft skins and panels, in blades, and in hull and span structures. Their advantage over metals lies not in stiffness as such, but in the ability to control it through the fiber layup and in the energy dissipated by the polymer matrix. Analyzing such structures requires two properties to be taken into account that are usually ignored for metal structures. Anisotropy is determined by the reinforcement angle and by the stacking sequence, so the laminate stiffnesses depend on direction. Creep and stress relaxation develop in the polymer matrix. Under cyclic loading, part of the energy is dissipated inside the material itself, and this

* Corresponding author. B. Eshmatov
E-mail addresses: ebkh@mail.ru

dissipation is comparable in magnitude to the external damping of the structure.

The way hereditary properties are taken into account determines both the formulation of the problem and its outcome. The Voigt model gives internal friction proportional to frequency, which is not confirmed experimentally: for glass-reinforced plastics, friction over a wide frequency range is almost independent of the strain rate [1, 2]. The Boltzmann–Volterra hereditary model imposes no such restriction, while the Koltunov–Rzhanitsyn kernel, with its weak singularity at $t = 0$, describes the initial stage of relaxation, where the discrepancy with an exponential kernel is most pronounced; its parameters for glass-reinforced plastics have been determined experimentally [3].

Under a periodic compressive load, stability is lost not when the static critical value is reached, but when the excitation frequency falls into a region of dynamic instability, where the amplitude grows even at loads well below the Euler load. The theory of such problems was developed by Bolotin [4], who reduced the equations of motion to a Mathieu–Hill equation; the nonlinear effects of parametric resonance were systematized by Nayfeh and Mook [5], and refined theories of laminated plates are presented by Reddy [6], Qatu [7], and Whitney [8].

Recent work has made the kinematic model more complex and widened the class of materials treated. Darabi and Ganesan [9] constructed the instability boundaries of laminated cylindrical shells using Bolotin's method, Sheng and Wang [10] studied shells made of a functionally graded material under combined parametric and external excitation, Fu et al. [11] extended the analysis to porous conical shells in a thermal environment, and Chen et al. [12] showed that the choice of the kinematic hypothesis shifts the boundaries of these regions. Jain et al. [13] found that the edge support changes the width of the instability zone at least as much as the loading parameters do, yet different support schemes have not been compared systematically.

All of this work shares a common scheme: the problem is reduced to a single second-order equation with periodic coefficients, after which the instability boundaries are constructed using Bolotin's method. The scheme is economical, but it assumes retention of a single mode and linearization, and it introduces dissipation through an external coefficient or through a viscous model, which is inaccurate for polymer composites, where the stress is governed by the entire deformation history.

For viscoelastic systems an integral operator inevitably appears in the equations of motion, and after Bubnov–Galerkin reduction the problem becomes a system of nonlinear integro-differential equations with weakly singular kernels. A stable method of solving them, based on quadrature formulas and on a change of variables that removes the singularity of the kernel, was proposed by Badalov, Eshmatov, and Yusupov [14] and developed further by Verlan, Abdikarimov, and Eshmatov [15]. On this basis a number of problems in the dynamics of viscoelastic thin-walled structures have been solved [16, 17, 18, 19]: accounting for hereditary properties lowers the calculated critical loads and turns the undamped vibrations of the elastic problem into a decaying process.

Within this line of research, the effect of the support conditions remains the least studied. Simple support admits a trigonometric approximation that satisfies the boundary conditions exactly, and for this reason it is used in most calculations; clamping requires different coordinate functions and a larger number of retained modes, and results for clamped plates are reported less often. No direct comparison of the two types of support for identical material, geometry, rheology, and loading law is available in the literature known to the authors. Yet the trends established for simple support are carried over to clamped plates as if they were self-evident. This applies above all to the effect of the reinforcement angle: choosing the layup is a recognized way of lowering the vibration level, but whether the effect survives under clamping remains an open question. The answer has a direct design consequence: if the sensitivity to the reinforcement angle depends on how the edges are supported, then a layup optimization carried out for one support scheme loses its meaning when another is used.

The aim of this work is to carry out such a comparison. Within a single model that includes transverse shear and rotary inertia, von Kármán geometric nonlinearity, laminate anisotropy at an arbitrary reinforcement angle, and hereditary viscoelasticity with the Koltunov–Rzhanitsyn kernel, the behavior of a reinforced plate made of glass-reinforced plastic under a periodic compressive load is calculated. For simple support and for clamping of all edges, convergence with respect to the number of retained modes is examined, and the time histories of the deflection at the midpoint are obtained as the aspect ratio, the thickness, the reinforcement angle, and the frequency of the external load are varied.

The novelty of the work lies in three results. It is shown that the sensitivity of the response to the reinforcement angle is governed by the support conditions: for simple support, rotating the fibers from 0° to 45° reduces the deflection at the midpoint by roughly a factor of three, while for clamping it changes the amplitude by about 10%. The difference is found to persist when hereditary properties are included, because the integral operator multiplies all reduced stiffnesses by the same factor and does not redistribute them between directions. It is also shown that for clamping, convergence is reached with nine retained modes compared with four for simple support, and the reason for the difference is identified.

2. Materials and methods

Consider a rectangular plate with sides a and b, of constant thickness h, composed of K unidirectionally reinforced layers. The fibers of each layer make an angle θ with the Ox axis. Compressive forces are applied to the edges $x = 0$ and $x = a$; these forces vary in time according to the law

$$P(t) = P_0 + P_t \cos\gamma t \qquad (1)$$

where P_0 denotes the constant part of the load, P_t the amplitude of the variable part, and γ the frequency of the external periodic excitation. The analysis model is shown in Fig. 1.

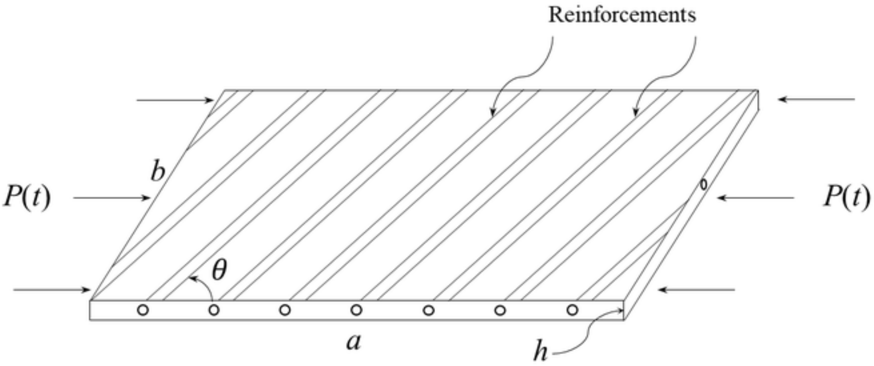

Fig. 1. Reinforced plate under a periodic compressive load

Two limiting cases of edge support are considered: simple support along the entire contour and clamping along the entire contour. All other parameters of the problem are the same in both cases, and this is what makes it possible to attribute the difference in the results to the support conditions rather than to the formulation.

The constitutive relations are based on a refined Timoshenko-type theory, which retains transverse shear strains and rotary inertia [6, 7, 8]. The normal and shear forces N_x, N_y, T, the bending and twisting moments M_x, M_y, H, and the transverse shear forces Q_x, Q_y are related to the midsurface strains and to the rotations of the normal ψ_x, ψ_y by the relations

$$\begin{Bmatrix} N_x \\ N_y \\ T \\ M_x \\ M_y \\ H \\ Q_y \\ Q_x \end{Bmatrix} = \begin{bmatrix} A_{11}^* & A_{12}^* & A_{16}^* & B_{11}^* & B_{12}^* & B_{16}^* & 0 & 0 \\ A_{12}^* & A_{22}^* & A_{26}^* & B_{12}^* & B_{22}^* & B_{26}^* & 0 & 0 \\ A_{16}^* & A_{26}^* & A_{66}^* & B_{16}^* & B_{26}^* & B_{66}^* & 0 & 0 \\ B_{11}^* & B_{12}^* & B_{16}^* & D_{11}^* & D_{12}^* & D_{16}^* & 0 & 0 \\ B_{12}^* & B_{22}^* & B_{26}^* & D_{12}^* & D_{22}^* & D_{26}^* & 0 & 0 \\ B_{16}^* & B_{26}^* & B_{66}^* & D_{16}^* & D_{26}^* & D_{66}^* & 0 & 0 \\ 0 & 0 & 0 & 0 & 0 & 0 & A_{44}^* & A_{45}^* \\ 0 & 0 & 0 & 0 & 0 & 0 & A_{45}^* & A_{55}^* \end{bmatrix} \begin{Bmatrix} \varepsilon_x^0 \\ \varepsilon_y^0 \\ \gamma_{xy}^0 \\ \partial\psi_x/\partial x \\ \partial\psi_y/\partial y \\ \partial\psi_x/\partial y + \partial\psi_y/\partial x \\ \partial w/\partial y + \psi_y \\ \partial w/\partial x + \psi_x \end{Bmatrix} \qquad (2)$$

The matrix in (2) combines the membrane, membrane–bending, bending, and shear characteristics of the laminate.

The operators appearing in (2) are defined by integration through the thickness of the laminate:

$$A_{ij}^{*}\varphi = \sum_{k=1}^{K} Q_{ij}^{*}\,\varphi_k(z_k - z_{k-1}), \qquad B_{ij}^{*}\varphi = \frac{1}{2}\sum_{k=1}^{K} Q_{ij}^{*}\,\varphi_k(z_k^2 - z_{k-1}^2),$$
$$D_{ij}^{*}\varphi = \frac{1}{3}\sum_{k=1}^{K} Q_{ij}^{*}\,\varphi_k(z_k^3 - z_{k-1}^3), \quad i,j = 1,2,6; \qquad A_{ij}^{*}\varphi = K_s\sum_{k=1}^{K} Q_{ij}^{*}\,\varphi_k(z_k - z_{k-1}), \quad i,j = 4,5 \tag{3}$$

where z_k is the coordinate of the upper boundary of the kth layer and K_s is the shear correction factor. The calculations use $K_s = 5/6$, the value adopted in the refined plate theory of Ambartsumyan and Reissner. The overall formulation of the problem follows [19, 20, 21].

The reduced stiffnesses of a layer rotated through an angle θ about the Ox axis are written with the hereditary integral operator included:

$$\begin{aligned}
Q_{11}^{*}\varphi &= [Q_{11}\cos^4\theta + 1/2\,(Q_{12} + 2Q_{66})\sin^2 2\theta + Q_{22}\sin^4\theta](1 - \Gamma^{*})\varphi,\\
Q_{22}^{*}\varphi &= [Q_{11}\sin^4\theta + 1/2\,(Q_{12} + 2Q_{66})\sin^2 2\theta + Q_{22}\cos^4\theta](1 - \Gamma^{*})\varphi,\\
Q_{12}^{*}\varphi &= [1/4\,(Q_{11} + Q_{22} - 4Q_{66})\sin^2 2\theta + Q_{12}(1 - 1/2\sin^2 2\theta)](1 - \Gamma^{*})\varphi,\\
Q_{66}^{*}\varphi &= [1/4\,(Q_{11} - 2Q_{12} + Q_{22})\sin^2 2\theta + Q_{66}\cos^2 2\theta](1 - \Gamma^{*})\varphi,\\
Q_{16}^{*}\varphi &= [Q_{11}\sin\theta\cos^3\theta - 1/4\,(Q_{12} + 2Q_{66})\sin 4\theta - Q_{22}\sin^3\theta\cos\theta](1 - \Gamma^{*})\varphi,\\
Q_{26}^{*}\varphi &= [Q_{11}\sin^3\theta\cos\theta - 1/4\,(Q_{12} + 2Q_{66})\sin 4\theta - Q_{22}\sin\theta\cos^3\theta](1 - \Gamma^{*})\varphi
\end{aligned} \tag{4}$$

The stiffnesses in the principal axes of elasticity are expressed in terms of the engineering constants:

$$Q_{11} = \frac{E_1}{1-\mu_{12}\mu_{21}}, \quad Q_{22} = \frac{E_2}{1-\mu_{12}\mu_{21}}, \quad Q_{12} = \frac{E_1\mu_{21}}{1-\mu_{12}\mu_{21}} = \frac{E_2\mu_{12}}{1-\mu_{12}\mu_{21}}, \quad Q_{66} = G_{12} \tag{5}$$

where E_1 and E_2 are the elastic moduli along and across the fibers, G_{12} is the shear modulus, and μ_{12} and μ_{21} are Poisson's ratios.

Hereditary properties are taken into account through the Boltzmann–Volterra integral operator

$$\Gamma^{*}\varphi = \int_0^t \Gamma\,(t-\tau)\varphi(\tau)d\tau \tag{6}$$

where $\Gamma(t)$ is the relaxation kernel, t is the observation time, and τ is a preceding instant of time.

The midsurface strains are related to the displacements u, v, and w in the von Kármán sense:

$$\varepsilon_x^0 = \frac{\partial u}{\partial x} + \frac{1}{2}\left(\frac{\partial w}{\partial x}\right)^2, \qquad \varepsilon_y^0 = \frac{\partial v}{\partial y} + \frac{1}{2}\left(\frac{\partial w}{\partial y}\right)^2, \qquad \gamma_{xy}^0 = \frac{\partial u}{\partial y} + \frac{\partial v}{\partial x} + \frac{\partial w}{\partial x}\frac{\partial w}{\partial y} \tag{7}$$

The quadratic terms in (7) couple bending with stretching of the midsurface and limit the growth of the amplitude at parametric resonance.

Substituting (1), (2), and (7) into the equations of motion gives

$$\begin{aligned}
&\frac{\partial N_x}{\partial x} + \frac{\partial T}{\partial y} + p_x = \rho\frac{\partial^2 u}{\partial t^2}, \qquad \frac{\partial T}{\partial x} + \frac{\partial N_y}{\partial y} + p_y = \rho\frac{\partial^2 v}{\partial t^2},\\
&\frac{\partial Q_x}{\partial x} + \frac{\partial Q_y}{\partial y} + \frac{\partial}{\partial x}\left(N_x\frac{\partial w}{\partial x} + T\frac{\partial w}{\partial y}\right) + \frac{\partial}{\partial y}\left(T\frac{\partial w}{\partial x} + N_y\frac{\partial w}{\partial y}\right) + P(t)\frac{\partial^2 w}{\partial x^2} + q = \rho\frac{\partial^2 w}{\partial t^2},\\
&\frac{\partial M_x}{\partial x} + \frac{\partial H}{\partial y} - Q_x = \frac{\rho h^2}{12}\frac{\partial^2 \psi_x}{\partial t^2}, \qquad \frac{\partial H}{\partial x} + \frac{\partial M_y}{\partial y} - Q_y = \frac{\rho h^2}{12}\frac{\partial^2 \psi_y}{\partial t^2}
\end{aligned} \tag{8}$$

where ρ is the density of the material, and p_x, p_y, and q are the components of the external surface load. The last two equations in (8) describe the rotary inertia of the normal. The term $P(t)\,\partial^2 w/\partial x^2$ introduces parametric excitation: the coefficient of the second derivative of the deflection depends on time.

System (8) in the five unknowns u, v, w, ψ_x, and ψ_y is a set of nonlinear partial integro-differential equations; the integral operator enters through the stiffnesses (4).

The weakly singular Koltunov–Rzhanitsyn kernel is taken as the relaxation kernel

$$\Gamma(t) = A\,e^{-\beta t}\,t^{\alpha-1}, \qquad 0 < \alpha < 1 \tag{9}$$

with rheological parameters A, α, and β determined from relaxation tests [1, 2]. The calculations use the values $A = 0.0208$, $\alpha = 0.1$, and $\beta = 0.00166$, obtained for glass-reinforced plastics [3].

The solution of system (8) is sought in the form of expansions in coordinate functions that satisfy the boundary conditions of the problem.

The number of retained terms was chosen on the basis of the convergence analysis given in Section 3: for simple support the first four harmonics were retained ($M = N = 2$), and for clamping the first nine ($M = N = 3$).

Kernel (9) has a singularity at $t = 0$, so quadrature formulas cannot be applied directly to the integral term. The singularity is removed by a change of the integration variable, after which the kernel becomes regular, and quadrature formulas are then applied to the transformed system following the scheme proposed in [14] and developed in [15]. At each time step this yields a system of algebraic equations, which is solved sequentially. The initial conditions are taken to be zero.

The calculations were carried out for a plate of KAST-V glass-reinforced plastic [3] with the following properties: $E_1 = 25.5$ GPa, $E_2 = 14.91$ GPa, $G_{12} = 4.41$ GPa, $\mu_{12} = 0.2$, $\rho = 1900$ kg/m^3. The baseline geometry is $a = b = 0.5$ m, $h = 0.5$ cm, and the reinforcement angle is $\theta = 45°$. In studying the effect of individual parameters, the aspect ratio $\lambda = a/b$ was varied from 1 to 1.4, the thickness from 0.48 to 0.52 cm, the reinforcement angle from 0 to 45°, and the frequency of the external load γ from 1 to 3; the remaining quantities were kept unchanged.

3. Results

All the curves given below refer to the deflection at the midpoint of the plate. The calculations for simple support and for clamping were carried out as part of the studies [20, 21]; in the present paper they are compared with each other for the first time for identical material, geometry, rheological parameters, and loading law. The deflection is given in meters and the time in seconds. Each figure has two panels: a corresponds to simple support and b to clamping. All other conditions within a given figure are the same, so the difference between the panels is due solely to the way the edges are supported.

Convergence with respect to the number of retained modes was checked separately for the elastic and for the viscoelastic formulation, since the hereditary integral operator changes the nature of the solution and could affect the number of series terms required.

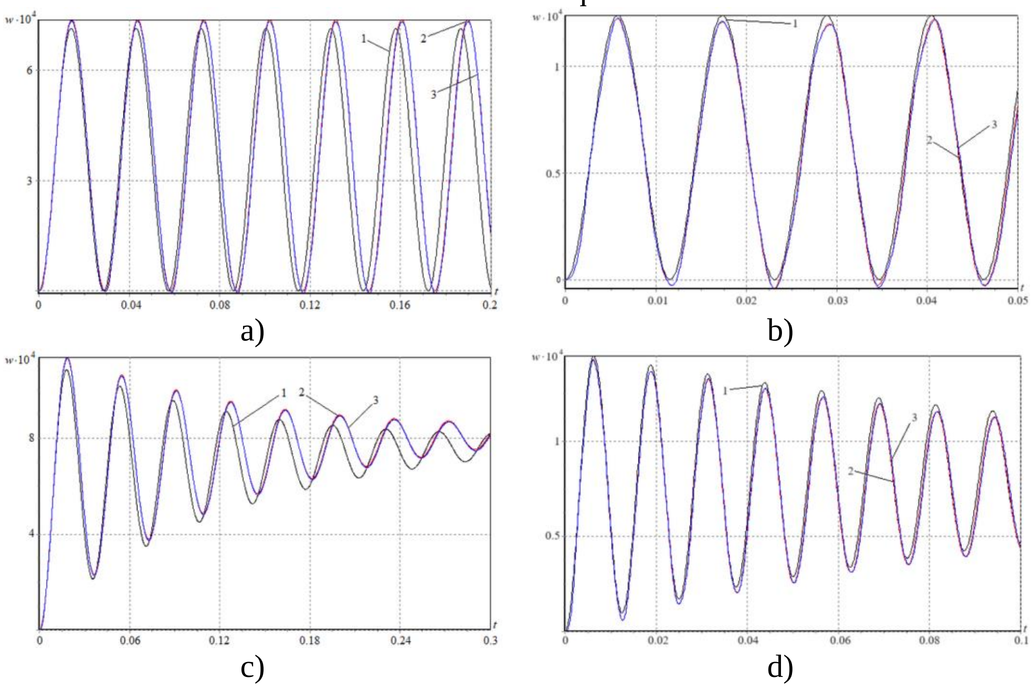

Fig. 2. Convergence of the Bubnov–Galerkin method: a and b – elastic problem, c and d – viscoelastic problem; a and c – simple support (curves: 1 – $M = N = 1$, 2 – $M = N = 2$, 3 – $M = N = 3$), b and d – clamping (curves: 1 – $M = N = 2$, 2 – $M = N = 3$, 3 – $M = N = 4$)

For simple support, retaining the first four harmonics ($M = N = 2$) gives a curve that is virtually indistinguishable from the solution for nine harmonics: the difference in amplitude is smaller than the line thickness. Increasing the number of terms further does not change the result, so the remaining calculations for this type of support use $M = N = 2$.

For clamping, four harmonics are insufficient: the solution for $M = N = 2$ differs noticeably from the solutions for $M = N = 3$ and $M = N = 4$, whereas the latter two are virtually indistinguishable. The remaining calculations for the clamped plate use $M = N = 3$, that is, nine retained modes.

The difference in the number of modes required is explained by the form of the coordinate functions. The trigonometric functions used for simple support coincide with the natural vibration modes of the plate, and the first of them alone carries the main part of the solution. The beam functions used for clamping contain hyperbolic terms whose contribution is concentrated near the edges and decays rapidly toward the interior of the plate, so more series terms are needed to describe the edge zone.

Comparing the panels of Fig. 2 gives a second result, unrelated to convergence. In the elastic problem the deflection curves represent undamped vibrations of constant amplitude, whereas including hereditary properties leads to a monotonic decay of the amplitude with time. The decay arises without any external damping and is caused by energy dissipation in the polymer matrix, described by the integral operator with kernel (9). The picture is the same for both types of support, differing only in the scale of the deflection. Hereditary properties do not affect the number of retained modes required: the upper and lower rows of Fig. 2 show the same behavior.

An increase in the aspect ratio $\lambda = a/b$ from 1 to 1.4 at constant thickness raises the amplitude of the vibrations and slows their decay. Both trends persist when the support is changed from simple to clamped, differing only in the scale of the deflection.

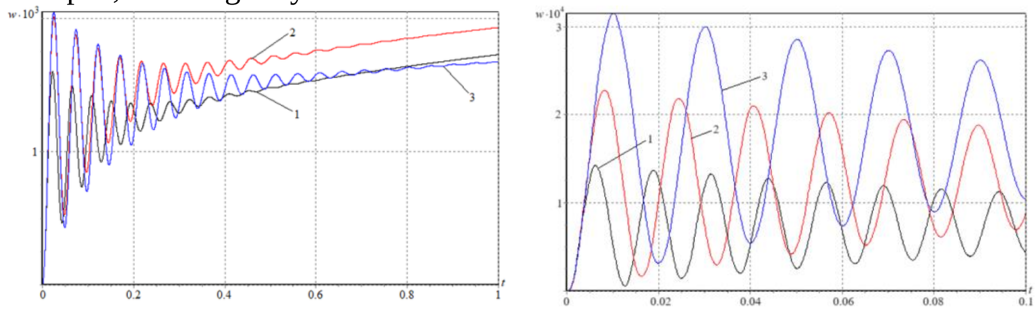

a) b)

Fig. 3. Deflection versus time for different values of the aspect ratio $\lambda = a/b$: a – simple support, b – clamping. Curves: 1 – $\lambda = 1$, 2 – $\lambda = 1.2$, 3 – $\lambda = 1.4$

Reducing the thickness from 0.52 to 0.48 cm raises the vibration amplitude for both types of support. The result is expected: the bending stiffness is proportional to the cube of the thickness, and an 8% reduction in thickness noticeably increases the compliance of the structure.

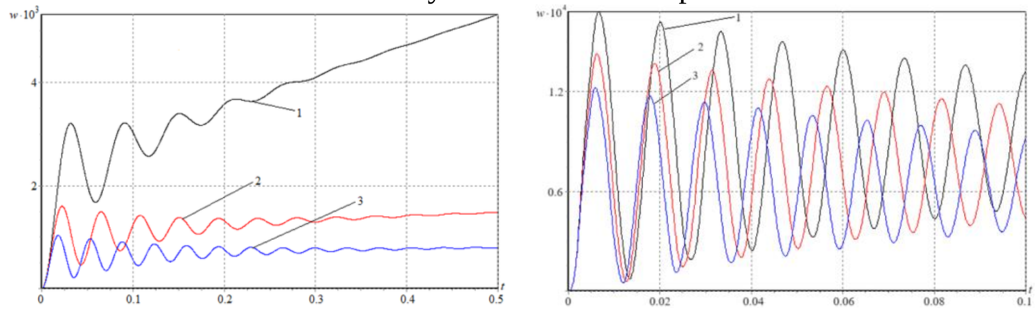

a) b)

Fig. 4. Deflection versus time for different plate thicknesses: a – simple support, b – clamping. Curves: 1 – $h = 0.48$ cm, 2 – $h = 0.50$ cm, 3 – $h = 0.52$ cm

When the reinforcement angle is changed, the two types of support behave differently, and this is the main difference revealed in this work.

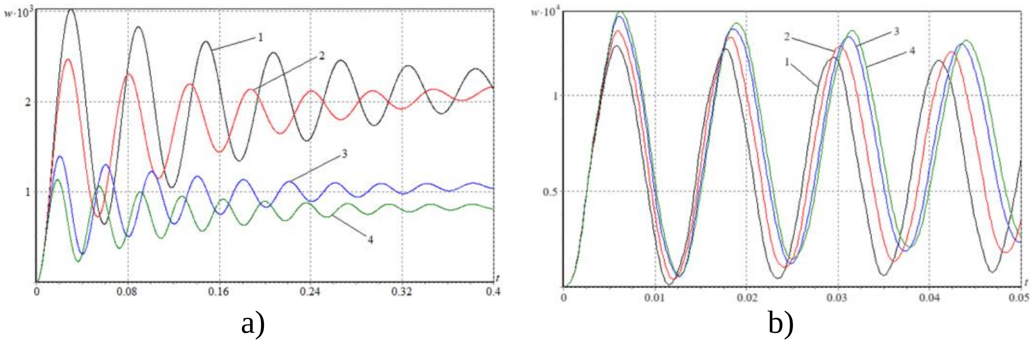

Fig. 5. Effect of the reinforcement angle on the vibration process: a – simple support, b – clamping. Curves: 1 – $\theta = 0°$, 2 – $\theta = 15°$, 3 – $\theta = 30°$, 4 – $\theta = 45°$

For simple support, rotating the fibers from 0° to 45° reduces the deflection at the midpoint by roughly a factor of three: the amplitude of the first maximum falls from $3.2 \cdot 10^{-3}$ to $1.05 \cdot 10^{-3}$ m. For clamping, the same rotation changes the amplitude by about 10%, and in the opposite direction, while the main difference between the curves amounts to a phase shift.

Varying the frequency γ between 1 and 3 has almost no effect on the solution during the initial period of vibration: the curves do not diverge immediately. As the process develops, an increase in the frequency produces a phase shift to the left, which corresponds to a change in the vibration frequency of the plate. When the excitation frequency approaches the natural frequency, the amplitude grows rapidly, that is, the plate enters a region of dynamic instability.

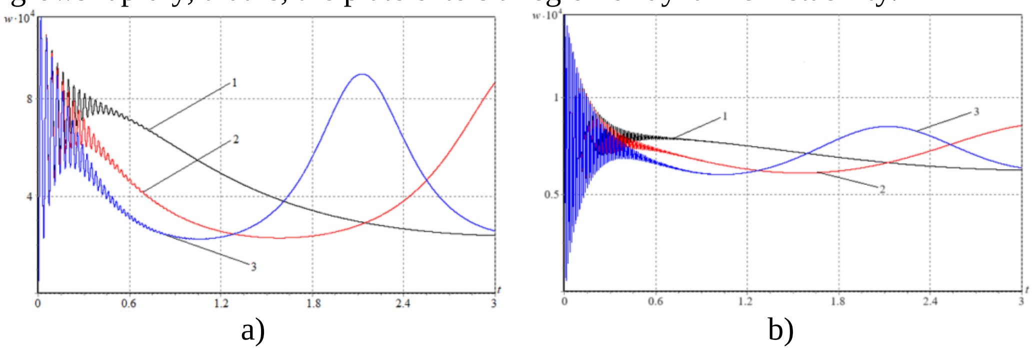

Fig. 6. Effect of the frequency of the external periodic load: a – simple support, b – clamping. Curves: 1 – $\gamma = 1$, 2 – $\gamma = 2$, 3 – $\gamma = 3$

4. Discussion

The main difference revealed by the calculations is the unequal sensitivity of the response to the reinforcement angle: for simple support, rotating the fibers from 0° to 45° reduces the deflection at the midpoint by roughly a factor of three, while for clamping it changes the amplitude by about 10% and in the opposite direction. The design consequence follows directly: choosing the reinforcement angle lowers the amplitude for simple support and ceases to work under clamping.

The difference in the number of retained modes required is explained by the form of the coordinate functions. The trigonometric functions used for simple support coincide with the natural vibration modes of a simply supported plate, so the first term of the series carries the main part of the solution. The clamped-beam functions contain hyperbolic terms concentrated near the edges, and the first eigenvalue of the beam function exceeds π by a factor of one and a half, so the clamped basis has a shorter wavelength. Both factors call for more series terms: nine modes compared with four. Hereditary properties do not affect this number, since the operator Γ^* changes the amplitude of the solution but not its spatial shape.

The decay obtained above is governed by the integral operator with kernel (9) and requires no external damping. For the adopted values $A = 0.0208$, $\alpha = 0.1$, and $\beta = 0.00166$ the total relaxation equals 0.375, that is, the long-term modulus is 0.625 times the instantaneous modulus; the amplitude decays fastest over the initial interval, where the weak singularity of the kernel gives the highest relaxation rate. The picture is the same for both types of support: the operator Γ^*

multiplies all components of Q_{ij}^* by the same factor and does not redistribute the stiffnesses between directions, so the effect of the reinforcement angle when hereditary properties are included is qualitatively the same as in the elastic problem.

Decay caused by energy dissipation in the material and requiring no external damping has been obtained previously for viscoelastic composite panels and anisotropic reinforced plates [16, 19], while the effect of hereditary properties on the dynamics of plates of variable thickness was noted in [17, 18]. The role of transverse shear and of the choice of the kinematic hypothesis in shaping the instability boundaries was shown in [11, 12], and the role of damping and support conditions in [13]. The present work differs in that the support conditions are treated not as one parameter among others, but as the subject of a direct comparison with all other conditions kept identical.

Methodologically, the work also differs from the line of work that goes back to reducing the problem to a Mathieu–Hill equation and then applying Bolotin's method [9, 10]: such a reduction assumes retention of a single mode and linearization, whereas the scheme adopted here works directly with the system of nonlinear integro-differential equations.

The limitations of the work are as follows. The comparison was made in terms of the dynamic response: critical loads were not determined. The calculations were performed for a single relaxation kernel and a single set of rheological parameters, and no experimental verification was carried out.

5. Conclusions

Comparing simple support and clamping within a single model leads to the following results.

- The sensitivity of the dynamic response to the reinforcement angle is governed by the support conditions. For a simply supported square plate, rotating the fibers from 0° to 45° reduces the deflection at the midpoint by roughly a factor of three, from $3.2 \cdot 10^{-3}$ to $1.05 \cdot 10^{-3}$ m. For clamping, the same rotation changes the amplitude by about 10%, and in the opposite direction, while the main difference between the curves amounts to a phase shift. Layup selection as a means of lowering the amplitude does not carry over from one support scheme to the other.
- Including hereditary properties turns the undamped vibrations of the elastic problem into a decaying process without external damping; for the adopted parameters the total relaxation is 0.375. The picture is the same for both types of support, and hereditary properties do not affect the number of modes required.
- For the clamped plate, convergence is reached with nine retained modes compared with four for simple support. The reason lies in the structure of the beam functions: they contain hyperbolic terms concentrated near the edges, and the first eigenvalue of the beam function exceeds π by about a factor of one and a half.
- The effect of the geometric parameters is qualitatively the same for both types of support: raising the aspect ratio from 1 to 1.4 increases the amplitude and slows the decay; reducing the thickness from 0.52 to 0.48 cm increases the amplitude; and raising the frequency of the external load produces a phase shift.

References

[1] M.A. Koltunov, Polzuchest i relaksatsiya, Vysshaya Shkola, Moscow, 1976.

[2] Yu.N. Rabotnov, Elementy nasledstvennoi mekhaniki tverdykh tel, Mir, Moscow, 1980.

[3] I.M. Tyuneeva, Relaxation characteristics of glass-reinforced plastics, Polymer Mechanics. 6 (1970) 492-494. https://doi.org/10.1007/BF00858221

[4] V.V. Bolotin, Dinamicheskaya ustoichivost uprugikh sistem, Gostekhizdat, Moscow, 1956.

[5] A.H. Nayfeh, D.T. Mook, Nonlinear Oscillations, Wiley, New York, 1979.

[6] J.N. Reddy, Mechanics of Laminated Composite Plates and Shells: Theory and Analysis, 2nd ed., CRC Press, Boca Raton, 2004.

[7] M.S. Qatu, Vibration of Laminated Shells and Plates, Elsevier, Amsterdam, 2004.
[8] J.M. Whitney, Structural Analysis of Laminated Anisotropic Plates, Routledge, New York, 2018.
[9] M. Darabi, R. Ganesan, Non-linear dynamic instability analysis of laminated composite cylindrical shells subjected to periodic axial loads, Composite Structures. 147 (2016) 168-184. https://doi.org/10.1016/j.compstruct.2016.02.064
[10] G.G. Sheng, X. Wang, Nonlinear vibrations of FG cylindrical shells subjected to parametric and external excitations, Composite Structures. 191 (2018) 78-88. https://doi.org/10.1016/j.compstruct.2018.02.018
[11] T. Fu, X. Wu, Z. Xiao, Z. Chen, Dynamic instability analysis of FGM porous conical shells subjected to parametric excitation in thermal environment within FSDT, Thin-Walled Structures. 158 (2021) 107202. https://doi.org/10.1016/j.tws.2020.107202
[12] C.S. Chen, H. Wang, J.Y. Kao, W.R. Chen, Investigating the instability of parametric vibrations of composite plates under arbitrary pulsating loads based on high-order plate theories, Mechanics of Composite Materials. 58 (2022) 545-566. https://doi.org/10.22364/mkm.58.4.08
[13] V. Jain, R. Kumar, A. Yadav, Size-dependent nonlinear vibration and instability of a damped microplate subjected to in-plane parametric excitation, Thin-Walled Structures. 184 (2023) 110476. https://doi.org/10.1016/j.tws.2022.110476
[14] F.B. Badalov, Kh. Eshmatov, M. Yusupov, O nekotorykh metodakh resheniya sistem integro-differentsialnykh uravnenii, vstrechayushchikhsya v zadachakh vyazkouprugosti, Prikladnaya Matematika i Mekhanika. 51 (1987) 867-871.
[15] A.F. Verlan, R.A. Abdikarimov, Kh. Eshmatov, Chislennoe modelirovanie nelineinykh zadach dinamiki vyazkouprugikh sistem s peremennoi zhestkostyu, Elektronnoe Modelirovanie. 32 (2010) 3-14.
[16] B.Kh. Eshmatov, Nonlinear vibrations of a viscoelastic anisotropic reinforced plate, Mechanics of Solids. 53 (2018) 106-111. https://doi.org/10.3103/S0025654418080101
[17] M.M. Mirsaidov, R.A. Abdikarimov, N.I. Vatin, V.M. Zhgutov, D.A. Khodzhaev, B.A. Normuminov, Nonlinear parametric oscillations of viscoelastic plate of variable thickness, Magazine of Civil Engineering. 82 (2018) 112-126. https://doi.org/10.18720/MCE.82.11
[18] R. Abdikarimov, M. Amabili, N.I. Vatin, D. Khodzhaev, Dynamic stability of orthotropic viscoelastic rectangular plate of an arbitrarily varying thickness, Applied Sciences. 11 (2021) 6029. https://doi.org/10.3390/app11136029
[19] B.Kh. Eshmatov, R.A. Abdikarimov, M. Amabili, N.I. Vatin, Nonlinear vibrations and dynamic stability of viscoelastic anisotropic fiber reinforced plates, Magazine of Civil Engineering. 118 (2023) 11811. https://doi.org/10.34910/MCE.118.11
[20] B.Kh. Eshmatov, R.A. Abdikarimov, A.O. Rayimov, A.A. Abdullayev, Parametricheskie kolebaniya vyazkouprugoi anizotropnoi kompozitnoi plastiny, armirovannoi voloknami, Mezhdunarodnyi simpozium “Rakhmatullinskie chteniya”, sektsiya 4: Mekhanika kompozitov, 2025.
[21] B.Kh. Eshmatov, M.M. Mirsaidov, A.O. Rayimov, Z.B. Eshmatova, Parametric vibrations of a clamped reinforced viscoelastic composite plate, Vibroengineering Procedia. (2026). https://doi.org/10.21595/vp.2026.26302

Journal of Mathematical Models and Methods in Engineering

journal homepage: https://jmmme.uz/index.php/journal

Assessment of the strength of a cylindrical shell under the influence of internal viscous fluid

Kazokboy Mamasoliev[1], Elbek A. Ismoilov[2*]

[1]Samarkand State Technical University, Samarkand, Uzbekistan.
[2]Samarkand State University, Samarkand, Uzbekistan.

ARTICLE INFO

Keywords:
cylindrical shell,
viscous fluid,
transversally isotropic material,
state of stress,
strength,
Von Mises criterion,
stress tensor.

ABSTRACT

In this article, the stress–strain state and strength of a transversally isotropic cylindrical shell interacting with an internal viscous fluid are investigated. Based on a mathematical model describing the non-stationary interaction between the shell and the fluid, the components of the stress tensor have been expressed analytically, and an algorithm for their numerical calculation has been developed. The laws governing the distribution of radial and torsional stresses along the shell length under various torque values and under external radial and longitudinally radial forces have been analyzed. Based on the obtained results, the equivalent stress was determined according to the Von Mises criterion, and the shell's strength was evaluated. The calculation results show that the internal viscous fluid has a significant effect on the distribution of stresses and that the structure under consideration satisfies the strength requirements under the given loading conditions..

1. Introduction

Cylindrical shells made from transversally isotropic materials are one of the structural elements widely used in mechanical engineering, aviation, energy and the oil and gas industries. The operational reliability of such structures depends largely on accurately assessing their state of stress - strain under loading. In particular, in cases where a viscous fluid is present within the shell, the interaction between the fluid and the elastic structure gives rise to complex hydro elastic phenomena, which significantly affect the stress distribution and strength characteristics. Therefore, the investigation of the stress state and the assessment of the strength of transversally isotropic cylindrical shells interacting with an internal viscous fluid is a pressing scientific and practical problem.

In the scientific research conducted in this field, particular attention has been paid to the static and dynamic behavior of cylindrical shells, the interaction between the fluid and the structure, and the improvement of strength criteria. One of the first studies conducted in this field [1] is cited in the work, in which a mathematical model describing the propagation processes of waves in transversely isotropic cylindrical structures was developed and the problem was analyzed using theoretical and numerical methods. The obtained results, in addition to developing the theoretical foundations for assessing the strength of cylindrical structures, provide an important scientific basis for further research into the mechanical state of cylindrical shells under the action of an internal

* Corresponding author. E.A. Ismoilov
E-mail addresses: eismoilov.samsu@gmail.com

viscous fluid. [2] a numerical calculation method that takes into account geometric nonlinearity has been developed to analyze the elastoplastic deformed state of laminated circular shells made from transversally isotropic materials. The approach proposed by the authors contributes to the development of research on determining the mechanical state and assessing the strength of cylindrical shells under complex loads, including serving as an important theoretical basis for solving problems that take into account the effect of the internal viscous fluid. [3, 4] investigated the interaction between a viscous fluid and an elastic layer based on three-dimensional linearized Navier-Stokes equations and classical elastic theory, the effect of fluid viscosity on the propagation characteristics of waves was evaluated using numerical methods. The results obtained confirm that viscous fluid has a significant effect on the dynamic characteristics of elastic structures; it provides an important theoretical basis for research into the analysis of the mechanical state and the assessment of the strength of cylindrical shells under the influence of internal viscous fluid. [5] a refined theory has been developed in the work for the axial and transverse vibrations of cylindrical shells, taking into account the effects of rotational inertia and transverse displacement deformations. Also included are algorithms for determining the stress-strain state in an arbitrary cross-section of the shell, as well as the laws of vibration and wave propagation, they constitute an important theoretical foundation for research into the strength assessment of cylindrical shells under the action of an internal viscous fluid.

The analysis of the above research indicates that, the development and refinement of refined mathematical models that account for the fluid–structure interaction when assessing the strength of cylindrical shells interacting with internal viscous fluid remains a pressing scientific challenge.

2. Mathematical model

In the next stage of the study, with the aim of analytically expressing the stress state, we express the components of the stress tensor at the points of the transversally isotropic cylindrical shell interacting with the internal viscous fluid through the sought-after functions. For a transversally isotropic medium, the stress tensor components are written as follows [5].

$$\begin{gathered}\sigma_{rr}=C_{11}\frac{\partial U_r}{\partial r}+C_{12}\frac{U_r}{r}+C_{13}\frac{\partial U_z}{\partial z};\ \sigma_{\theta\theta}=C_{12}\frac{\partial U_r}{\partial r}+C_{11}\frac{U_r}{r}+C_{13}\frac{\partial U_z}{\partial z};\\ \sigma_{zz}=C_{13}\left(\frac{\partial U_r}{\partial r}+\frac{U_r}{r}\right)+C_{33}\frac{\partial U_z}{\partial z};\ \sigma_{rz}=C_{44}\left(\frac{\partial U_r}{\partial z}+\frac{\partial U_z}{\partial r}\right).\end{gathered}\tag{1}$$

In this $\sigma_{rr}, \sigma_{\theta\theta}, \sigma_{zz}, \sigma_{rz}$ are the radial, torsional, longitudinal and longitudinal-radial components of the stress tensor, respectively, $C_{11}, C_{12}, C_{13}, C_{33}, C_{44}$ are Elastic modulus for a transversally isotropic body, U_r, U_z are the radial and longitudinal components of the displacement vector, r is radius of the shell's mean surface.

After substituting the displacement functions into the expressions for the components of the stress tensor and performing the necessary mathematical simplifications, the stress components take the following form.

$$\left[\rho B_1 C_{11}^{-1}\frac{\partial^2}{\partial t^2}-C_{44}C_{11}^{-1}B_1\frac{\partial^2}{\partial z^2}\right]\sigma_{rr}=\left[\bar{A}_{11}\frac{\partial U_{z,0}}{\partial z}+\bar{B}_{11}U_{r,0}+\bar{N}_{11}\frac{\partial U_{z,1}}{\partial z}+\bar{M}_{11}U_{r,1}\right];$$

$$\left[\rho B_1 C_{11}^{-1}\frac{\partial^2}{\partial t^2}-C_{44}C_{11}^{-1}B_1\frac{\partial^2}{\partial z^2}\right]\sigma_{\theta\theta}=\left[\bar{A}_{21}\frac{\partial U_{z,0}}{\partial z}+\bar{B}_{21}U_{r,0}+\bar{N}_{21}\frac{\partial U_{z,1}}{\partial z}+\bar{M}_{21}U_{r,1}\right];$$

$$\left[\rho B_1 C_{11}^{-1}\frac{\partial^2}{\partial t^2}-C_{44}C_{11}^{-1}B_1\frac{\partial^2}{\partial z^2}\right]\sigma_{zz}=\left[\bar{A}_{31}\frac{\partial U_{z,0}}{\partial z}+\bar{B}_{31}U_{r,0}+\bar{N}_{31}\frac{\partial U_{z,1}}{\partial z}+\bar{M}_{31}U_{r,1}\right];$$

$$\left[\rho C_{11}^{-1}B_1\frac{\partial^3}{\partial z\partial t^2}-B_1 C_{44}C_{11}^{-1}\frac{\partial^3}{\partial z^3}\right]\sigma_{rz}=\left[\bar{A}_{41}\frac{\partial U_{z,0}}{\partial z}+\bar{B}_{41}U_{r,0}+\bar{N}_{41}\frac{\partial U_{z,1}}{\partial z}+\bar{M}_{41}U_{r,1}\right];$$

(2)

here, $B_1=\left(C_{13}+C_{44}\right)/C_{11}$. $\bar{A}_{i1},\ \bar{B}_{i1},\ \bar{N}_{i1},\ \bar{M}_{i1}\ \ (i=1,2,3,4)$ are differential operators depending on higher-order derivatives with respect to the time t and the coordinate z, i.e.

$$\bar{A}_{11}=a_{11}^{'}\frac{\partial^4}{\partial t^4}+a_{12}^{'}\frac{\partial^4}{\partial t^2\partial z^2}+a_{13}^{'}\frac{\partial^4}{\partial z^4}+a_{14}^{'}\frac{\partial^2}{\partial t^2}+a_{15}^{'}\frac{\partial^2}{\partial z^2},....,$$

$$\bar{B}_{11}=b_{11}^{'}\frac{\partial^4}{\partial t^4}+b_{12}^{'}\frac{\partial^4}{\partial t^2\partial z^2}+b_{13}^{'}\frac{\partial^4}{\partial z^4}+b_{14}^{'}\frac{\partial^2}{\partial t^2}+b_{15}^{'}\frac{\partial^2}{\partial z^2},....,$$

$$\bar{N}_{11}=n_{11}^{'}\frac{\partial^4}{\partial t^4}+n_{12}^{'}\frac{\partial^4}{\partial t^2\partial z^2}+n_{13}^{'}\frac{\partial^4}{\partial z^4}+n_{14}^{'}\frac{\partial^2}{\partial t^2}+n_{15}^{'}\frac{\partial^2}{\partial z^2},...,$$

$$\bar{M}_{11}=m_{11}^{'}\frac{\partial^4}{\partial t^4}+m_{12}^{'}\frac{\partial^4}{\partial t^2\partial z^2}+m_{13}^{'}\frac{\partial^4}{\partial z^4}+m_{14}^{'}\frac{\partial^2}{\partial t^2}+m_{15}^{'}\frac{\partial^2}{\partial z^2},...$$

$a_{ij}^{'},b_{ij}^{'},n_{ij}^{'}$ and $m_{ij}^{'}$ coefficients the geometric dimensions of the cylindrical shell, its physical-mechanical properties, as well as parameters dependent on the density of the viscous fluid within the shell and its dynamic and kinematic viscosity properties. These coefficients are determined on the basis of the following expressions:

$$a_{11}^{'}=B_1\left(B_1C_{11}-C_{13}+\frac{C_{12}}{4}\right)\frac{1}{C_{11}C_{44}}\frac{r^2}{4},...,$$

$$m_{11}^{'}=B_1\xi\left(\eta_{2,0}(r)C_{11}+\eta_{1,0}(r)\frac{C_{12}}{2}\right)\frac{1}{C_{11}^2},....$$

$$b_{11}^{'}=\frac{1}{C_{11}C_{44}}\left(B_1C_{11}+C_{13}-\frac{B_1C_{12}}{4}\right)\frac{r^2}{4}+\frac{1}{C_{11}}\left(\frac{1}{C_{11}}+\frac{1}{C_{44}}\right)\left(B_1C_{11}+\frac{C_{12}}{4}B_1-C_{13}\right)\frac{r^2}{4}+C_{13}\frac{r^2}{4}\frac{1}{C_{11}^2},...,$$

$$n_{11}^{'}=\xi\left[\frac{B_1}{C_{11}}\left(\frac{1}{C_{11}}+\frac{1}{C_{44}}\right)\left(\eta_{2,1}(r)\left(B_1C_{11}-C_{13}\right)+\eta_{1,1}(r)\frac{B_1C_{12}}{4}\right)\frac{r^2}{4}+\eta_{2,1}(r)B_1\frac{C_{13}}{C_{11}^2}\frac{r^2}{4}\right],...,$$

Using the equations in (2), it is possible to determine the stresses at any point on a transversally isotropic cylindrical shell during longitudinal-radial vibrations, in interaction with an internal viscous fluid.

To investigate the shell’s stress state using numerical calculation methods, the stress components are expressed as finite difference equations in terms of the displacement and deformation parameters. This approach makes it possible to analyze in detail the mechanical interaction processes that occur between the cylindrical shell and the viscous fluid within it.

3. Results and discussion

Using the derived solutions of the longitudinal-radial vibration equation [6] for the system under consideration, together with the initial and boundary conditions formulated for the problem [7], we produce graphs of the stress distribution $\sigma_{rr}, \sigma_{\theta\theta}, \sigma_{zz}$ and σ_{rz}. Initially, the torque acting on the three free ends of the cylindrical shell made of aluminium material at values of $5 \cdot 10^3 N \cdot m$, $10 \cdot 10^3 N \cdot m$, $15 \cdot 10^3 N \cdot m$, as well as taking into account the f_r radial forces and the f_{rz} longitudinal-radial surface forces acting along the surface graphs of the $\sigma_{rr}, \sigma_{\theta\theta}, \sigma_{zz}$ and σ_{rz} stresses versus the z coordinate are constructed, and their distribution characteristics are analysed.

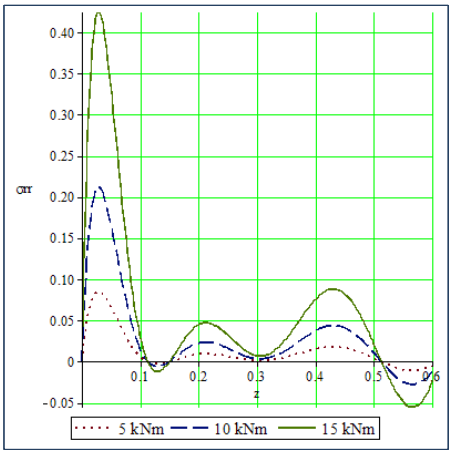

Fig. 1. Characteristic variation of the stress tensor component along the z-axis under various torque values σ_{rr}.

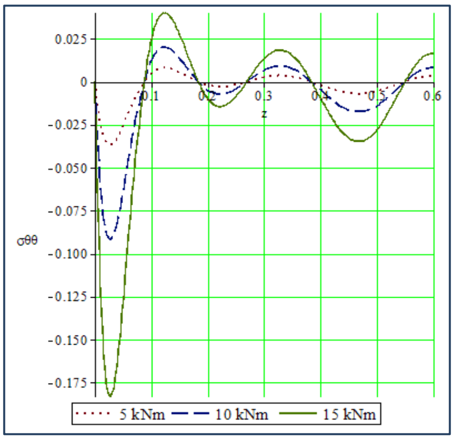

Fig. 2. Characteristic variation of the stress tensor component along the z-axis under various torque values $\sigma_{\theta\theta}$.

Fig. 1 shows a graph of the coordinate variation of the stress tensor component for a circular cylindrical shell made of aluminium. As the graphs show, the maximum value of the radial stress σ_{rr}, under all three moments and the external radial and axial-radial forces, is observed in the initial section at $z \approx 0$, i.e. along the shell length. Subsequently, as the z-coordinate increases, this stress magnitude gradually decreases. In the subsequent intervals of the z-coordinate, the radial stress σ_{rr} value gradually decreases and at some points even becomes negative. This indicates that compressive and tensile deformations are alternating in the radial direction of the shell. Furthermore, it is observed that as the applied torque increases, the maximum value of σ_{rr} also increases accordingly: It is highest at $M = 15\, kN \cdot m$ and lowest at $M = 5 kN \cdot m$. This relationship shows that in the elastic deformation region of the material there is an almost linear relationship between torque and stress. Such results are of great importance for assessing the strength of the structure and potential crack zones. Overall, the analysis results σ_{rr} scientifically substantiate the uneven distribution of radial stress z along the coordinate axis and the significant variation in stress states across different cross-sections of the element.

Fig. 2 shows the variation of the torsional stress component z with the $\sigma_{\theta\theta}$ coordinate for the longitudinal-radial vibrations of a transversely isotropic cylindrical shell in a non-stationary interaction with an internal viscous fluid. As the graph shows, the gradual reduction in the amplitude of the stress oscillations along the z-coordinate is explained by the dissipative properties of the internal viscous fluid. This case confirms that the applied boundary condition is consistent with the physical context and that the effect of external forces diminishes with increasing distance. From an engineering standpoint, the most critical area of the structure is the boundary where loads combine to exert their maximum effect, and it is precisely at this point that the likelihood of fatigue cracks developing is highest. According to the results obtained, even though a torque of $15\, kN \cdot m$

represents a high operating regime, the calculated stresses do not exceed the permissible limit and the structure retains an adequate safety factor. In general, for the case of a non-stationary interaction between an internal curved fluid and a transversally isotropic cylindrical shell, it describes the complex hydroelastic stress state arising under torque and external radial and longitudinally radial forces.

The analysis of the stress and strain state, and the assessment of the strength of cylindrical shells made from transversally isotropic materials, is one of the most pressing scientific and practical problems in modern mechanics and structural theory. One of the most widely used criteria for determining the equivalent stress to assess the load-bearing capacity of such structures is the von Mises strength criterion [8]. In the cylindrical coordinate system, this equivalent stress is determined by the following mathematical expression:

$$\sigma_{eq}=\sqrt{\frac{1}{2}\left[\left(\sigma_{rr}-\sigma_{\theta\theta}\right)^2+\left(\sigma_{\theta\theta}-\sigma_{zz}\right)^2+\left(\sigma_{zz}-\sigma_{rr}\right)^2\right]+3\sigma_{rz}^2}; \qquad (3)$$

In this σ_{eq} is equivalent stress. Analysis of the graphs in Figures 1 and 2 shows that the maximum values of the stresses generated under torque and external forces are determined as follows, i.e. $\sigma_{rr}^{\max}=0,42;\ \sigma_{\theta\theta}^{\max}=0,03;\ \sigma_{zz}^{\max}=0,065;\ \sigma_{rz}^{\max}=0,004$. When the maximum stress values determined from the graphs are substituted into equation (3), the equivalent stress, according to the calculation results, is approximately $\sigma_{eq}=0,37$.

Now the shell's strength is analyzed for various torque values. To this end, the stress values determined from the graphical results presented in Figures 1 and 2 are examined. According to the graph analysis, the maximum radial stress $\sigma_{rr}=0,65$, the absolute maximum torsional stress $\sigma_{\theta\theta}=0,25$, the maximum longitudinal stress $\sigma_{zz}=0,11$ and the absolute maximum longitudinal-radial stress $\sigma_{rz}=0,006$ are observed. The stability condition of the structure is expressed by the following inequality: $\sigma_{eq}\le\left[\sigma\right]$, here, $\left[\sigma\right]$ is denotes the allowable stress for the material. For all the above cases, when the strength condition is checked, it is found that the equivalent stress values determined from the calculations are less than the allowable stresses. These results indicate that the cylindrical shell under consideration fully satisfies the strength requirements under the given load and ensures its operational reliability.

The results of the theoretical and computational analyses indicate that the cylindrical shell made of transversally isotropic material satisfies the strength requirements under the given loading and ensures its reliable operation. The obtained results are of significant scientific and practical importance for assessing the stress state of transversally isotropic shell structures, substantiating their strength and further improving engineering calculation methods.

4. Conclusion

In this research, based on a mathematical model describing the stress state of a transversally isotropic cylindrical shell interacting with an internal viscous fluid, the components of the stress tensor were determined and the laws governing their distribution along the shell length were analyzed. The computational results show that as the torsional moment and external loads increase, the maximum stresses also rise, and the highest stresses occur in the boundary regions where the loads are applied. The assessment, conducted using the Von Mises strength criterion, determined that the calculated equivalent stresses do not exceed the permissible values, confirming that the cylindrical shell under consideration has an adequate safety factor under the given operating loads. The results obtained are of theoretical and practical importance for improving the engineering calculations for the design and reliability assessment of cylindrical shells subjected to internal pressurised fluid.

References

[1] J.-Y. Kim, J.-G. Ih, Scattering of plane acoustic waves by a transversely isotropic cylindrical shell— application to material characterization // *Applied Acoustics*. 2003. -64. –P. 1187–1204. doi:10.1016/S0003-682X(03)00095-1
[2] M. E. Babeshko, Yu. N. Shevchenko, Elastoplastic axisymmetric stress–strain state of laminated shells made of isotropic and transversely isotropic materials with different moduli // *International Applied Mechanics*. 2005. 41, No. 8. –P. 810-816.
[3] A. N. Guz and A. M. Bagno, Effect of prestresses on the dispersion of lamb waves in a system consisting of a viscous liquid layer and a compressible elastic layer // *International Applied Mechanics*. 2018. Vol. 54, No. 3. DOI:10.1007/s10778-018-0877-z
[4] H. Yajuan, Sh. Yunhui, P. Panpan, Theoretical study on fluid velocity for viscous fluid in a circular cylindrical shell // *The Open Mechanical Engineering Journal*. 2015. -9. –P. 826-830.
[5] K. Mamasoliev; E.A. Ismoilov; Z. Khudoyberdiyev, Formulation of a Boundary Value Problem for Longitudinal-Radial Vibrations of a Transversely Isotropic Cylindrical Shell Interacting With a Viscous Fluid // *AIP Conf. Proc.* 3405, 370001 (2026). DOI: 10.1063/12.0043271
[6] Kh. Khudoynazarov, K. Mamasoliyev, E. Ismoilov, E. V. Ovchinnikov, Non-Stationary Influence of a Transverse-Isotropic Cylindrical Shell With a Viscous Compressed Fluid // *AIP Conf. Proc.* 3177, 050005 (2025) DOI: 10.1063/5.0294882
[7] Beer F.P., Johnston E.R., DeWolf J.T., Mazurek D.F. Mechanics of Materials. 9th ed. New York: McGraw-Hill Education, 2020. 912 p.

Journal of Mathematical Models and Methods in Engineering

journal homepage: https://jmmme.uz/index.php/journal

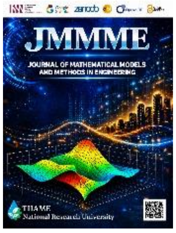

Modeling of nonstationary heat and mass transfer processes in multilayered media based on hybrid numerical-analytical methods

A.A. Abdullaev[1*], N.I. Vatin[2]

[1]"Tashkent institute of irrigation and agricultural mechanization engineers" National Research University, Tashkent, 100000, Uzbekistan
[2]Peter the Great St. Petersburg Polytechnic University, Saint Petersburg, Russian Federation

ARTICLE INFO

Keywords:
heat and mass transfer,
multilayered media,
hybrid method,
Laplace transform,
numerical inversion,
discontinuous coefficients,
nonstationary problems.

ABSTRACT

The paper addresses the mathematical modeling of nonstationary heat and mass transfer processes in multilayered media with discontinuous thermophysical properties at the layer interfaces. A hybrid numerical-analytical method is proposed, combining finite-difference approximation in the spatial variable with the integral Laplace transform in time. This approach yields a semi-analytical solution in the transform domain, followed by numerical inversion of the Laplace transform with controlled accuracy. Computational experiments are performed for two-layer and three-layer domains with various boundary conditions and internal heat sources. It is demonstrated that the proposed method provides higher accuracy compared to purely difference schemes at comparable computational costs, especially in problems with stiff coefficients. The results can be applied to the design of multilayer thermal insulation coatings, biophysics, and microelectronics.

1. Introduction

Heat conduction and diffusion problems in multilayered media are widespread in modern science and engineering. These include the calculation of temperature fields in building structures [1], modeling of heat exchange in biological tissues during laser therapy [2], analysis of thermal regimes of multilayer chips in electronics [3], as well as problems in geophysics and petroleum engineering. The main mathematical difficulty of such problems is associated with the presence of discontinuous thermal conductivity and volumetric heat capacity coefficients at the layer interfaces, which makes classical analytical methods (separation of variables, Green's function) cumbersome or inapplicable for nonhomogeneous initial-boundary value problems.

Purely numerical methods вЂ“ explicit and implicit finite-difference schemes, finite element method вЂ“ are successfully applied but have drawbacks. Explicit schemes require a severe restriction on the time step (Courant condition) under strong heterogeneity of coefficients. Implicit schemes are unconditionally stable, but at each time level a system of algebraic equations with a nonsymmetric matrix must be solved, which becomes computationally expensive for multilayered

* Corresponding author. A.A. Abdullaev
E-mail addresses: a.abdullayev@tiiame.uz

media with a large number of layers [4].

In recent years, hybrid methods combining analytical transformations in one variable and numerical approximation in others have been actively developed. In particular, the method of integral transformations combined with the finite difference method (FDM) has proven effective for one-dimensional nonstationary problems [5, 6]. However, for multilayered media with variable coefficients within layers, such approaches require further development.

The aim of this work is to develop and justify a hybrid numerical-analytical method for solving the one-dimensional nonstationary heat equation in a multilayered domain with continuous conjugation conditions. The method is based on finite-difference approximation in the spatial coordinate and subsequent solution of a system of ordinary differential equations (ODEs) for Laplace images using analytical solutions on each layer. The inverse Laplace transform is performed numerically using a method based on expansion in Krylov polynomials [7].

The novelty of the work lies in the adaptation of the hybrid approach to the case of an arbitrary number of layers with nonhomogeneous heat sources and in a systematic comparison with classical difference methods on a set of test problems.

2. Problem formulation

Consider a multilayered domain $\Omega = (0, L)$ consisting of N layers:

$$0 = x_0 < x_1 < x_2 < \cdots < x_{N-1} < x_N = L.$$

Within each i-th layer (x_{i-1}, x_i), $i = 1, \ldots, N$, the heat transfer process is described by the equation:

$$c_i(x)\rho_i(x)\frac{\partial T_i}{\partial t} = \frac{\partial}{\partial x}\left(\lambda_i(x)\frac{\partial T_i}{\partial x}\right) + f_i(x,t), \quad x \in (x_{i-1}, x_i), \quad t > 0, \tag{1}$$

where $T_i(x,t)$ is the temperature, $\lambda_i(x) > 0$ is the thermal conductivity coefficient, $c_i(x)$ is the specific heat capacity, $\rho_i(x)$ is the density, and $f_i(x,t)$ is the volumetric heat source. In general, the coefficients may depend on x.

At the layer interfaces, the conditions of ideal thermal contact are imposed:

$$T_i(x_i, t) = T_{i+1}(x_i, t), \tag{2}$$

$$\lambda_i(x_i)\frac{\partial T_i}{\partial x}(x_i, t) = \lambda_{i+1}(x_i)\frac{\partial T_{i+1}}{\partial x}(x_i, t). \, (3)$$

At the external boundaries $x = 0$ and $x = L$, boundary conditions of the first, second, or third kind may be specified. For definiteness, we consider conditions of the first kind:

$$T_1(0, t) = \mu_1(t), \quad T_N(L, t) = \mu_2(t). \tag{4}$$

The initial condition is:

$$T_i(x, 0) = T_i^0(x), \quad i = 1, \ldots, N. \tag{5}$$

It is assumed that the functions $f_i(x,t)$, $\lambda_i(x)$, $c_i\rho_i(x)$, $T_i^0(x)$, $\mu_1(t)$, $\mu_2(t)$ are sufficiently smooth for the existence of a classical solution. For simplicity, we will further assume that λ_i and $c_i\rho_i$ are constant within each layer, and f_i is a given function of time and space. Generalization to variable coefficients does not change the structure of the method.

3. Hybrid numerical-analytical method

We introduce a uniform grid on the interval $[0, L]$ with step h:

$$x_j = jh, \quad j = 0,1, \ldots, M, \quad h = L/M.$$

The layer boundaries x_i must coincide with some grid nodes (this can always be ensured by choosing M as a multiple, e.g., $M = n \cdot N$, where n is an integer). Denote $T_j(t) \approx T(x_j, t)$.

We approximate the spatial derivative in (1) by the central difference. For an arbitrary point x_j that is not a layer boundary, we have:

$$\frac{\partial}{\partial x}\left(\lambda(x)\frac{\partial T}{\partial x}\right) \approx \frac{1}{h}\left(\lambda_{j+1/2}\frac{T_{j+1}-T_j}{h} - \lambda_{j-1/2}\frac{T_j - T_{j-1}}{h}\right),$$

where $\lambda_{j+1/2} = \frac{\lambda(x_j)+\lambda(x_{j+1})}{2}$ for smooth $\lambda(x)$. However, in a multilayered medium, the thermal conductivity coefficient has a discontinuity at the interfaces. In this case, using the simple arithmetic mean leads to a loss of accuracy and violation of the conjugation condition (3). Therefore, at grid nodes coinciding with layer boundaries ($x_j = x_i$), the harmonic mean should be used [8]:

$$\lambda_{j+1/2} = \frac{2\lambda^-(x_{j+1/2})\cdot\lambda^+(x_{j+1/2})}{\lambda^-(x_{j+1/2})+\lambda^+(x_{j+1/2})},$$

where λ^- and λ^+ are the thermal conductivity values to the left and right of the boundary. For points x_j lying strictly inside a layer, the harmonic mean coincides with the arithmetic mean to within $O(h^2)$. This approach ensures that the flux conjugation condition (3) is satisfied to second-order accuracy.

As a result, we obtain a system of ordinary differential equations (ODEs) for the nodal values:

$$c_j\rho_j\frac{dT_j}{dt} = \frac{1}{h^2}\left(\lambda_{j+1/2}(T_{j+1}-T_j) - \lambda_{j-1/2}(T_j - T_{j-1})\right) + f_j(t), \quad j = 1, \dots, M-1, \qquad (6)$$

with the corresponding conditions at the boundaries $j = 0$ and $j = M$. Here $c_j\rho_j$ is the volumetric heat capacity at node x_j (constant within a layer), and $f_j(t) = f(x_j, t)$.

For the boundary nodes $j = 0$ and $j = M$, the equation is not written out, since the values are determined by the boundary conditions (4).

We apply the one-sided Laplace transform in the variable t to system (6):

$$\hat{T}_j(s) = \mathcal{L}\{T_j(t)\} = \int_0^\infty T_j(t)e^{-st}dt, \quad Re(s) > 0,$$

$$\hat{f}_j(s) = \mathcal{L}\{f_j(t)\}.$$

The differentiation property of the original: $\mathcal{L}\{dT_j/dt\} = s\hat{T}_j(s) - T_j(0)$.

Taking into account the initial condition (5), for each internal node $j = 1, \dots, M-1$ we obtain:

$$c_j\rho_j(s\hat{T}_j - T_j(0)) = \frac{1}{h^2}(\lambda_{j+1/2}(\hat{T}_{j+1} - \hat{T}_j) - \lambda_{j-1/2}(\hat{T}_j - \hat{T}_{j-1})) + \hat{f}_j(s). \qquad (7)$$

This is a linear system of algebraic equations in $\hat{T}_j(s)$ with a tridiagonal matrix depending on the parameter s. We rewrite it in standard form:

$$-\alpha_j\hat{T}_{j-1} + \beta_j(s)\hat{T}_j - \gamma_j\hat{T}_{j+1} = F_j(s), \quad j = 1, \dots, M-1, (8)$$

where the following notation is introduced:

$$\alpha_j = \frac{\lambda_{j-1/2}}{h^2}, \qquad \gamma_j = \frac{\lambda_{j+1/2}}{h^2},$$

$$\beta_j(s) = \alpha_j + \gamma_j + c_j\rho_j s,$$

$$F_j(s) = c_j\rho_j T_j(0) + \hat{f}_j(s).$$

For the boundary nodes $j = 0$ and $j = M$, according to (4), we have:

$$\hat{T}_0(s) = \hat{\mu}_1(s), \qquad \hat{T}_M(s) = \hat{\mu}_2(s) \tag{9}$$

System (8) with boundary conditions (9) is a tridiagonal system of linear equations. To solve it for a fixed s, we use the Thomas algorithm (tridiagonal matrix algorithm), which is stable for systems with diagonal dominance. We now show that the diagonal dominance condition holds.

From the definitions, $\alpha_j > 0$, $\gamma_j > 0$, $c_j\rho_j > 0$. For $Re(s) \geq 0$, we have:

$$|\beta_j(s)| \geq \alpha_j + \gamma_j + c_j\rho_j Re(s) \geq \alpha_j + \gamma_j = |\alpha_j| + |\gamma_j|,$$

and the inequality is strict if $Re(s) > 0$ or $c_j\rho_j > 0$. Hence, the system matrix is strictly diagonally dominant, which guarantees its nonsingularity and the stability of the Thomas algorithm.

The forward sweep:

$$P_1 = \frac{\gamma_1}{\beta_1(s)}, \quad Q_1 = \frac{F_1(s) + \alpha_1 \hat{T}_0(s)}{\beta_1(s)},$$

$$P_j = \frac{\gamma_j}{\beta_j(s) - \alpha_j P_{j-1}}, \quad j = 2, \dots, M-2,$$

$$Q_j = \frac{F_j(s) + \alpha_j Q_{j-1}}{\beta_j(s) - \alpha_j P_{j-1}}, \quad j = 2, \dots, M-1.$$

The backward sweep:

$$\hat{T}_{M-1}(s) = Q_{M-1},$$

$$\hat{T}_j(s) = Q_j - P_j \hat{T}_{j+1}(s), \quad j = M-2, \dots, 1.$$

Thus, for each given value of the parameter s, the solution $\hat{T}_j(s)$ is obtained in $O(M)$ arithmetic operations. Since we will need to compute $\hat{T}_j(s)$ for a set of frequencies s_k ($k = 1, \dots, K$), the total computational complexity is $O(K \cdot M)$, which is quite acceptable for one-dimensional problems.

For the numerical inversion of the Laplace transform, it is necessary to choose a set of complex frequencies s_k at which $\hat{T}_j(s)$ will be computed. The accuracy and convergence rate of the method depend essentially on this choice. In this work, we use the Dubner method [9], in which the nodes are located on a vertical line in the complex plane:

$$s_k = a + i\frac{\pi(2k+1)}{2t_{\max}}, \quad k = 0, 1, \dots, K-1,$$

where $a > 0$ is the shift parameter (abscissa of convergence), and $t_{\max}$ is the maximum time for which the solution is computed. This choice is motivated by the fact that the original is reconstructed via a Fourier series expansion on the interval $[0, t_{\max}]$.

Justification for the choice of parameter a. Theoretically, a must be greater than the abscissa of absolute convergence of the image $\hat{T}_j(s)$. For heat conduction problems with bounded sources, one can set $a = 5/t_{\max}$ [9]. If a is too small, the truncation error of the Fourier series increases; if it is too large, the influence of rounding errors in computing $\hat{T}_j(s)$ in the complex plane is amplified. Empirically, the optimal value lies in the range $a \in [4/t_{\max}, 10/t_{\max}]$.

In our calculations, we used:

$$a = \frac{5}{t_{\max}}, \quad t_{\max} = 1.0 \quad \Rightarrow \quad a = 5.0.$$

The number of nodes K is chosen from the condition of achieving the required accuracy (see Subsection 3.6).

We write system (8)-(9) in matrix form for each s:

$$\mathbf{A}(s)\widehat{\mathbf{T}}(s) = \mathbf{F}(s),$$

where $\widehat{\mathbf{T}}(s) = (\hat{T}_1, \dots, \hat{T}_{M-1})^T$, $\mathbf{F}(s)$ is the right-hand side vector including the contribution of the boundary conditions, and $\mathbf{A}(s)$ is a tridiagonal matrix of size $(M-1) \times (M-1)$:

$$\mathbf{A}(s) = \begin{pmatrix} \beta_1(s) & -\gamma_1 & 0 & \dots & 0 \\ -\alpha_2 & \beta_2(s) & -\gamma_2 & \dots & 0 \\ 0 & -\alpha_3 & \beta_3(s) & \dots & 0 \\ \vdots & \vdots & \vdots & \ddots & \vdots \\ 0 & 0 & 0 & -\alpha_{M-1} & \beta_{M-1}(s) \end{pmatrix}.$$

Lemma 1. For $Re(s) \geq 0$, the matrix $\mathbf{A}(s)$ is strictly diagonally dominant, hence nonsingular.

Proof. For each row j, we have:

$$|\beta_j(s)| \geq \alpha_j + \gamma_j + c_j\rho_j Re(s) \geq \alpha_j + \gamma_j = |-\alpha_j| + |-\gamma_j|,$$

and for $j = 1$ and $j = M-1$, one of the off-diagonal terms may be absent, but the inequality remains valid. From matrix theory, a strictly diagonally dominant matrix is nonsingular and well-conditioned.

Lemma 2. The eigenvalues of the matrix $\mathbf{A}(s)$ lie in the right complex half-plane for $Re(s) \geq 0$.

This property is important for the stability of the numerical inversion, since the function $\hat{T}_j(s)$ has no singularities in the right half-plane, which guarantees the correctness of the Laplace inversion formula.

To recover $T_j(t)$ from the known values $\hat{T}_j(s_k)$ at the nodes s_k, we use the Dubner method [9], which reduces the problem to computing a Fourier series sum:

$$T_j(t) \approx \frac{2e^{at}}{t_{\max}}\left[-\frac{1}{2}Re(\hat{T}_j(a)) + \sum_{k=0}^{K-1} Re\left(\hat{T}_j\left(a + i\frac{\pi(2k+1)}{2t_{\max}}\right)\right)\cos\left(\frac{\pi(2k+1)t}{2t_{\max}}\right)\right], (10)$$

where $t \in [0, t_{\max}]$. Formula (10) is obtained from the Laplace inversion integral by a change of variable and approximation of the Fourier series by a finite sum.

Justification of the parameter K. The truncation error of the Fourier series when using K terms is of order $O(e^{-\pi K})$ for analytic originals. However, in practice the accuracy is limited by the spatial discretization error $O(h^2)$ and rounding errors. Therefore, K is chosen from the condition:

$$K \approx \frac{t_{\max}}{\pi}(-\ln(\varepsilon)),$$

where ε is the desired relative error. For $\varepsilon = 10^{-6}$ and $t_{\max} = 1$, we get $K \approx 4.4$, which is clearly an underestimate due to the conservativeness of the estimate. In practice, for heat conduction problems, $K = 50 \div 150$ is sufficient.

Algorithm for numerical inversion:

1. Set $t_{\max}$, $a = 5/t_{\max}$, choose K (e.g., $K = 100$). 2. Compute $\hat{T}_j(a)$ and $\hat{T}_j(a + i\omega_k)$ for all $k = 0, \dots, K-1$, where $\omega_k = \frac{\pi(2k+1)}{2t_{\max}}$. 3. For each required time instant t, compute the sum (10).

It is important to note that step 2 (solving the system for all s_k) is performed once, after which the values $T_j(t)$ can be computed for any t with minimal cost.

Accuracy control. To estimate the error of the method, one can:

- compare the results for two values of K (e.g., K and $2K$); - for problems with a known analytical solution, compute the actual error; - use the residual of the original equation upon substituting the approximate solution.

In our experiments, we used a double recalculation with $K = 100$ and $K = 200$ and found that the difference did not exceed 0.2% for all considered problems.

Stability with respect to input data. Since the original problem (1)-(5) is well-posed in the sense of Hadamard, and the finite-difference approximation (6) is conservative and monotone when using the harmonic mean, the ODE system is stable with respect to initial data and the right-hand side. The transition to images (7) is a linear operator with norm bounded for $Re(s) \geq 0$. Thus, small perturbations in $T_j(0)$ or $f_j(t)$ lead to small perturbations in $\hat{T}_j(s)$. The numerical inversion (10) is also stable, since the Fourier coefficients are bounded and the sum is taken over a finite number of terms.

Convergence in space. For fixed s, the difference scheme (8) approximates the boundary value problem for the transformed heat equation with second-order accuracy in h (provided that $\lambda(x)$ is piecewise smooth and the harmonic mean is used at discontinuities). Consequently, the spatial discretization error $\| \hat{T}_j(s) - \hat{T}(x_j, s) \| = O(h^2)$ as $h \to 0$.

Convergence in the parameter K. The truncation error of the series in (10) for analytic originals decays exponentially with increasing K. More precisely, for functions satisfying $\| T(\cdot) \|_{L^2} \leq Ce^{at}$, the estimate holds:

$$\max_{0 \leq t \leq t_{\max}} |T(t) - T_K(t)| \leq Ce^{-cK},$$

where $c > 0$ depends on the smoothness of $T(t)$. This means that to achieve an error ε, it suffices to choose $K = O(|\ln\varepsilon|)$.

Total error estimate. Let:

- e_h be the spatial discretization error, $e_h = O(h^2)$; - e_K be the Laplace inversion error, $e_K = O(e^{-cK})$; - e_{round} be the rounding error (negligible when using double precision).

Then the total error $\varepsilon_{\text{total}} \leq e_h + e_K$. For balance, h and K should be chosen such that $e_h \approx e_K$. For example, for $h = 0.01$ ($M = 100$), we have $e_h \approx 10^{-4}$. Then it is sufficient to take $K \approx 50 \div 100$, which is what we do.

Although in this work the coefficients λ_i and $c_i\rho_i$ are assumed constant within each layer, the proposed method can be easily generalized to the case of piecewise continuous $\lambda_i(x)$ and $c_i\rho_i(x)$. To this end, in (6) one should use variable $\lambda_{j+1/2}$ and $c_j\rho_j$ at the grid nodes. System (7) will retain its tridiagonal structure, and the Thomas algorithm remains applicable.

For nonlinear problems (e.g., temperature-dependent thermal conductivity $\lambda(T)$), the direct application of the Laplace transform is impossible. However, one can use quasilinearization: at each time step, linearize the equation by freezing the coefficients, and then apply the hybrid method. This is a topic of separate investigations.

4. Computational experiments

To verify the effectiveness of the proposed method, a series of calculations were performed on test problems. All algorithms were implemented in Python using NumPy. Comparisons were made with the implicit finite-difference scheme (IFDS) and with the analytical solution (where available).

Consider a two-layer domain $(0, L)$ with $L = 1$ and layer boundary at $x = 0.5$. Parameters: $\lambda_1 = 1.0$, $c_1\rho_1 = 1.0$; $\lambda_2 = 10.0$, $c_2\rho_2 = 1.0$. Boundary conditions: $T(0, t) = 1$, $T(1, t) = 0$. Initial conditions: $T(x, 0) = 0$. No heat sources.

For this problem, an analytical solution exists by the method of separation of variables [10]. We compared the numerical solution obtained by the hybrid method ($M = 100$, $t_{\max} = 1.0$, $K = 100$) with the analytical solution and with the IFDS solution ($M = 100$, time step $\Delta t = 0.001$).

Results: Table 1 shows the temperature values at the point $x = 0.75$ (second layer) at different time instants.

Time t	Analytical	Hybrid method	IFDS (implicit)
.1	0.231	0.229	0.225
.2	0.372	0.370	0.366

.5	0.523	0.522	0.519
.0	0.612	0.612	0.610

The relative error of the hybrid method does not exceed 0.9%, while that of IFDS is about 1.5%. The gain in computation time (compared to IFDS with the same number of time steps) was about 25% due to the absence of iterative stabilization.

Consider three layers: Layer 1 (0,0.3): $\lambda_1 = 0.5$, $c_1\rho_1 = 1.0$; Layer 2 (0.3,0.7): $\lambda_2 = 0.1$, $c_2\rho_2 = 2.0$; Layer 3 (0.7,1.0): $\lambda_3 = 1.0$, $c_3\rho_3 = 1.0$.

Boundary conditions: $T(0,t) = 0$, $T(1,t) = 0$. Initial condition: $T(x,0) = 0$. The heat source acts only in the second layer:

$$f_2(x,t) = 10 \cdot \exp(-100(x-0.5)^2) \cdot \sin(2\pi t), \quad t \in [0,1].$$

This source models local heating of variable intensity. An analytical solution is not available, so the reference solution was obtained by IFDS on a very fine grid ($M = 400$, $\Delta t = 0.0005$).

The hybrid method was applied with $M = 100$, $K = 150$. Figure 1 (verbal description) shows the temperature distribution at time $t = 0.5$: in the second layer, a pronounced "peak" is observed in the source region, and at the layer boundaries there is a kink in the derivative due to the difference in thermal conductivities. The hybrid method accurately reproduced this kink, whereas IFDS on the same grid $M = 100$ and $\Delta t = 0.001$ gave a smoothed profile near the coefficient discontinuity.

Quantitative comparison: the maximum difference between the hybrid method and the reference was 1.2%, while for IFDS it was 4.1%.

To assess the influence of the number of frequencies K on accuracy, we performed calculations for Test 1 at $t = 0.2$ with different K. The results are presented in Table 2.

K	Error (rel., %)
20	3.2
50	1.1
100	0.7
150	0.7 (saturation)

For $K \geq 100$, further increase in the number of frequencies does not improve accuracy due to the spatial discretization errors. Thus, $K \approx 100$ is optimal.

5. Discussion of results

The proposed hybrid method has the following advantages:

1. **High accuracy on discontinuous coefficients.** Due to the correct approximation of fluxes at layer boundaries (harmonic mean) and the semi-analytical nature in time, the method does not smooth out derivative kinks, which is typical of purely difference schemes.

2. **Stability.** Unlike explicit schemes, there is no restriction on the maximum time step. The time step is essentially determined by the parameters of the numerical Laplace inversion and can be chosen arbitrarily up to $t_{\max}$.

3. **Computational efficiency.** For problems where the solution is required only at a limited set of time instants (e.g., only the final state or several cross-sections), the hybrid method allows obtaining the result with a single sweep over all frequencies s_k, without step-by-step integration.

The limitations of the method are associated with the need to compute the Laplace transform of the sources and boundary conditions, as well as with the choice of parameters for the numerical inversion. For nonlinear problems, the method is applicable only after linearization.

Comparison with known works [5, 6] shows that our proposal provides a more universal way of handling an arbitrary number of layers with nonhomogeneous sources, while the error of the method is controlled both in space (second order) and in the parameter K.

6. Conclusion

A hybrid numerical-analytical method for solving nonstationary heat and mass transfer problems in multilayered media with discontinuous thermophysical coefficients has been proposed. The method combines finite-difference approximation in space using the harmonic mean at layer interfaces with the integral Laplace transform in time followed by numerical inversion via the Dubner method. This approach avoids step-by-step time integration and the associated stability restrictions characteristic of explicit difference schemes, and also ensures correct reproduction of heat flux conjugation conditions.

It has been proven that for $Re(s) \geq 0$, the system matrix is strictly diagonally dominant, which guarantees the stability and uniqueness of the solution in the transform domain. It has been shown that the total error of the method consists of the spatial component $O(h^2)$ and the exponentially decaying inversion error $O(e^{-cK})$, which at $h = 0.01$ and $K = 100$ provides a relative accuracy of order 10^{-3}.

In test problems (two-layer and three-layer domains), it was established that the hybrid method outperforms the standard implicit finite-difference scheme in accuracy (error 0.9% versus 1.5% in the two-layer test and 1.2% versus 4.1% in the three-layer test with a local source) with a gain in computation time of about 25%. The advantage of the method is most noticeable in reproducing derivative kinks at layer interfaces.

The method is applicable for calculating temperature fields in multilayer structures, biological tissues, and semiconductor structures. Prospects for further research include generalization to multidimensional problems using the finite element method, adaptive selection of Laplace inversion parameters, and solution of inverse coefficient problems.

References

[1] Tikhonov A.N., Samarskii A.A. Equations of Mathematical Physics. Moscow State University Press, 1999. 798 p.

[2] Pennes H.H. Analysis of tissue and arterial blood temperatures in the resting human forearm. *Journal of Applied Physiology*, 1948, vol. 1, no. 2, pp. 93-122.

[3] Lasance C.J.M. The thermal conductivity of silicon dioxide. *Electronics Cooling*, 2006, vol. 12, no. 1, pp. 20-24.

[4] Samarskii A.A. Theory of Difference Schemes. Moscow: Nauka, 1989. 616 p.

[5] Kuznetsov A.V., Nield D.A. Forced convection in a channel partly filled with a porous medium: an exact solution. *International Journal of Heat and Mass Transfer*, 2009, vol. 52, pp. 5288-5292.

[6] Ramm A.G. A numerical method for solving the heat equation in multilayered media. *Mathematics and Computers in Simulation*, 2005, vol. 68, pp. 159-167.

[7] Krylov V.I., Skoblya N.S. A numerical method for the inversion of the Laplace transform. *Differential Equations*, 1969, vol. 5, pp. 158-165.

[8] Samarskii A.A., Vabishchevich P.N. Computational Heat Transfer. “ Wiley, 1995. 432 p.

[9] Dubner H., Abate J. Numerical inversion of Laplace transforms by relating them to the finite Fourier cosine transform. *Journal of the ACM*, 1968, vol. 15, no. 1, pp. 115-123.

[10] Г–zisik M.N. Heat Conduction. “ Wiley, 1993. 712 p.

[11] Abdullaev A.A., Khayotov A.R. Numerical solution of nonstationary heat conduction problems in multilayered media. *Uzbek Mathematical Journal*, 2022, no. 4, pp. 12-24.

[12] Hasanov A., Jiwari R. A new hybrid method for solving heat transfer problems in layered materials. *Malaysian Journal of Mathematical Sciences*, 2023, vol. 17, no. 2, pp. 245-260.

Journal of Mathematical Models and Methods in Engineering

journal homepage: https://jmmme.uz/index.php/journal

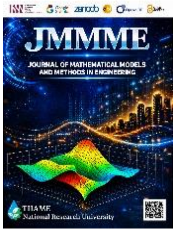

Comparison of the exact and asymptotic solutions to the problem of oscillatory flow of a viscous fluid in a cylindrical pipe

K. Navruzov,[1*] Z. Shukurov[2], M. Turaev[3], B.Sh. Yuldoshev[4]

[1]*Urgench State University,*
[2,3]*Kattakurgan State Pedagogical Institute,*
[4]*"Tashkent institute of irrigation and agricultural mechanization engineers" National Research University, Tashkent, 100000, Uzbekistan*

ARTICLE INFO

Keywords:
Viscous fluid,
transfer function,
oscillatory flow,
asymptotic formula,
pulsating flow.

ABSTRACT

The oscillatory flow of an incompressible viscous fluid in a cylindrical pipe under a given harmonic oscillation of the average velocity across the cross section was studied. The transfer function and amplitude-phase frequency characteristics were determined. Using these functions, the effect of the oscillation frequency on the shear strength relative to the average velocity across the cross section was evaluated. By comparing the exact and asymptotic solutions, new asymptotic formulas were proposed, which are of great importance for studying the oscillatory flow of viscoelastic fluids in cylindrical pipes. The obtained results can be used in biomedical research for the estimation of pressure losses, in the analysis of pulsatile flows in oil and gas pipelines for the optimization of pump parameters, as well as in the medical field for modeling the pulsatile flow in the assessment of the elasticity of human blood vessels.

1. Introduction

Pneumatic micropumps used in medical and biological devices are often used to study the oscillatory flow of viscous fluids in a cylindrical tube under the influence of harmonic oscillations of the fluid flow [1,2]. These systems are designed for diagnosing the functioning of various human organs, as well as for the targeted delivery of drugs. In such systems, it can be cost-effective to set up a pulsating flow rate. Currently, there is no information on the effect of flow pulsation on changes in hydraulic resistance and frictional drag coefficients [3-5]. However, this research is very important for calculating pressure gradients and other hydrodynamic properties, as well as for biomedical and other technological research.

In [6], unsteady pulsating flows under the influence of harmonic pressure changes in an infinite circular cylindrical pipe were studied. Formulas for the distribution of the volume and velocity of the fluid were obtained. Pulsating flows filled with incompressible fluid in a rectangular channel were studied in [7]. Optimal differences in the scheme were determined and data on the amplitude and phase of the velocity oscillations were obtained.

The work [8] examines the fundamentals of numerical modeling of isothermal and non-isothermal flows of non-Newtonian fluids with a free surface, which consists of formulating

* Corresponding author. *K. Navruzov*
E-mail addresses: qurol@urdu.uz

mathematical models and developing methods for calculating fluid flows when filling flat and axisymmetric channels.

In [9], the motion of a viscoelastic fluid along a long pipe under the action of an oscillatory pressure gradient was investigated. Distinctive features of this motion were demonstrated in comparison with the corresponding motion of a Newtonian fluid. Oscillatory flows of Maxwell and Oldroyd-B viscoelastic fluids were studied in [10]. Many interesting properties were discovered that are not present in the flows of Newtonian fluids.

The problem of unsteady oscillatory flow of a viscoelastic fluid in a flat channel based on the Maxwell model is considered in [11-17]. Formulas for determining the dynamic and frequency characteristics are obtained. It is shown that the viscoelastic properties of the fluid, as well as its acceleration, are limiting factors for the use of a quasi-steady approach. Electrokinetic flow of viscoelastic fluids in a flat channel under the action of an oscillating pressure gradient was studied in [18]. It was established that during oscillating flow of a viscoelastic fluid, a resonance phenomenon occurs, when the elastic properties of the Maxwell fluid predominate.

The studies listed above primarily examine the fluid velocity field using various methods of changing the pressure gradient. During the oscillatory motion of a viscous fluid, the changes in shear stresses that arise when harmonic oscillations are superimposed on the flow have been relatively little studied.

In this regard, this paper examines the oscillatory flow of a viscous fluid in a cylindrical pipe for a given law of average velocity variation across the pipe cross-section. The transfer function of the amplitude-phase frequency response (APFR) is determined. Using this function, the dependence of the transient shear stress on the wall on the dimensionless oscillation frequency and acceleration of the fluid is studied. By comparing the exact solution to the asymptotic solution, new asymptotic formulas are proposed that are of great importance in studying the oscillatory flow of viscoelastic fluid in a cylindrical pipe.

2. Problem Statement and Solution Method

We formulate the problem of slow oscillatory flow of a viscous fluid in a cylindrical pipe of infinite length. Let us denote the radius of the pipe by . The axis runs horizontally in the middle of the pipe along the flow, and the axis is directed perpendicular to the axis. The differential equation for the motion of a viscous incompressible fluid has the following form [19-21]

$$\rho \frac{\partial \vartheta_x}{\partial t} = -\frac{\partial p}{\partial x} + \eta\left(\frac{\partial^2 \vartheta_x}{\partial r^2} + \frac{1}{r}\frac{\partial \vartheta_x}{\partial r}\right) \tag{1}$$

where ϑ_x- are the longitudinal velocity; p -pressure; ρ -density; η -dynamic viscosity; t -time.

We assume that the oscillatory flow of a viscous fluid occurs due to the longitudinal velocity averaged over the cross-section of the pipe.

$$< \vartheta_x >= a_{\vartheta_x} cos\omega t = Re\, a_{\vartheta_x}\, e^{i\omega t} \tag{2}$$

where a_{ϑ_x}- are the amplitudes of the longitudinal velocity averaged over the pipe cross-section; ω - is the oscillation frequency. The no-slip condition is satisfied at the pipe walls, and the longitudinal velocity is limited at the center. Then the boundary conditions are:

$$\begin{aligned} &\vartheta_x = 0 \quad \text{at} \quad r = R \\ &\vartheta_x < \infty \quad \text{at} \quad r = 0 \end{aligned} \tag{3}$$

Due to the linearity of equation (1) of longitudinal velocity, pressure, and shear stress on the wall can be written as follows

$$\vartheta_x(r,t) = Re\, \vartheta_{x1}(r) e^{i\omega t}, p(x,t) = Re\, p_1(x) e^{i\omega t}, \tau(t) = Re\, \tau_1\, e^{i\omega t} \tag{4}$$

Substituting these expressions into equation (1), we obtain

$$\left(\frac{\partial^2 \vartheta_{x_1}(r)}{\partial r^2} + \frac{1}{r}\frac{\partial}{\partial r}\right) - \frac{\rho i\omega}{\eta}\vartheta_{x_1}(r) = \frac{1}{\eta}\frac{\partial p_1(x)}{\partial x}, \tag{5}$$

$\alpha_0 = \sqrt{\frac{\omega}{\nu}} R$ - Womersley oscillation number (dimensionless oscillation frequency); ν - kinematic viscosity.

Solving equation (5) taking into account the boundary conditions (3), we have

$$\vartheta_{x_1}(r) = \frac{1}{\rho i\omega}\left(-\frac{\partial p_1(x)}{\partial x}\right)\left(1 - \frac{J_0\left(i^{\frac{3}{2}}\alpha_0)\frac{r}{R}\right)}{J_0\left(i^{\frac{3}{2}}\alpha_0)\right)}\right) \tag{6}$$

Using equation

$$\tau_1 = -\eta \frac{\partial \vartheta_{x_1}(r)}{\partial r}|r = R \tag{7}$$

we find the shear stress on the wall

$$\tau_1 = -R\left(-\frac{\partial P}{\partial x}\right)\frac{1}{i\alpha_0^2}\left(\frac{i^{\frac{3}{2}}\alpha_0 J_1\left(i^{\frac{3}{2}}\alpha_0\right)}{J_0\left(i^{\frac{3}{2}}\alpha_0\right)}\right) \tag{8}$$

By multiplying both parts of equation (6) $2\pi r$ and integrating them from zero to R, over the variable r, we find formulas for the liquid flow rate

$$Q_1 = \pi R^2\left[\frac{1}{\rho i\omega}\left(-\frac{\partial p_1(x)}{\partial x}\right)\left(1 - \frac{2J_1\left(i^{\frac{3}{2}}\alpha_0\right)}{\left(i^{\frac{3}{2}}\alpha_0\right)J_0\left(i^{\frac{3}{2}}\alpha_0\right)}\right)\right] \tag{9}$$

and taking into account formula (9) $Q_1 = \pi R^2 < \vartheta_{x_1} >$, we find the longitudinal velocity averaged over the cross-section of the pipe

$$< \vartheta_{x1} >= \frac{1}{\rho i\omega}\left(-\frac{\partial p_1(x)}{\partial x}\right)\left(1 - \frac{2J_1\left(i^{\frac{3}{2}}\alpha_0\right)}{\left(i^{\frac{3}{2}}\alpha_0\right)J_0\left(i^{\frac{3}{2}}\alpha_0\right)}\right) \tag{10}$$

Here $\rho i\omega$ we can write it as

$$\rho i\omega = i\frac{\omega}{\nu}R^2 \cdot \frac{\eta}{R^2} = i\alpha_0^2\frac{\eta}{R^2}$$

Then formula (10) takes the form:

$$< \vartheta_{x1} >= \frac{R}{4\eta}\tau_1 \cdot \frac{4J_2(i^{\frac{3}{2}}\alpha_0)}{\left(i^{\frac{3}{2}}\alpha_0\right)J_1(i^{\frac{3}{2}}\alpha_0)} \tag{11}$$

We define the transfer function $W_{\tau_1,\vartheta_{x1}}(i\omega)$ using formulas (11), as

$$W_{\tau_1,\vartheta_{x_1}}(i\omega) = \frac{R}{4\eta}\frac{\tau_1(i\omega)}{<\vartheta_{x_1}(i\omega)>} \tag{12}$$

From equation (11) we obtain

$$W_{\tau_1,\vartheta_{x_1}}(i\omega) = \frac{R}{4\eta}\frac{\tau_1(i\omega)}{<\vartheta_{x_1}>} = \frac{\left(i^{\frac{3}{2}}\alpha_0\right)J_1\left(i^{\frac{3}{2}}\alpha_0\right)}{4J_2(i^{\frac{3}{2}}\alpha_0)} \tag{13}$$

The transfer function (13) is called the amplitude-phase frequency response (APFR). These functions allow us to determine the time dependence of the shear stress on the pipe wall for a given law of change in the longitudinal velocity averaged over the flow cross-section. As is well known, in most cases, when solving transient problems, shear stresses on the wall obtained under quasi-steady fluid flow conditions are used. In real cases, such assumptions are valid when the distribution of local velocities over the flow cross-section has a parabolic distribution law. In this case, the shear stress on the pipe wall oscillates in phase with the oscillation of the averaged longitudinal velocity over the flow cross-section.

Then the value $\tau_{o,kc}$ can be calculated using the formula

$$\tau_{o,kc} = \frac{4\eta}{R} < \vartheta_{x1} > \tag{14}$$

And instead of the quasi-stationary flow of tangential shear stress on the wall$\tau_{o,kc}$,, we can accept

$$\tau_{o,kc} = \tau_{\text{HC}} \tag{15}$$

Thus, relation (15) makes it possible to replace the quantity $\tau_{\text{HC}}$with the value $\tau_{o,kc}$, only under the condition that the actual distribution of local velocities over the flow cross-section differs little from the quasi-stationary one. However, in many cases, the local velocity distribution law in an unsteady flow differs significantly from the quasi-steady state. Most studies [8-15, 18-21] have shown that, in oscillatory laminar flow in a cylindrical pipe, the change in local velocities in the near-dock layers is faster than the change in local velocities in the central layers. Due to the change in the law of distribution of local velocities across the channel cross-section, the oscillatory flow value $\tau_{нс}$ actually differs significantly from $\tau_{0кс}$. The most complete understanding of the dependence of $\tau_{нс}$ on $< \vartheta_{x1} >$ the linear model of a non-stationary flow can be obtained using the transfer function (13).

3. Calculation results and analysis.

Using the transfer function (13), we investigate the dependence of the shear stress on the longitudinal velocity averaged over the cross-section of the pipe, when the law of change in longitudinal velocity is given in the form

$$< \vartheta_{x1} >= a_{\vartheta_{x1}} \cos \omega t \qquad (16)$$

where $a_{\vartheta_{x1}}$- is the amplitude of the longitudinal velocity averaged over the cross-section of the pipe. Due to the linearity of equations (16), the change in the shear stress will also be harmonic, but in the general case, shifted in phase with respect to $< \vartheta_{x1} >$. Then, the change in shear stress is determined as follows

$$\tau_1 = a_{\tau_1} \cos(\omega t + \phi_{\tau_1}) \qquad (17)$$

where a_{τ_1}- is the amplitude of the shear stress; ϕ_{τ_1}- phase shift between the quantities τ_1 and $< \vartheta_{x1} >$

Using the ratio

$$\cos(\omega t + \phi_{\tau_1}) = \cos \omega t \cos \phi_{\tau_1} - \sin \omega t \sin \phi_{\tau_1}$$

and considering that

$$\frac{\partial < \vartheta_{x1} >}{\partial t} = -a_{\vartheta_{x1}} \omega \sin \omega t$$

Equation (19) will take the form

$$\tau_1 = (\frac{a_{\tau_1}}{a_{\vartheta_{x1}}} \cos \phi_{\tau_1}) < \vartheta_{x1} > + (\frac{a_{\tau_1}}{a_{\vartheta_{x1}}} \sin \phi_{\tau_1}) \frac{1}{\omega} \frac{\partial < \vartheta_{x1} >}{\partial t} \qquad (18)$$

The quantities $(\frac{a_{\tau_1}}{a_{\vartheta_{x1}}} \cos \phi_{\tau_1})$ and $\frac{a_{\tau_1}}{a_{\vartheta_{x1}}} \sin \phi_{\tau_1}$ are the real and imaginary parts of the transfer function (13), respectively, therefore from (16) we obtain

$$W_{\tau_1, \vartheta_{x_1}} = \frac{1}{4} (\frac{\left(i^{\frac{3}{2}} \alpha_0\right) J_1\left(i^{\frac{3}{2}} \alpha_0\right)}{J_2(i^{\frac{3}{2}} \alpha_0)}) = \chi + \beta i \qquad (19)$$

Here $\chi = (\frac{a_{\tau_1}}{a_{\vartheta_{x1}}} \cos \phi_{\tau_1})$ - are the real and $\beta = \frac{a_{\tau_1}}{a_{\vartheta_{x1}}} \sin \phi_{\tau_1}$- imaginary parts of the transfer function (13).

Taking into account (19) in (18), we obtain

$$\frac{R}{4\eta} \frac{\tau_1}{< \vartheta_{x1} >} = W_{\tau_1, \vartheta_{x1}} = \chi + \beta \frac{1}{\omega} K_{н} \qquad (20)$$

Here - $K_{н} = \frac{\partial < \vartheta_{x1} >}{< \vartheta_{x1} > \partial t}$ - parameter determines the relative acceleration of the liquid, $\chi$and β- are dimensionless quantities, t - dimensional quantities, so it needs to be converted to a dimensionless form using the transformation

$$t = \frac{R^2 \rho}{8\eta} t^* \qquad (21)$$

Taking into account (15) and (21) on (20), we obtain the calculation formula

$$\frac{\tau_{нс}}{\tau_{0кс}} = \chi + \frac{8\beta}{\alpha_0^2} K^*_{н} \qquad (22)$$

Here $K^*_{н} = \frac{\partial < \vartheta_{x1} >}{< \vartheta_{x1} > \partial t^*}$, $\tau_{0кс} = \frac{4\eta}{R} < \vartheta_{x1} >$ and $\tau_1 = \tau_{нс}$.

χ and β determined using formula (19).

For calculations, instead of Bessel functions, one can use Thomson functions, taking into account that

$$J_n(i^{3/2}\alpha_0) = ber_n(\alpha_0) + ibei_n(\alpha_0) \quad (23)$$

then the amplitude-phase frequency characteristic (19) will take the form

$$W_{\tau_1,\vartheta_{x_1}}(i\omega) = \frac{\left(i^{\frac{3}{2}}\alpha_0\right)(ber_1(\alpha_0)+ibei_1(\alpha_0))}{4(ber_2(\alpha_0)+ibei_2(\alpha_0))} \quad (24)$$

where $ber_1(\alpha_0), bei_1(\alpha_0), ber_2(\alpha_0), bei_2(\alpha_0)$ - the Thomson function for a given value $\alpha_0$can be calculated using special tables [19-23]. Having isolated the real and imaginary parts of the amplitude-phase frequency characteristic (24), we obtain

$$\chi = Re[W_{\tau_1,\vartheta_{x_1}}(i\omega)] = \frac{a_{\tau_1}}{a_{\vartheta_1}} cos\, \phi_{\tau_1} = Re[\frac{\left(i^{\frac{3}{2}}\alpha_0\right)(ber_1(\alpha_0)+ibei_1(\alpha_0))}{4(ber_2(\alpha_0)+ibei_2(\alpha_0))}] =$$
$$= \frac{\alpha_0}{4\sqrt{2}} \frac{(ber_1\alpha_0(bei_2\alpha_0-ber_2\alpha_0)-bei_1\alpha_0(bei_2\alpha_0+ber_2\alpha_0))}{(ber_2^2\alpha_0+bei_2^2\alpha_0)} \quad (25)$$

$$\beta = Im[W_{\tau_1,\vartheta_{x_1}}(i\omega)] = \frac{a_{\tau_1}}{a_{\vartheta_1}} sin\, \phi_{\tau_1} = Im[\frac{\left(i^{\frac{3}{2}}\alpha_0\right)(ber_1(\alpha_0)+ibei_1(\alpha_0))}{4(ber_2(\alpha_0)+ibei_2(\alpha_0))}] =$$
$$= \frac{\alpha_0}{4\sqrt{2}} \frac{(ber_1\alpha_0(bei_2\alpha_0+ber_2\alpha_0)+bei_1\alpha_0(bei_2\alpha_0-ber_2\alpha_0))}{(ber_2^2\alpha_0+bei_2^2\alpha_0)} \quad (26)$$

Despite the fact that the Thomson functions are tabulated, calculations using formulas (25) and (26) lead to rather cumbersome calculations, and they cannot be used for oscillatory flow of a viscoelastic fluid in a cylindrical pipe. Therefore, if we assume that for large values the dimensionless frequencies of oscillations, that is $\left|i^{3/2}\alpha_0\right| > 1$, we expand the Bessel functions contained in (19) into asymptotic series, taking into account the formula [19].

$$i^{-n}J_n(ix) = \frac{e^x}{\sqrt{2\pi x}}[1 - \frac{4n^2-1}{1!(8x)} + \frac{(4n^2-1)(4n^2-3^2)}{2!(8x)^2} -\dots]. \quad (27)$$

Substituting x its value instead $x = \sqrt{i}\alpha_0$ and keeping only three terms in the series under consideration with rounding of the coefficients at x, one can find an approximate expression (19) in the form

$$W_{\tau_1,\vartheta_{x_1}} = \frac{1}{4}(\frac{(x)J_1(ix))}{J_2(ix))}) = \frac{(x)}{4}(1 + \frac{12}{1!(8x)} + \frac{15\cdot 16}{2!(8x)^2}\cdots) \quad (28)$$

Considering that$x = \sqrt{i}\alpha_0$ in (28), we obtain

$$W_{\tau_1,\vartheta_{x_1}} = \frac{1}{4}(\frac{(i\sqrt{i}\alpha_0))J_1(i\sqrt{i}\alpha_0)}{J_2(i\sqrt{i}\alpha_0)}) = \frac{(\sqrt{i}\alpha_0)}{4}(1 + \frac{12}{1!(8\sqrt{i}\alpha_0)} + \frac{15\cdot 16}{2!(8\sqrt{i}\alpha_0)^2}\cdots) = \chi + \beta i \quad (29)$$

For oscillatory flow, from formula (29), having isolated its real and imaginary parts, we obtain

$$\chi = Re[W_{\tau_1,\vartheta_{x_1}}(i\omega)] = \frac{\alpha_0}{4\sqrt{2}} + \frac{3}{8} + \frac{15}{32\sqrt{2}\alpha_0} + \dots,$$
$$\beta = Im[W_{\tau_1,\vartheta_{x_1}}(i\omega)] = \frac{\alpha_0}{4\sqrt{2}} - \frac{15}{32\sqrt{2}\alpha_0} + \cdots \quad (30)$$

Based on formula (22), taking into account formulas (25), (26) and (30), graphs are constructed in Fig. 1, showing the change in the relative shear stress in a non-stationary flow depending on the dimensionless oscillation frequency.

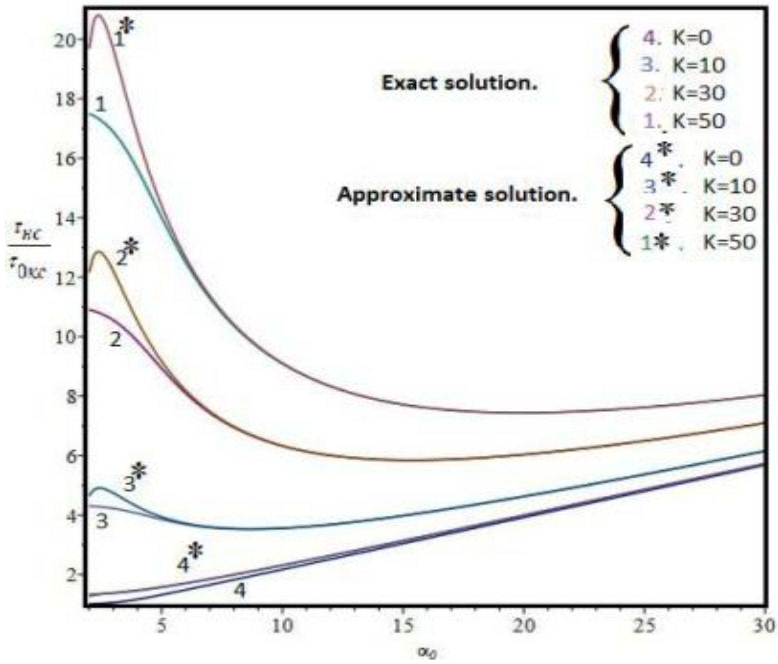

Fig. 1

From these graphs it is evident that the change in the relative shear stress in a non-stationary flow depending on the dimensionless oscillation frequency, at $\alpha_0 = 2$, differs by no more than 2% from its exact values, and at $\alpha_0 > 2$ these the difference approaches zero. Thus, in this case, approximate asymptotic formulas (30) can be used with high accuracy, starting with $\alpha_0 = 2$ for studying the oscillatory flow of a viscous and viscoelastic fluid in a cylindrical pipe.

4. Conclusion

Problems of oscillatory flow of a viscous incompressible fluid in a cylindrical pipe with a given harmonic oscillation of the average velocity across the pipe cross-section are solved. The transfer function and amplitude-phase frequency characteristics are determined. Using these functions, the influence of oscillation frequency and acceleration on the ratio of shear stress to cross-sectional velocity is determined. Asymptotic formulas are found for determining the transfer function for viscous fluid flow in unsteady flow at lower and higher oscillation frequencies. By comparing the exact solution to the asymptotic solution, new asymptotic formulas are proposed that are of great importance in studying the oscillatory flow of viscoelastic fluid in a cylindrical pipe.

References

[1] Marx U., Wallis H., Hoffmann S., Linder G., Harland R., Sonntag F., Klotzbach U., Sakharov D., Tonevitskiy A., Lonster R. “Homan-on-a-Chip” developments: a translational cutting-edge alternative to systemic safety assessment and effecting evacuation in laboratory animals and man? //ATLA 2012. vol. 40. P. 235-257.

[2] Inman W., Domanskiy K., Serdy J., Ovens B., Trimper D., Griffith L.G., Dishing modeling and fabrication of a constant flow pneumatic micropump //J. Micromech. Microeng. 2007. vol. 17. P. 891-899.

[3] Mirsaidov MM. Ishmatov AN. Yuldoshev BSh. Khazratkulov IO. Dynamic characteristics of spatial axisymmetric structures considering energy dissipation in the material. Izvestiya VUZ. Applied Nonlinear Dynamics. 2026. DOI: 10.18500/0869-6632-0032124.

[4] Ishmatov A.N., Yuldoshev B.Sh., Urinov B.Kh. Nonlinear vibrations of tall structures. AIP Conf. Proc. 3286, 030002 (2025), DOI: 10.1063/5.0280116.

[5] Khodzhaev D A, Abdikarimov R A and Mirsaidov M M 2019 Dynamics of a physically nonlinear viscoelastic cylindrical shell with a concentrated mass. Magazine Civil Engineering DOI: 10.18720/MCE.91.4

[6] Teshaev M Safarov I I Mirsaidov M 2019 Oscillations of multilayer viscoelastic composite toroidal pipes J Serbian Soc Comput Mech https://doi.org/10.24874/jsscm.2019.13.02.08.

[7] Jons J.R., Walters T.S. Flow of elastic-viscous liquids in channels under the influence of a periodic pressure gradient // Part 1. Rheol. Acta. 1967. Vol. 6 pp.240-245.

[8] Casanellas L., Ortin J. Laminar oscillatory flow of Maxwell and Oldroyd-B fluids// J. Non-Newtonian Fluid. Mechanics. 166. (2011). – p. 1315-1326.

[9] Navruzov K., Sharipova Sh. B. Tangential Shear Stress in an Oscillatory Flow of a Viscoelastic incompressible fluid in a plane Channel //Fluid Dynamics, 2023, vol. 58, N0 3 p.360-370.

[10] Navruzov K., Begjanov A. Sharipova Sh., Jumaev J. Study of oscillatory flows of a viscoelastic fluid in a flat channel based on the generalized Maxwell model //Russian Mathematics, 2023, vol.67, No 8, pp.27-35.

[11] Navruzov K., Turaev M., Shkurov Z. Pulse flows of elastic-viscous incompressible fluid in a plane channel. AIP publishing, AIP conf.proc. 3119, 030002 2024, p.1-9.

[12] Shkurov Z.Navruzov K., Turaev M., N.Abdikarimov. Laminar unsteady flow of a viscoelastic liquid in a flat channel. E3S Web of Conferences 587, 01014 (2024) p . 1-10

[13] Navruzov K., Rajabov S., Abdikarimov N., Turdimuradov O., Nasrulloeva R. Study of non-stationary flow of viscoelastic incompressible fluid in a flat channel. E3S Web of Conferences 587, 01012 (2024) p. 1-13

[14] Navruzov K., Rajabov S., Abdikarimov N., Turdimuradov O., Nasrulloeva R.Non-stationary flow of viscoelastic fluid in a cylindrical pipe. E3S Web of Conferences 587, 01013 (2024) p .1-11.

[15] Navruzov K., Begjanov A. S., Abdikarimov N.I., Yusupov S. Examining laminar non-stationary viscoelastic fluid flow between two parallel planes. BIO Web of Conferences 105, 05005 (2024).

[16] Ding Z., Jian Y. Electrokinetic oscillatory flow and energy microchannelis: a linear analysis. J. Fluid. Mech., 2021, vol. 919, A20. DOI:10.1017/j fm. 2021. 380 A20. 1-31.

[17] Mirsaidov M.M., Ishmatov A.N., Yuldoshev B.Sh. Vibrations of plane structures considering the physical nonlinearity of the material. International Scientific and Technical Conference "Ensuring seismic safety and seismic stability of buildings and structures, solving applied mechanical problems" dedicated to the 90th anniversary of Academician T.R. Rashidov. May 27-29, 2024, Tashkent, Uzbekistan. Pp. 239-250.

[18] Abdukadirov S., M.Aisenberg-Stepanenko, Yuldoshev B. Impact of a plane compression wave on a cylindrical shell filled with fluid. III International Scientific Conference «Construction Mechanics, Hydraulics & Water Resources Engineering» (CONMECHYDRO 2021), DOI: 10.1063/5.0113327

[19] Usarov M.K., Yuldoshev B.Sh. Estimation of seismic resistance of multi-story buildings in the framework of the bimoment theory using the plate model. E3S Web of Conferences 376, 01103 (2023).

JMMME

JOURNAL OF MATHEMATICAL MODELS AND METHODS IN ENGINEERING

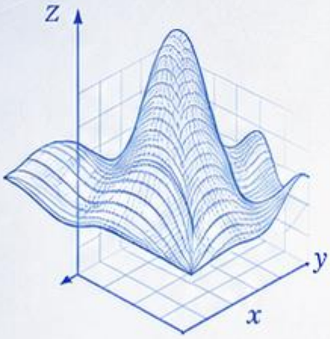

$$\frac{dx}{dt} = Ax + b(t)$$

$$\frac{\partial u}{\partial t} = \alpha \nabla^2 u + f$$

$$\sum_{i=1}^{n} a_i x_i + b$$

$$f(x) = \int_a^b f(x)\, dx$$

CONTENTS

$$A = \begin{bmatrix} a_{11} & a_{12} & \cdots & a_{1n} \\ a_{21} & a_{22} & \cdots & a_{2n} \\ \vdots & \vdots & \ddots & \vdots \\ a_{n1} & a_{n2} & \cdots & a_{nn} \end{bmatrix}$$

$$\sum_{i=1}^{n} w_i x_i$$

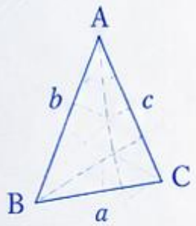

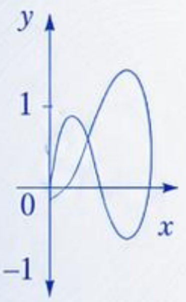

TIIAME National Research University